PERFORMANCE OF LDPC DECODER WITH ACCURATE LLR METRIC IN LDPC-CODED PILOT-ASSISTED OFDM SYSTEM

LI ZHI PING

(B.E., South China University of Technology; M.Eng., Xi'an Jiaotong University)

A THESIS SUBMITTED FOR

THE DEGREE OF MASTER OF ENGINEERING

DEPARTMENT OF ELECTRICAL AND COMPUTER

ENGINEERING

NATIONAL UNIVERSITY OF SINGAPORE

2011

Acknowledgements

I would like to take this opportunity to convey my deepest and sincere gratitude to people without whom I would not have completed this thesis successfully.

First and foremost, I would like to express my deepest gratitude to my advisor, Professor Kam Pooi Yuen, for devoting the time to guiding me with great enthusiasm and patience during the entire course of the research project. Despite his busy schedule, he met me regularly to obtain updates on the project progress and to ensure that I am progressing in the right direction. Such meeting has provided me with opportunity to learn valuable knowledge on research methodology, critical thinking and the right way to present my work, all of which will help me become a good researcher and have far reaching effects on my professional life.

I would also like to acknowledge the support and advice I received from PhD student Mr. Yuan Hai Feng. I've drawn inspiration from his wonderful research work. We had a lot great technical discussions via email. I really appreciate his great patience when dealing with the technical problems raised by me.

Special thanks go to Dr. Li Yan for her guidance on channel modeling. I am also very thankful to Dr. Wu Ming Wei for giving me detailed instruction on how to use the High Performance Computing (HPC) facility for accelerating the simulation. I also got much insightful feedback from her during my graduate seminars.

My gratitude is extended to all the professors who have educated me during my graduate study. Their professionalism has always inspired and enlightened me. I totally enjoyed their teaching and the knowledge I've learnt from their lecture laid a solid foundation for me to carry out the research.

Finally, I would like to thank my family. I thank my mom, dad and sister for their unconditional love and sacrifice. I am also very grateful to my husband, Liu Jin Xiang, and two lovely daughters, Liu Xin Yi and Liu Pei Shan, who have been the greatest source of strength and support in my life. This thesis is dedicated to them all.

Table of Contents

Abstract

Modern communication systems are increasingly adopting advanced technologies such as OFDM modulation and LDPC codes. OFDM modulation is spectrally efficient and able to mitigate the multipath fading in the wireless channel, whereas the LDPC code is a very powerful error correcting code with a near Shannon-limit performance. A common practice in OFDM system is to transmit pilots on some subcarriers periodically along with the data subcarriers for the purpose of channel estimation. The combination of these technologies is becoming the trend of many modern wireless communication standards. Hence, in this thesis, we study a LDPC-coded pilot-assisted OFDM system with the focus on how to optimally insert pilot and which LLR metric to use in the LDPC decoder, in order to achieve the best performance.

The thesis starts with a literature review on OFDM modulation, LDPC codes and pilot-assisted communication. Based on the knowledge of these technologies, we first study the LDPC-coded pilot-assisted single-carrier communication system over Rayleigh flat fading channel. Based on the pilot-aided MMSE channel estimator, two LLR metrics, namely PSAM-LLR and A-PSAM-LLR, are defined and their impact on the BER performance is studied through simulation. Secondly, we study the LDPC-coded pilot-assisted OFDM system over multipath fading channel. Similarly, pilot-aided MMSE channel estimator is used and two LLR metrics are derived for the OFDM system. Simulation is conducted for the OFDM system with different configurations. The simulations serve several purposes. One objective is to investigate the optimal pilot spacing in various scenarios. Another objective is to compare the two LLR metrics in terms of decoder performance and implementation complexity.

List of Tables

List of Figures

List of Acronyms

AM	Amplitude Modulation
A-PSAM-LLR	Approximate Pilot Symbol Assisted Modulation Log Likelihood Ratio
AWGN	Additive White Gaussian Noise
BER	Bit Error Rate
BPSK	Binary Phase Shift Keying
CDMA	Code Division Multiple Access
CIR	Channel Impulse Response
CP	Cyclic Period
CSI	Channel State Information
DAB	Digital Audio Broadcasting
DFT	Discrete Fourier Transform
DMT	Discrete Multi-tone Modulation
DVB-S2	Digital Video Broadcasting – Satellite – Second Generation
DVB-T	Digital Video Broadcasting - Terrestrial
Eb/No	Energy per Bit to Noise Power Spectral Density Ratio
FDMA	Frequency Division Multiple Access
FEC	Forward Error Correction
FFT	Fast Fourier Transform
FIR	Finite Impulse Response
GSM	Global System for Mobile Communications
ICI	Inter-Carrier Interference
IDE	Integrated Development Environment
IDFT	Inverse Discrete Fourier Transform
IEEE	Institute of Electrical and Electronics Engineers
IFFT	Inverse Fast Fourier Transform

ISI	Inter-Symbol Interference
ITU	International Telecommunication Union
ITU-T	ITU Telecommunication Standardization Sector
LAN	Local Area Network
LDPC	Low Density Parity Check
LLR	Log-likelihood Ratio
LMMSE	Linear Minimum Mean Square Error Estimator
LS	Least-Squares
MAN	Metropolitan Area Network
MATLAB	Matrix Laboratory
MIMO	Multiple Input Multiple Output
MLE	Maximum Likelihood Estimator
MMSE	Minimum Mean Square Error
MMSEE	Minimum Mean Square Error Estimator
MSE	Mean Square Error
OFDM	Orthogonal Frequency Division Multiplexing
PAT	Pilot-aided Transmission
PSAM	Pilot Symbol Assisted Modulation
PSAM-LLR	Pilot Symbol Assisted Modulation Log Likelihood Ratio
PSK	Phase Shift Keying
QAM	Quadrature Amplitude Modulation
QPSK	Quadrature Phase Shift Keying
SNR	Signal-to-Noise Ratio
TDMA	Time Division Multiple Access
WCDMA	Wideband Code Division Multiple Access
WSSUS	Wide Sense Stationary Uncorrelated Scattering

CHAPTER 1   INTRODUCTION

In this chapter, we firstly review some important technologies that emerge in the last decades and contribute enormously to the modern digital communication. These key techniques, including the Orthogonal Frequency Division Multiplexing (OFDM) modulation, Low Density Parity Check (LDPC) code and Pilot-aided Transmission (PAT), will be the main subjects of the thesis. Following the literature review, the motivation of the research is introduced. Finally, the outline of the thesis will be given.

1.1   New Technologies in Modern Digital Communication

We are now living in the information age. It is a digital world where people are connected via internet and mobile phones anytime and anywhere. Hence, there is an increasing demand for fast and reliable digital communications. To meet the demand, some new technologies are proposed and soon become the driving force of the thriving information age. For instance, the Orthogonal Frequency Division Multiplexing (OFDM) is proposed as multicarrier modulation technique with robustness to fading channel. The LDPC code is proposed as a powerful error correcting code with near Shannon-limit performance. Pilot-aided Transmission (PAT) is a technique that enables the receiver to estimate the channel with the assistance of inserted pilots. Nowadays, these technologies have seen their applications in many new generation communications systems and become key contributors to the rapid advance in the modern communication world.

1.1.1   OFDM System

Orthogonal Frequency Division Multiplexing (OFDM) is a digital multi-carrier modulation technique which uses a large number of orthogonal sub-carriers to carry data. The history of OFDM dates back to 1960s when frequency-division multiplexing or multi-tone systems were employed in military applications —for example, by Bello [35], Zimmerman et al [36] [37]. Later, Chang [13] [38] proposed Orthogonal Frequency Division Multiplexing which employs multiple carriers overlapping in the frequency domain. Saltzberg [39] studied a parallel quadrature amplitude modulation (AM) data transmission system which meets Chang's criteria and finds it achieves good performance over band-limited dispersive transmission media. The breakthrough came when Weinstein and Ebert [14] in 1971 suggested the use of the Discrete Fourier Transform (DFT) to replace the banks of sinusoidal generators and the demodulators to significantly reduce the implementation complexity of OFDM modems.

OFDM has become popular for several reasons. It divides the high-rate data stream into sub-channels which carry only a slow-rate data stream, thus it is robust in combating multipath fading in wireless channels. Its equalization filter design is simple. The

implementation of Fast Fourier Transform / Inverse Fast Fourier Transform (FFT/IFFT) is practical and affordable. The guard interval between symbols eliminates inter-symbol interference (ISI).

Because of its advantages, OFDM is now widely used in wideband communication system. For instance, it has been chosen as the standard for European terrestrial digital video broadcasting (DVB-T) and digital audio broadcasting (DAB), the IEEE 802.11a (local area network, LAN) and the IEEE 802.16a (metropolitan area network, MAN) standards. The combination of multiple-input multiple-output (MIMO) wireless technology with OFDM is employed in the next generation (4G) broadband wireless communications.

1.1.2 LDPC

Low Density Parity Check (LDPC) code is a linear error correcting code with sparse parity check matrix. It was proposed by Gallager [19] in his PhD thesis in 1962. Unfortunately, it was mostly ignored for years until Tanner [20] in 1981 suggested bipartite graph be used to represent the structure of LDPC code. It was Mackay and Neal who finally brought it to the attention of the research community in 1999 ([40], [21]).

Because of its near Shannon-limit performance and low complexity of the iterative decoder, the LDPC code now emerges as the contender to Turbo code in many communication systems. In 2003, an LDPC code beat several turbo codes to be chosen as the error correcting code in the new DVB-S2 standard for the satellite transmission of digital television. In 2008, LDPC beats convolutional codes and turbo codes as the Forward Error Correction (FEC) scheme for the ITU-T G.hn standard. LDPC is also used in 10GBase-T Ethernet.

1.1.3 Pilot Assisted Transmission

Pilot Assisted Transmission (PAT) is a technique which aids the channel estimation. It refers to multiplexing pilots (known symbols) into the transmitted signal. The receiver can exploit the pilot symbols for many purposes like channel estimation and tracking, receiver adaptation and optimal decoding. PAT is prevalent in modern communication systems. The GSM (Global System for Mobile Communications) system includes 26 pilot bits in the middle of every packet. The North America TDMA (Time Division Multiple Access) standard puts pilot symbols at the beginning of each packet. Third generation systems such as WCDMA and CDMA-2000 transmit pilots and data simultaneously.

The history of PAT dates back to 1989 when it was introduced for single-carrier system by Moher and Lodge [41]. It was Cavers [12] who coined the now widely used term Pilot Symbol Assisted Modulation (PSAM) and provided a thorough performance analysis that generalizes the design of pilot assisted transmissions.

Pilot assisted transmission in multi-carrier system like OFDM system has been explored by many researchers. Two types of pilot insertions are generally considered. The first is block type pilot insertion, in which all the subcarriers are used for pilot transmission. Channel estimation algorithm can be Least-Squares (LS) or Minimum Mean Square Error (MMSE). The computational complexity of LS/MMSE estimator can be reduced by a low-rank channel estimator using singular value decomposition [7][28]. Once the channel estimation is obtained, it can either be applied to the successive symbols or a decision-directed channel equalizer can be implemented for channel tracking.

While the block type pilot scheme may suffice for slowly fading channel, it often fails to track the rapidly fading channel [42], [7]. To solve the problem, comb type pilot scheme is proposed, in which pilots and data symbols are both transmitted in each OFDM symbol. Channel estimation in comb type pilot arrangement can have different approaches. The first methodology is to estimate the frequency domain channel response at pilot subcarriers with LS or MMSE criteria [28], then perform interpolation to obtain the channel estimation at data subcarriers. The interpolation methods can be piecewise-constant and piecewise-linear filter [30], second-order polynomial interpolation [28], low-pass interpolation [31], or spline cubic interpolation [31]. The second methodology is to use maximum likelihood estimator (MLE) [9] or the Bayesian minimum mean square error estimator (MMSEE) [9][42] to obtain the frequency-domain channel response.

Apart from the one-dimensional estimation, some researchers have investigated the pilots in frequency-time grid and derive 2-D Wiener filter [43][44][45]. The 2-D Wiener filter can be further simplified into cascaded two 1-D Wiener filter in the time-domain and frequency domain without compromise in the performance.

Optimal placement of pilot tones is an interesting research area. For 1-D estimation, Negi and Cioffi [29] suggests that pilots tones shall be equally spaced and the number of pilots shall be no less than the maximum channel length. For 2-D estimation, based on the Nyquist sampling theorem, it is suggested that the spacing of pilot tones in frequency domain depend on the maximum excess delay of the channel, and the spacing of pilot tones in time domain depend on the maximum Doppler spread [43][44][50].

In this thesis, we only consider MMSE channel estimation with comb type pilots. 2-D time-frequency estimation is beyond the scope of the thesis.

1.2 Research Motivation

In the literature, we can find a lot of research done in the pilot-based channel estimation, but very little research is conducted in finding the optimal Log-likelihood Ratio (LLR) metric for a LDPC-coded pilot-based OFDM system to achieve the best decoding performance. The LDPC decoding is well-known for its iterative nature, in which the LLR metric initialization is critical. In the literature, it is generally assumed that receiver has a priori knowledge of

channel and a conventional formula for LLR metric is derived under such assumption. However, in practical applications, receiver need to estimate the channel from the received pilot symbols inserted periodically in the data stream. In this case, a common practice is to modify the conventional metric by simply replacing the actual channel with the estimated channel. However, there is a better approach. In [1], Haifeng et al. studies the LDPC-coded pilot-aided single-carrier system transmitted over Rayleigh flat fading channel and proposes a new LLR metric by taking both the channel estimation and estimation mean square error into account. By comparison with the conventional approach, the new algorithm is demonstrated to have superior performance particularly in high Signal-to-Noise Ratio (SNR) range.

It is therefore of interest to study if it is possible to generalize the new LLR metric into the OFDM system transmitted over frequency selective fading channel. That is how our work is motivated. We will not only derive the LLR metric for the pilot-assisted OFDM system but also investigate the effect of different pilot placement on the system performance.

1.3 Thesis Organization

The rest of the thesis is organized as follows.

Chapter 2 reviews the basics of the LDPC code, including its encoding and decoding algorithms. A typical LDPC code and its performance is illustrated.

Chapter 3 reviews the Pilot Symbol Assisted Modulation (PSAM) and introduces the PSAM in single-carrier and OFDM system.

Chapter 4 studies the LDPC-coded pilot-assisted single-carrier system over Rayleigh flat fading channel. The Linear Minimum Mean Square Error Estimator (LMMSE) estimator based on the received pilot is obtained and the two LLR metrics are defined. Simulation result with different LLR metrics is presented.

Chapter 5 studies the LDPC-coded pilot-assisted OFDM system over multipath fading channel. Comb-type pilot insertion is adopted. Two LLR metrics are derived based on the LMMSE channel estimation with received pilots. Simulation is conducted on OFDM system by varying parameters such as FFT point, pilot spacing, maximum delay spread, power delay profile, etc. The simulation result is presented and discussed. Some interesting observation and comments are made regarding the optimal pilot spacing and the best LLR metric.

Chapter 6 makes conclusion and discusses about the future work.

CHAPTER 2   LDPC CODES

This chapter introduces the basics of LDPC codes. First, the history of LDPC code is presented, followed by the introduction of the Tanner graph, which is a graphic representation of LDPC code. Second, the encoder and decoder of LDPC are introduced with detailed explanation on probability-domain decoder and log-domain decoder. The LLR metric initialization as an essential step to a successful decoding will be discussed for Additive White Gaussian Noise (AWGN) channel and Rayleigh flat fading channel.   Finally, a typical LDPC code and its performance will be given.

2.1   History of LDPC Codes

LDPC codes were invented by Gallager [19] in his 1963 Ph.D thesis. Gallager proposed a specific construction of regular LDPC code and a hard decoding algorithm. However, Gallager's work was forgotten for decades. Tanner [20] in 1981 proposed Tanner graph to graphically represent LDPC code. Tanner graph is a bipartite graph constituting two groups of nodes. There are edges between the nodes in different groups, but there are no edges connecting nodes within the same group. Tanner graph is also forgotten for many years, until MacKay [21] in 1999 rediscovered Gallager's work and claimed the LDPC code has near-Shannon performance.

Ever since then, LDPC has become a hot research field and attracted intensive research efforts worldwide. With the merits of LDPC codes being recognized, LDPC codes are now adopted as the coding scheme by more and more digital communication standards.

2.2   Basics of LDPC Codes

LDPC code is a special class of linear block codes. For a code rate r = k / m LDPC code, the message has k-bits, the codeword has n-bits, and m = n - k. The parity matrix H is a m x n matrix. Denote the codeword C as a row vector with length n, then the codeword C shall satisfy the equation $HC^T = 0$.

The characteristic of LDPC code is that it has sparse parity check matrix which means that the number of 1's per column and per row in the parity check matrix is small compared with the column number and row number. The number of 1's in a row is called the weight of that row, and the number of 1's in a column is called the weight of that column. If rows have equal weights and columns have equal weights, it is called a "regular LDPC code", otherwise it is called "Irregular LDPC code".

2.3   Graphical Representation by Tanner Graph

A LDPC code can be conveniently described by a graphical representation known as a Tanner graph which was firstly proposed by Tanner. Tanner graph is a bipartite diagram which

consists of two groups of nodes. One group consists of check nodes, while the other group consists of variable nodes. Variable nodes represent the bits in the codeword, while check nodes represent the parity check equations. For a (n,k) LDPC code, there are n variable nodes and (n-k) check nodes. A regular (d_v,d_c)-LDPC code means that each variable node has d_v neighboring check nodes, and each check node has d_c neighboring variable nodes.

The connection between variable nodes and check nodes is determined by the parity check matrix H. For a parity check matrix H given in Equation (2.1), its Tanner graph is shown in Figure 2-1.

$$H = \begin{bmatrix} 0 & 1 & 0 & 1 & 1 & 0 & 0 & 1 \\ 1 & 1 & 1 & 0 & 0 & 1 & 0 & 0 \\ 0 & 0 & 1 & 0 & 0 & 1 & 1 & 1 \\ 1 & 0 & 0 & 1 & 1 & 0 & 1 & 0 \end{bmatrix}$$

(2.1)
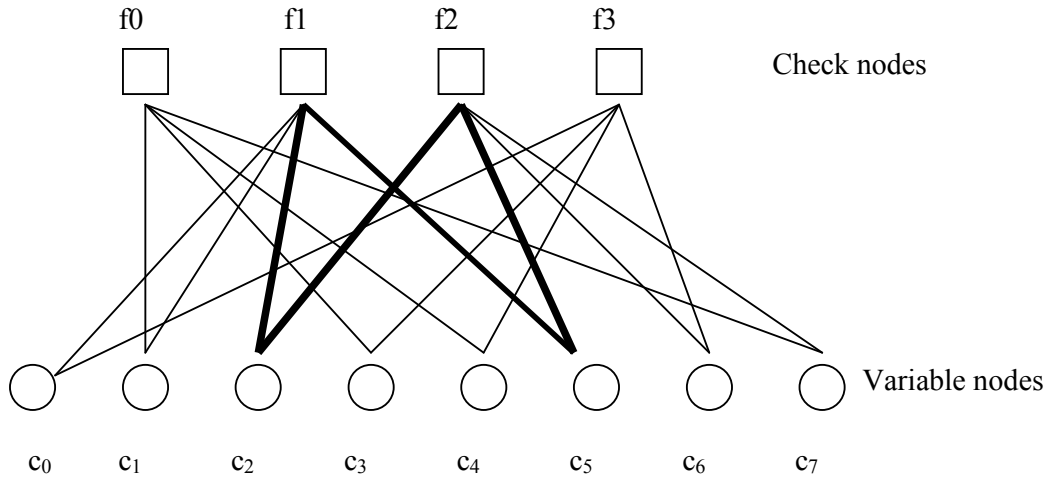
Figure 2-1   Graphical representation of a LDPC code by a Tanner Graph

A cycle of length n in a Tanner graph is a path which starts and ends in the same node and comprises n edges. Girth of a Tanner graph is defined as the shortest cycle in the graph. Apparently the shortest possible cycle in any Tanner graph is 4. In the above example, a path with cycle 4 is highlighted in bold lines. Any 2×2 submatrix in H consisting of four 1's is an indication of girth 4. To construct a good LDPC code, we need ensure that H contains no girth of 4 as it would degrade the performance of LDPC decoding.

2.4   LDPC Encoder

A straightforward implementation of LDPC encoding is to use the generation matrix G. The codeword can be obtained simply by $C = Gm$. In systematic encoding, G can be

derived from parity matrix H. However, as G is normally not a sparse matrix, the calculation of $C = Gm$ cannot achieve linear time encoding.

A popular implementation of LPDC encoder uses LU decomposition which is detailed as following. For a M x N matrix H, where M < N. H can be written as $H = \begin{bmatrix} A \mid B \end{bmatrix}$, where A is a M x M matrix, B is a M x (N-M) matrix. The codeword C consists of the message bits s and the check bits c. We denote the codeword C as $C = \begin{bmatrix} c & s \end{bmatrix}$, where s is a (N - M) x 1 row vector, c is a M x 1 row vector.

The codeword C shall satisfy the equation $HC^T = 0$. Hence $\begin{bmatrix} A & B \end{bmatrix}\begin{bmatrix} c \\ s \end{bmatrix} = 0$

We have $Ac + Bs = 0 \Rightarrow Ac = Bs$

If A can be LU decomposed into A=LU, then $LUc = Bs$

Let $y = Uc$, then $Ly = Bs$

The parity check bit c can be obtained with the following steps:

1) Solve the equation $Ly = Bs$ by forward substitution to obtain y.

2) Solve the equation $Uc = y$ by backward substitution to obtain c

The codeword is $C = \begin{bmatrix} c & s \end{bmatrix}$

In the case that matrix A is singular, we need to reorder the columns of H to ensure A is nonsingular. If H is not a full rank matrix, then the data rate can be actually higher.

2.5 LDPC Decoder

LDPC decoding is an iterative decoding, known as belief propagation, or sum-product, or message passing algorithm. Despite the different names, they refer to the same algorithm. In each iteration, variable nodes and check nodes exchange message and update the status information. The message that is passed along an edge is extrinsic information. Therefore, the message passed from a variable node v to a check node c will incorporate all incoming messages from v's neighboring check nodes excluding c. Likewise, the message passed from a check node c to a variable node v will incorporate all incoming messages from c's neighboring variable nodes excluding v. After a few iterations, the variable nodes will make a decision of the value of its bit based on its present status, and produce the decoder output.
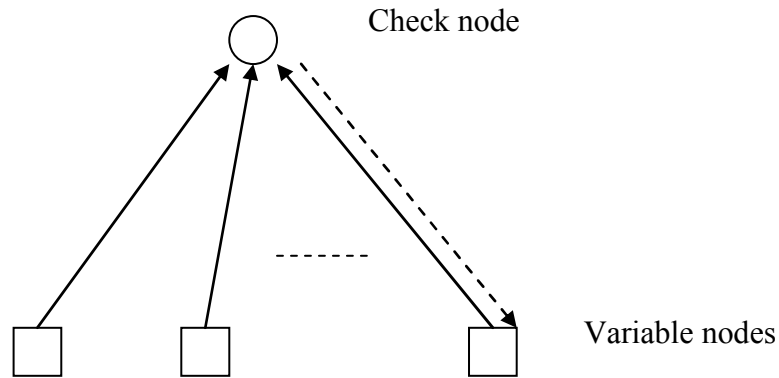
Figure 2-2   Output message from check node to variable node
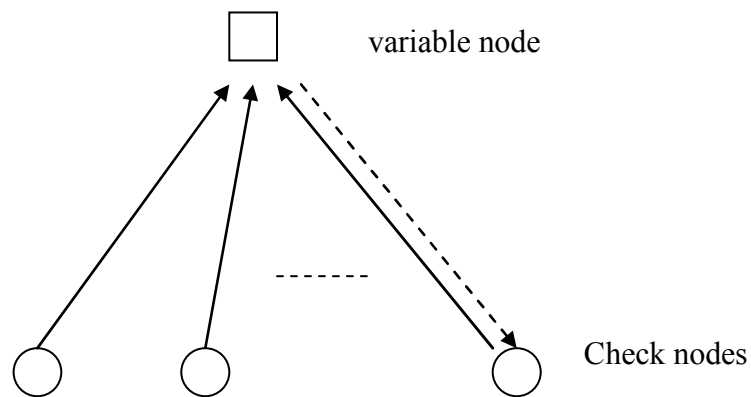
Figure 2-3   Output message from variable node to check node

There are several variants of the algorithm, namely, hard-decision decoding, probability-domain decoding and log-domain decoding. The latter two are soft-decision algorithm, which has much better performance than the hard-decision decoder. The log-domain decoder can be further simplified to min-sum decoder. All these decoding algorithms share similar structure, except that the messages have different forms.

All algorithms consist of these steps:

    1) Initialization

    2) Check node update

    3) Variable node update

    4) Verify parity check equation. Quit if successful, otherwise go to 2)

In the following, the probability-domain decoder and log-domain decoding algorithm will be introduced in details.

2.5.1 Probability-Domain Decoder

The message that is passed in the probability-domain decoder is the probability of each bit being 1 or 0.

Some notations used in the description of this decoding algorithm are:

q_{ij} - Message sent by the variable node i to check node j. The message consists of a pair of values $q_{ij}(0)$ and $q_{ij}(1)$, representing the amount of belief that the bit is 0 or 1.

r_{ji} - Message sent by the check node j to variable node i. The message consists of a pair of values $r_{ji}(0)$ and $r_{ji}(1)$, representing the amount of belief that the bit is 0 or 1.

The probability-domain decoder consists of following steps:

1. Initialization

For variable node i, the probability of the transmitted bit c_i on condition of the received value y_i is $\Pr(c_i = 0 | y_i)$ and $\Pr(c_i = 1 | y_i)$. Hence, the output message from variable node i to any check nodes j will be

$$q_{ij}(0) = \Pr(c_i = 0 | y_i)$$
$$q_{ij}(1) = \Pr(c_i = 1 | y_i)$$

(2.2)

We denote $P_i = \Pr(c_i = 1 | y_i)$

2. Check node update

$$r_{ji}(0) = \frac{1}{2} + \frac{1}{2} \prod_{i' \in V_j \setminus i} \left(1 - 2q_{i'j}(1)\right)$$
$$r_{ji}(1) = 1 - r_{ji}(0)$$

(2.3)

Here $V_j \setminus i$ represents all the variable nodes connected to check nodes j except the variable node i.

3. Variable node update

$$q_{ij}(0) = K_{ij}(1 - P_i) \prod_{j' \in C_i \setminus j} r_{j'i}(0)$$
$$q_{ij}(1) = K_{ij} P_i \prod_{j' \in C_i \setminus j} r_{j'i}(1)$$

(2.4)

Here $c_i \setminus j$ represents all the check nodes connected to variable node i except the check node j.

The parameter K_{ij} is determined by the condition $q_{ij}(0) + q_{ij}(1) = 1$.

    4.   Decision making and parity check equation verification

Each variable node will update the estimate of the bit with all the incoming messages, as well as the probability based on the received value y_i.

$$\begin{aligned} Q_i(0) &= K_i(1 - P_i)\prod_{j \in C_i} r_{ji}(0) \\ Q_i(1) &= K_i P_i \prod_{j \in C_i} r_{ji}(1) \end{aligned} \tag{2.5}$$

The parameter K_i is determined by the condition $Q_i(0) + Q_i(1) = 1$.

The decision rule will be:

$$\hat{c}_i = \begin{cases} 1 & if \ Q_i(1) > Q_i(0) \\ 0 & else \end{cases} \tag{2.6}$$

Check if $\hat{c}_i$ satisfies all the parity check equations $\hat{c}_i H^T = 0$. If yes, the algorithm terminates successfully, otherwise go to the step 2 if iteration has not exceeded the limit.

2.5.2 Log-Domain Decoder

The message that is passed in the log-domain decoder is the LLR metric of each bit. With LLR, the multiplications in the iteration will be replaced by addition operation. Hence, log-domain decoder can reduce computational complexity and avoid the numerical instability caused by multiplications of probabilities over large number of iterations.

The log-domain decoder can be derived from probability-domain decoder by replacing the probability value by the LLR.

The notation of LLR used in the log-domain decoders include:

$$L(c_i) = \log \frac{\Pr(c_i = 0 \mid y_i)}{\Pr(c_i = 1 \mid y_i)} \tag{2.7}$$

$$L(q_{ij}) = \log \frac{q_{ij}(0)}{q_{ij}(1)} \tag{2.8}$$

$$L(r_{ji}) = \log \frac{r_{ji}(0)}{r_{ji}(1)} \tag{2.9}$$

$$L(Q_i) = \log \frac{Q_i(0)}{Q_i(1)} \tag{2.10}$$

The log-domain decoder consists of following steps:

1. Initialization

$$L(c_i) = \log \frac{\Pr(c_i = 0 \mid y_i)}{\Pr(c_i = 1 \mid y_i)} \tag{2.11}$$

$$L(q_{ij}) = L(c_i) \tag{2.12}$$

2. Check node update

Separate $L(q_{ij})$ into a sign and absolute magnitude. Let

$$\begin{aligned}
L(q_{ij}) &= \alpha_{ij}\beta_{ij} \\
\alpha_{ij} &= sign[L(q_{ij})] \\
\beta_{ij} &= abs[L(q_{ij})]
\end{aligned} \tag{2.13}$$

Then

$$L(r_{ji}) = \left[\prod_{i' \in V_j \setminus i} \alpha_{i''j} \right] * \phi\left(\sum_{i' \in V_j \setminus i} \phi(\beta_{i''j}) \right) \tag{2.14}$$

Here $\phi(x) = -\log\left(\tanh(\frac{1}{2}x) \right)$ which has the property that $\phi^{-1}(x) = \phi(x)$

$V_j \setminus i$ represents all the variable nodes connected to check nodes j except the variable node i

3. Variable node update

$$L(q_{ij}) = L(c_i) + \sum_{j' \in C_i \setminus j} L(r_{j'i}) \tag{2.15}$$

Here $C_i \setminus j$ represents all the check nodes connected to variable node i except the check node j

4. Decision making and parity check equation verification

Each variable node will update the estimate of the bit with all the incoming messages, as well as the probability based on the received value y_i.

$$L(Q_i) = L(c_i) + \sum_{j \in C_i} L(r_{ji}) \tag{2.16}$$

The decision rule will be:

$$\hat{c}_i = \begin{cases} 1 & if \ L(Q_i) < 0 \\ 0 & else \end{cases} \tag{2.17}$$

Check if $\hat{c}_i$ satisfies all the parity check equations $\hat{c}_i H^T = 0$. If yes, the algorithm terminates successfully, otherwise go to the step 2 if iteration has not exceeded the limit.

2.6   LLR Metric Initialization

The LLR metric initialization is essential to the log-domain LDPC decoder. The LLR of a received symbol represents the reliability of the symbol being transmitted as 1 or 0. The log-likelihood ratio is defined as

$$\lambda_i = \log \frac{P(s_i = 1 | r_i)}{P(s_i = 0 | r_i)} \tag{2.18}$$

Here s_i is the ith transmitted bit and r_i is the corresponding received signal.

We will derive the LLR metric for Binary Phase Shift Keying (BPSK) signaling in AWGN channel and Rayleigh flat fading channel.

2.6.1 AWGN Channel

For BPSK signaling in AWGN channel, the received signal can be expressed as:

$$r_i = s_i + n_i \tag{2.19}$$

Here $s_i = \pm\sqrt{E_s}$ is the transmitted signal, and n_i is Gaussian noise with zero mean and variance σ^2, $N(0, \sigma^2)$. Using Bayes rule, the LLR can be written as

$$\lambda_i = \log \frac{P(r_i | s_i = 1) P(s_i = 1) / P(r_i)}{P(r_i | s_i = 0) P(s_i = 0) / P(r_i)} = \log \frac{P(r_i | s_i = 1)}{P(r_i | s_i = 0)} \tag{2.20}$$

Here we assume that 0 and 1 are equally likely to be transmitted: $P(s_i = 1) = P(s_i = 0)$

As the noise is Gaussian, we get

$$\lambda_i = \log \frac{\frac{1}{\sqrt{2\pi}\sigma} \exp\left[-\left(r_i - \sqrt{E_s}\right)^2 / 2\sigma^2 \right]}{\sqrt{2\pi}\sigma \exp\left[-\left(r_i + \sqrt{E_s}\right)^2 / 2\sigma^2 \right]} = \frac{2\sqrt{E_s}}{\sigma^2} r_i = \frac{4\sqrt{E_s}}{N_0} r_i \tag{2.21}$$

Here $N_0 = 2\sigma^2$

2.6.2 Rayleigh Flat Fading Channel

For BPSK signaling in slow frequency-nonselective Rayleigh flat flading channel with AWGN, following Jake's isotropic scattering model [2], the received symbol is expressed as:

$$r_i = c_i s_i + n_i \tag{2.22}$$

Here $s_i = \pm\sqrt{E_s}$ is the transmitted signal, and n_i is zero-mean complex AWGN noise whose real and imaginary parts are jointly normal and independent. We denote the noise as $n_i = x_i + jy_i$, where $x_i \sim N(0, \sigma^2)$, $y_i \sim N(0, \sigma^2)$. c_i is the Rayleigh fading channel gain which can be modeled as a correlated, zero-mean, complex Gaussian process with its real and imaginary part being independent and identically distributed $N(0, \sigma_c^2)$. The autocorrelation of c_i shall be

$$R_i = E\left[C_n C_{n-i}{}^*\right] = 2\sigma_c{}^2 J_0(2\pi f_d T_s i) \tag{2.23}$$

Here f_d is the maximum Doppler shift in Hz, T_s is the symbol period in second. $J_0(\cdot)$. is the Bessel function of the first kind of order zero. The parameter $f_d T_s$ is called Doppler fade rate.

The LLR for the above Rayleigh flat fading channel is expressed as:

$$\lambda_i = \ln\frac{P\left(s_i = \sqrt{E_s}\,\middle|\,c_i, r_i\right)}{P\left(s_i = -\sqrt{E_s}\,\middle|\,c_i, r_i\right)} \tag{2.24}$$

Using Bayes rule, the LLR can be rewritten as

$$\begin{aligned}\lambda_i &= \ln\frac{P\left(r_i\,\middle|\,c_i, s_i = \sqrt{E_s}\right)}{P\left(r_i\,\middle|\,c_i, s_i = -\sqrt{E_s}\right)} \\[2mm] &= \ln\frac{\exp\left\{-\left|r_i - c_i\sqrt{E_s}\right|^2 \middle/ N_0\right\}}{\exp\left\{-\left|r_i + c_i\sqrt{E_s}\right|^2 \middle/ N_0\right\}} \\[2mm] &= \frac{4\sqrt{E_s}}{N_0}\mathrm{Re}\left[r_i c_i{}^*\right]\end{aligned} \tag{2.25}$$

Here $N_0 = 2\sigma^2$

The above expression of λ_i is a well-known LLR metric used in the literature [51][52].

2.7   A Typical LDPC Code and its Performance

We select a rate-1/2 LDPC code for our simulation. The code is downloaded from the website founded and maintained by Dr. David J.C. MacKay who rediscovered the LDPC code in 1999 and has been active in LDPC research ever since. He shared a lot of LDPC codes with various code lengths and code rates in his website [27]. These LDPC codes can be used as benchmark of performance.

The selected code is named "PEGirReg504x1008" by Dr. MacKay. It is constructed by Progressive Edge Growth method and has very good performance. Dr. MacKay provides the parity check matrix of the code in a specially formatted file called Alist file. The brief description of the code is as follows.

Table 2-1   PEGirReg504x1008 (N=1008, K=504, M=504, R= 0.5)

Alist file	Parity check matrix
Author	Xiao-Yu Hu, IBM Zurich research labs
N	1008
M	504
comment	Progressive Edge Growth construction attempts to maximize girth, and empirically gives very good codes. The best known code with these parameters (N,M). [Best in the sense of performance on AWGN]

Computer simulations are conducted to show the performance of the code in both AWGN channel and Rayleigh flat fading channel. Two typical Doppler fade rates are tested, which are $f_d T_s$ =0.02 and $f_d T_s$ =0.005. The performance with ideal LLR metric is summarized in Table 2-2. Note that the notation "NA" used in Table 2-2 is the abbreviation for "not available". The bit error rate (BER) performance is evaluated at different Eb/No which is the Energy per Bit to Noise Power Spectral Density Ratio. E_b is the energy per bit, while N_0 is noise power spectral density. The BER versus Eb/No curves are plotted in Figure 2-4 and Figure 2-5.

Table 2-2   BER performance of LDPC code (1008, 504) over AWGN channel and Rayleigh flat fading channel

AWGN Channel		Rayleigh Channel $f_d T_s$ =0.02		Rayleigh Channel $f_d T_s$ =0.005	
Eb/No (dB)	BER	Eb/No (dB)	BER	Eb/No (dB)	BER
0.00	1.43E-01	0	2.06E-01	0	2.03E-01
0.25	1.25E-01	1	1.75E-01	1	1.65E-01
0.50	1.00E-01	2	1.26E-01	2	1.19E-01
0.75	6.60E-02	3	5.55E-02	3	7.05E-02
1.00	3.57E-02	4	1.30E-02	4	3.66E-02
1.25	1.27E-02	5	1.26E-03	5	1.50E-02
1.50	3.09E-03	6	1.40E-04	6	5.79E-03
1.75	6.60E-04	7	NA	7	1.87E-03
2.00	1.01E-04	8	NA	8	5.33E-04
2.25	1.06E-05	9	NA	9	1.55E-04
2.50	NA	10	NA	10	4.55E-05
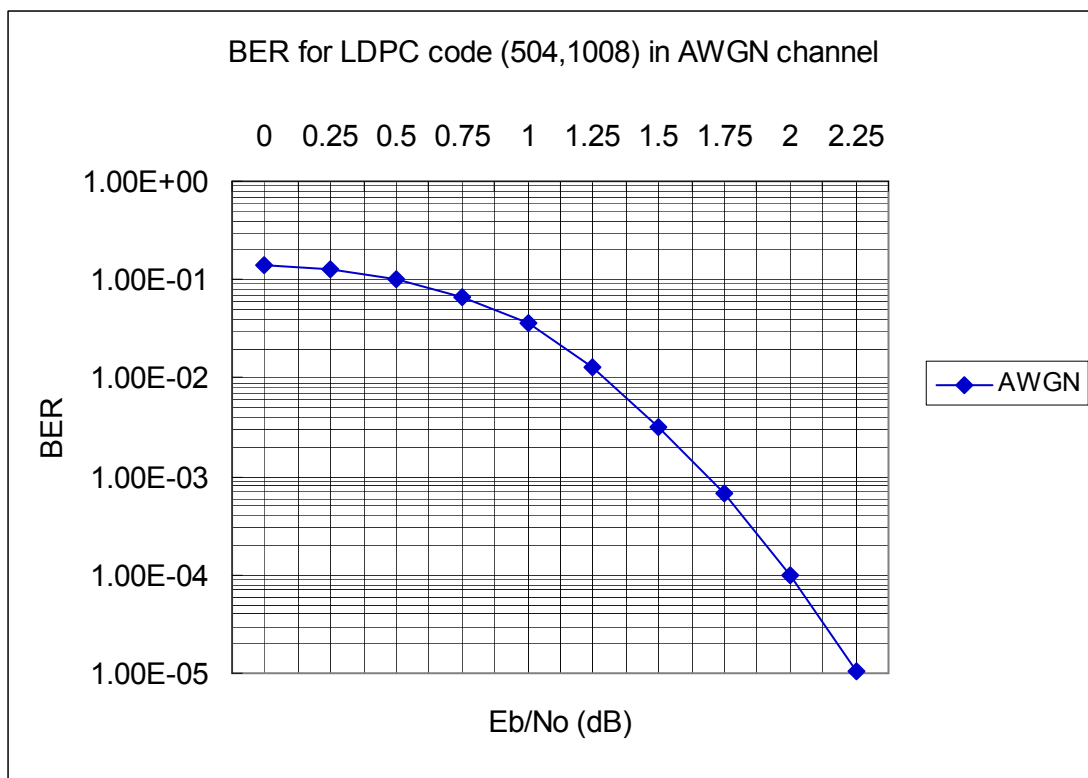
Figure 2-4   BER performance of LDPC over AWGN channel
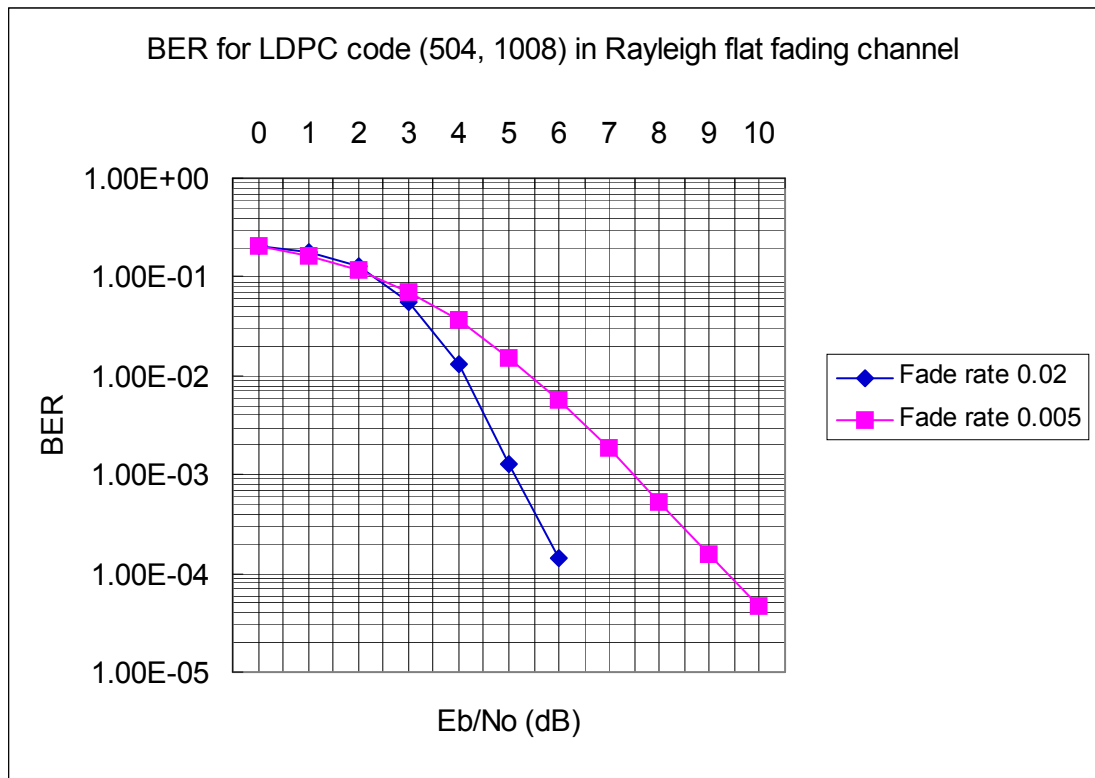
Figure 2-5   **BER performance of LDPC code (504,1008) over Rayleigh flat fading channel**

CHAPTER 3 PILOT-ASSISTED COMMUNICATIONS

In this chapter, we introduce Pilot Symbol Assisted Modulation (PSAM), followed by its application in the single-carrier system and OFDM system.

3.1 Pilot Symbol Assisted Modulation (PSAM)

Pilot Symbol Assisted Modulation (PSAM), also known as Pilot Assisted Transmission (PAT), is a transmission scheme in which known pilot symbols are interleaved with data symbols periodically. Some advantages of PSAM include that it does not affect the transmitted pulse shape or peak-to-average power ratio, and has straightforward implementation. As the pilot symbols and their placement in the data stream are known by the receiver, the received pilot symbols can be exploited for purposes like synchronization, channel estimation, optimal decoding, etc.

PSAM technology can be applied to both single-carrier system and multi-carrier system like OFDM. The details will be given in the subsequent clauses.

3.2 PSAM in Single-Carrier System

The single-carrier system is a traditional system, in which the data modulate a single carrier. Cavers [12] did the first solid analytical work on PSAM in a single-carrier system over Rayleigh flat fading channel. His pioneering work is classic and has ever since been cited by many researchers.

PSAM transmission is formatted as M-symbol frames with one being the known pilot symbol and the remaining (M-1) being data symbols. The transmitted frame structure is shown in Figure 3-1.

P	D	…	D	P	D	…	D

← M symbols →← M symbols →

| P | : pilot symbol |

| D | : data symbol |
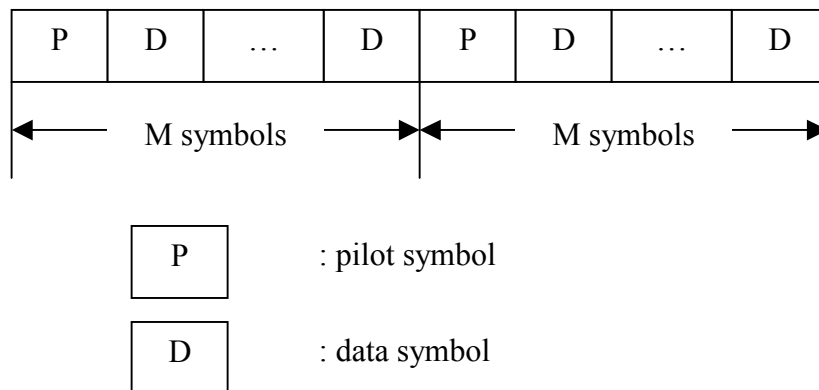
Figure 3-1   Transmitted frame structure of PSAM

Cavers has found that for PSAM in Rayleigh flat fading channel, the rate of pilot symbol insertion must be at least the Nyquist rate of the fading process, so that

$$M < \left(2 f_d T\right)^{-1} \tag{3.1}$$

Here T is the symbol duration, f_d is the relative Doppler shift between transmitter and receiver.

The receiver assumes that the channel statistic is known and uses Wiener filter to make an estimate of the channel gain at any data symbol based on K received pilots. The choice of K is a tradeoff between computational complexity and performance. It is found that K need not exceed 8 in general [12].

3.3 PSAM in OFDM System

3.3.1 OFDM System

Orthogonal Frequency Division Multiplexing (OFDM) is also known as discrete multi-tone modulation (DMT). It is a technique that allows the data stream to modulate a number of orthogonal carriers simultaneously and the modulated carriers are transmitted in parallel. With each subcarrier at the nulls of spectrum of other subcarriers, the OFDM system is much more spectral efficient than the conventional FDMA (Frequency Division Multiple Access) system. Also the inter carrier interference (ICI) can be eliminated. The OFDM system can be easily implemented with the Discrete Fourier Transform (DFT) and Inverse Discrete Fourier Transform (IDFT), which are the key signal processing modules in the transmitter and receiver. By selecting the DFT length N to be power of 2, IDFT and DFT can be implemented efficiently by IFFT and FFT for acceleration.

The baseband model of OFDM is shown in Figure 3-2.
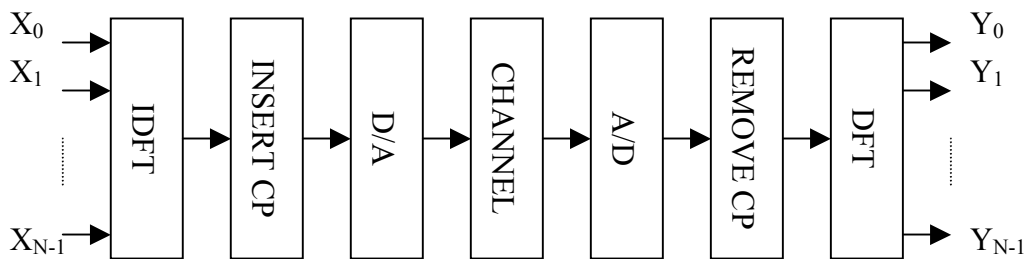
Figure 3-2 **Baseband model of an OFDM system**

In the transmitter, random bits are mapped to $\{X_k\}$ according to the chosen modulation scheme such as BPSK, QPSK (Quadrature Phase Shift Keying), etc. The IDFT transforms the symbols $\{X_k\}$ into OFDM symbol $\{x_n\}$. The Cyclic Period (CP) extends part of OFDM cyclically to eliminate the ICI and ISI. The D/A converts the digital signal to analog signal to be transmitted over the mobile channel.

In the receiver, the A/D converts the analog signal to discrete samples. The CP is discarded. DFT is performed on $\{y_n\}$ to obtain the demodulated symbols $\{Y_k\}$.

Denote N as the IDFT/DFT length, the IDFT/DFT is defined as

$$x_n = IDFT(X_k) = \sum_{k=0}^{N-1} X_k e^{j2\pi kn/N} \qquad n = 0,1,...,N-1$$

$$Y_k = DFT(y_n) = \frac{1}{N}\sum_{n=0}^{N-1} y_n e^{-j2\pi kn/N} \qquad k = 0,1,...,N-1$$

(3.2)

3.3.2 Block-type and Comb-type Pilots

There has been a lot of research on PSAM in OFDM system. There are basically two methods of inserting the pilots [28]. They are named block type and comb type, respectively. The two schemes are illustrated in Figure 3-3.

(a): Block-type pilots   (b): Comb-type pilots
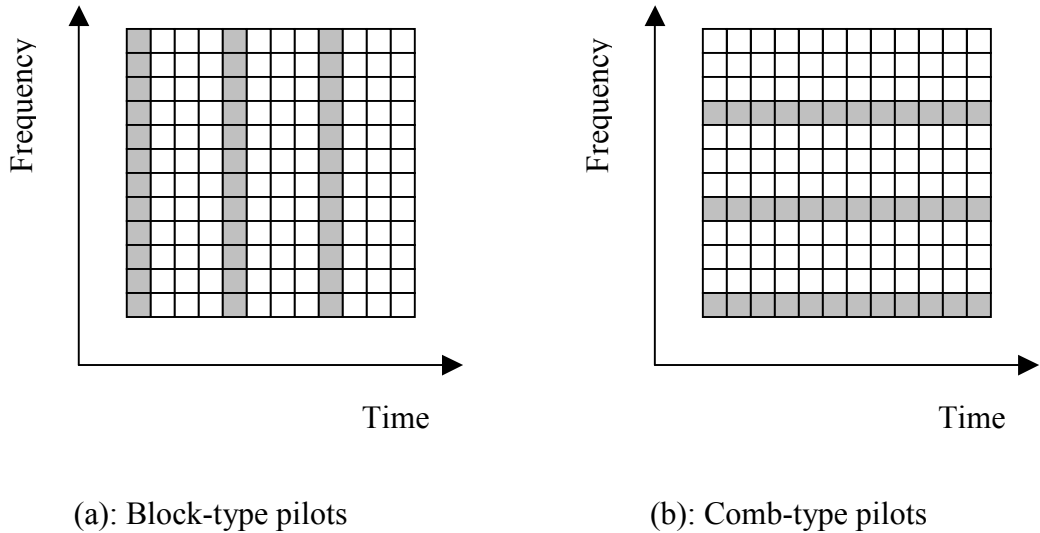
Figure 3-3   Two different types of pilot subcarrier arrangement

In the block-type pilot arrangement, the pilots are inserted at all subcarriers in one OFDM symbol, but absent in the subsequent (M-1) OFDM symbols. The receiver may

estimate the channel once and use the estimation directly or implement a decision-directed channel equalizer for successive (M-1) OFDM symbols.

In the comb-type pilot arrangement, the pilots are inserted at a number of equally spaced subcarriers in every OFDM symbol. The receiver may estimate the channel at the pilot subcarriers and interpolate them to obtain the channel estimation at data subcarriers.

Negi and Cioffi [29] suggested that the two schemes perform equally well for a time-invariant channel, but the comb-type scheme can better track a time-varying channel than the block-type scheme. In this thesis, we will focus on the comb-type pilot arrangement.

3.3.3 Optimal Pilot Placement in Comb-type Scheme

Pilots inserted in the OFDM symbol affects spectrum utilization, data throughput and the channel estimation accuracy. Decreasing the number of pilots will improve the spectral efficiency and data throughput, but may lead to insufficient channel estimation and degrade the system performance. On the other hand, increasing the number of pilots will ensure accurate channel estimation, but may decrease the spectral efficiency and data throughput too much. Hence, the optimal selection of pilots is an important issue. Too densely placed pilots or too sparsely placed pilots shall both be avoided.

There have been some findings in the literature. Negi and Cioffi [29] suggested that for accurate estimation, the number of pilots shall be no less than the maximum channel length. Moreover, equally spaced pilot tones are the best among other placement schemes when the channel is AWGN.

3.3.4 Channel Estimation and Interpolation

To obtain the channel estimate at data subcarriers, we can firstly estimate the channel at the pilot subcarriers based on LS or MMSE criteria, then interpolate the estimate to obtain channel at data subcarriers. A number of interpolation filters are proposed in the literature. Rinne and Renfors [30] proposed piecewise-constant and piecewise-linear interpolators. Hsieh et al. [28] proposed the piecewise second-order polynomial interpolation. Coleri et al. [31] compared different interpolation algorithms such as linear interpolation, second order interpolation, low-pass interpolation, spline cubic interpolation and time domain interpolation.

An alternative approach is to use the maximum likelihood estimator (MLE) and the Bayesian minimum mean square error estimator (MMSEE) , as proposed by Morelli et al. [9]. We will use the LMMSE estimator in this thesis.

CHAPTER 4   LDPC-CODED PILOT-ASSISTED SINGLE-CARRIER SYSTEM

This chapter will discuss the performance of LDPC code in pilot-assisted BPSK-modulated single-carrier communication system. The objective is to derive the LLR metric of each LDPC bit based on MMSE channel estimation. Simulation shows that the PSAM-LLR metric, which takes account of both the channel estimation and estimation mean square error has better performance than A-PSAM-LLR, which is a conventional LLR metric.

4.1   System Model

We consider a system shown in Figure 4-1
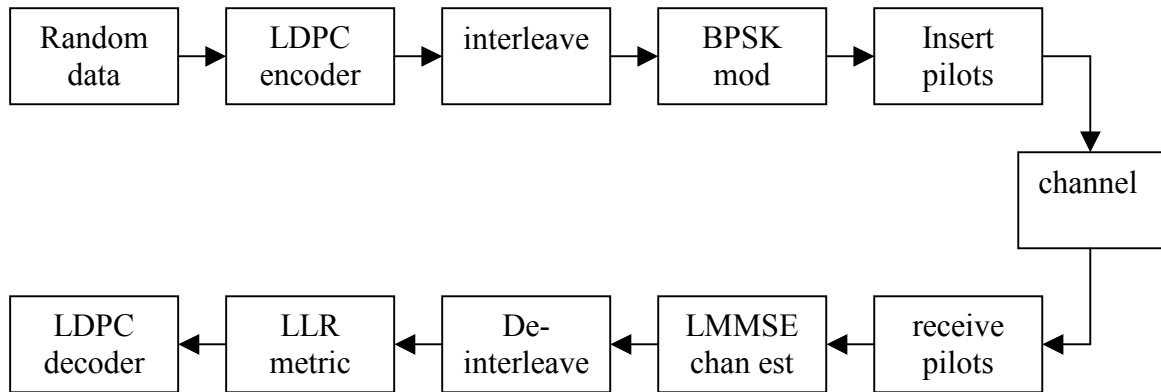
Figure 4-1   System model for LDPC-coded pilot-assisted single-carrier system over Rayleigh flat fading channel

In the transmitter, random bits are encoded into LDPC codewords. Interleaver permutes the coded bits to spread the burst of errors. After BPSK modulation, pilot symbols are inserted periodically. The frames with mixed pilot and data symbols are transmitted over the Rayleigh flat fading channel.

In the receiver, perfect timing synchronization is assumed. The pilot symbols are received and used for channel estimation. The deinterleaver restores the bit order. LLR metric for each bit is calculated based on the pilot-aided channel estimation. The LDPC decoder performs the decoding with the LLR metric. BER is calculated by comparing the transmitted and received bits.

Interleaver and deinterleaver is essential for fading channel which causes the burst errors. There are different types of interleaver, some are deterministic, some are random.   A classic deterministic interleaver is a block interleaver which consists of M x N array. The interleaver

takes in the bits by column and produces output bits by row. The deinterleaver is also a M x N array. The received bits enter the deinterleaver by rows and leave by columns. We will choose a deterministic block interleaver in the simulation.

Pilots are inserted periodically, as shown in Figure 4-2. We denote the pilot spacing as B. Pilot spacing is an important parameter as its selection is a tradeoff between performance and spectrum efficiency.

P	D_0	D_1	…	D_{B-1}	P	D_0	D_1	…	D_{B-1}

$\longleftarrow$ Pilot spacing B $\longrightarrow$ $\longleftarrow$ Pilot spacing B $\longrightarrow$
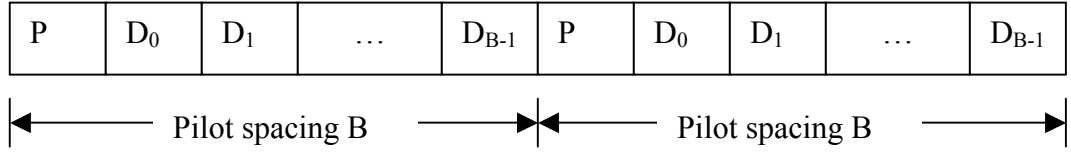
Figure 4-2   Pilot insertion with pilot spacing B

As mentioned in chapter 2.6, the Rayleigh flat fading channel model is

$$r(i) = c(i)s(i) + n(i) \tag{4.1}$$

Here $s(i)$ and $r(i)$ are transmitted and received symbol, respectively. $c(i)$ represents the multiplicative factor introduced by the fading channel. $c(i)$ and noise $n(i)$ are both modeled as independent complex Gaussian process. The autocorrelation of the channel gain is

$$R(i) = E\left[C(n)C(n-l)^*\right] = 2\sigma_c^2 J_0\left(2\pi f_d T_s i\right) \tag{4.2}$$

4.2   Receiver Algorithm

4.2.1   Channel Estimation

For data reception, the channel gain $c(i)$ that is unknown to the receiver need to be estimated based on the received pilots. The selection of estimator is important. In general, an estimator can estimate an unknown parameter θ from an observed vector $\mathbf{X}$. A general estimator is given by

$$\hat{\theta} = g(\mathbf{X}) \tag{4.3}$$

There are different estimators depending on the selection of function g(.) and whether the parameter θ is viewed as a deterministic or random variable. When we choose g(.) to be linear function and treat the parameter θ as a random variable, we have Linear Minimum Mean Square Error (LMMSE) Estimator which is a linear estimator that minimizes the mean

square error (MSE). LMMSE estimator is equivalent to Wiener filter. The LMMSE estimator is given by

$$\hat{\theta} = \left(\mathbf{R}^{-1}\mathbf{P}\right)^H \mathbf{X} \tag{4.4}$$

Here $\mathbf{R} = \mathrm{E}\left[\mathbf{X}\mathbf{X}^H\right]$ is a $\mathrm{N} \times \mathrm{N}$ autocorrelation matrix, $\mathbf{P} = \mathrm{E}\left[\theta^*\mathbf{X}\right]$ is a $\mathrm{N} \times 1$ cross-correlation vector.

The minimum mean square error is

$$\xi_{\min} = \mathrm{E}\left[|\theta|^2\right] - \mathbf{P}^H \mathbf{R}^{-1} \mathbf{P} \tag{4.5}$$

We will select LMMSE estimator to solve the channel estimation problem. The estimator input/output is illustrated in Figure 4-3. The input to the estimator is a series of received pilot symbols $r(i)$, while the output is the estimate of Rayleigh flat fading channel gain $c(j)$ based on MMSE criterion.

$\{r(i), i = Bm; m = 0,1,...\}$ → [LMMSE estimator] → $\{\hat{c}(j), j = Bm + k, m = 0,1,...; k = 1,..., B - 1\}$
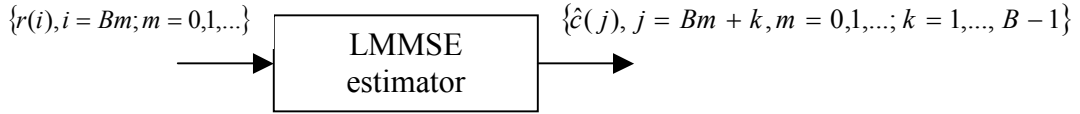
Figure 4-3   LMMSE estimator for channel estimation

For estimation of the channel gain $c(j)$, we may choose the input vector $\mathbf{X}$ to be a $(2W \times 1)$ vector, which comprises $2W$ pilot symbols closest to the data symbols in the time. Considering the symmetry property of the channel statistics, we choose W pilot symbols received before and after the time index j, as illustrated in Figure 4-4.

$$c(j)$$
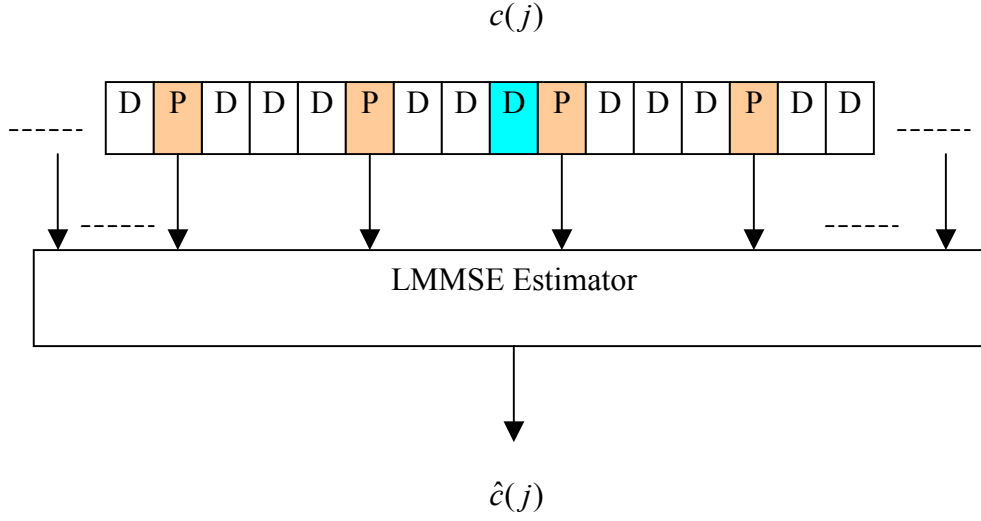
Figure 4-4   Input and output of the LMMSE estimator

Specifically, if we denote $j = Bm + k$, the input vector $\mathbf{X}$ is given by

$$\mathbf{X} = \begin{bmatrix} \mathbf{X}(\mathbf{0}) \\ \mathbf{X}(1) \\ ... \\ \mathbf{X}(2W-1) \end{bmatrix} = \begin{bmatrix} r(B(m-W+1)) \\ r(B(m-W+2)) \\ ... \\ r(B(m+W)) \end{bmatrix} \tag{4.6}$$

Hence, the ith element of vector $\mathbf{X}$ can be expressed as

$$\mathbf{X}(i) = r(B(m-W+1+i)), i = 0,1,...,2W-1 \tag{4.7}$$

The autocorrelation matrix $\mathbf{R} = E[\mathbf{X}\mathbf{X}^H]$ and $\mathbf{P} = E[c(j)^* \mathbf{X}]$ shall be calculated. The details are explained in the following.

The element $\mathbf{R}(j_1, j_2)$ is defined as

$$\begin{aligned} \mathbf{R}(j_1, j_2) &= E[\mathbf{X}(j_1)\mathbf{X}^*(j_2)] \\ &= E[r(B(m-W+1+j_1)) \cdot r^*(B(m-W+1+j_2))] \\ &= E[r(i_1) \cdot r^*(i_2)] \end{aligned} \tag{4.8}$$

Here $i_1 = B(m-W+1+j_1)$ and $i_2 = B(m-W+1+j_2)$

Considering the channel statistic property, we have

$$\begin{aligned} E[r(i_1) \cdot r^*(i_2)] &= E[(s(i_1)c(i_1) + n(i_1)) \cdot (s(i_2)c(i_2) + n(i_2))^*] \\ &= E_s 2\sigma_c^2 J_0(2\pi f_d T_s(i_1 - i_2)) + 2\sigma^2 \delta(i_1 - i_2) \end{aligned} \tag{4.9}$$

Here E_s is the average symbol energy. $\delta(.)$ is Dirac delta function.

Hence,

$$\mathbf{R}(j_1, j_2) = E_s 2\sigma_c^2 J_0(2\pi f_d T_s B(j_1 - j_2)) + 2\sigma^2 \delta(B(j_1 - j_2)) \quad (4.10)$$

The element $\mathbf{P}(i)$ is

$$
\begin{aligned}
\mathbf{P}(i) &= \mathrm{E}[c(j)^* \mathbf{X}(i)] \\
&= \mathrm{E}[c(Bm + k)^* r(B(m - W + 1 + i))] \\
&= \sqrt{E_s} \, 2\sigma_c^2 J_0[2\pi f_d T_s(B(-W + 1 + i) - k)]
\end{aligned}
\quad (4.11)
$$

Hence, the LMMSE estimation of $c(j)$ is

$$\hat{c}(j) = (\mathbf{R}^{-1}\mathbf{P})^H \mathbf{X} \quad (4.12)$$

And the minimum mean square error is

$$\xi_{\min} = 2\sigma_c^2 - \mathbf{P}^H \mathbf{R}^{-1} \mathbf{P} \quad (4.13)$$

4.2.2 LLR Metric

As discussed in chapter 2.6, if the receiver has prior knowledge of the channel gain $c(i)$ of the Rayleigh flat fading channel, the LLR metric for the BPSK-modulated bit is given by

$$
\begin{aligned}
\lambda(i) &= \ln \frac{P(r(i)|c(i), s(i) = \sqrt{E_s})}{P(r(i)|c(i), s(i) = -\sqrt{E_s})} \\
&= \frac{4\sqrt{E_s}}{N_0} \mathrm{Re}[r(i)c(i)^*]
\end{aligned}
\quad (4.14)
$$

However, $c(i)$ is unknown to the receiver in most situations and can only be estimated with pilots. In that case, what is the LLR metric that leads to optimal BER performance? Two LLR metrics can be found in the literature. The first LLR metric is widely used and is derived by replacing $c(i)$ with $\hat{c}(i)$:

$$\lambda(i) = \frac{4\sqrt{E_s}}{N_0} \mathrm{Re}[r(i)\hat{c}(i)^*] \quad (4.15)$$

The second LLR metric was recently proposed by Haifeng et al. [1]. It takes into account not only the estimated channel gain $\hat{c}(i)$, but also the minimum mean square error $\xi_{\min}$

$$\lambda(i) = \frac{1}{\dfrac{E_s}{N_0}\xi_{min}(i)+1}\left\{\frac{4\sqrt{E_s}}{N_0}\,\mathrm{Re}\!\left[r(i)\hat{c}(i)^*\right]\right\} \qquad (4.16)$$

The second LLR metric is literally the first LLR metric multiplied with a scaling factor which accounts for the channel estimation error ξ_{min}. When the estimator error is very small, i.e. $\xi_{min} \to 0$, the second LLR metric will be approximated to the first LLR metric. In [1], the second LLR metric is termed PSAM-LLR (Pilot Symbol Assisted Modulation Log Likelihood Ratio), whereas the first LLR metric is termed A-PSAM-LLR (Approximate Pilot Symbol Assisted Modulation Log Likelihood Ratio). It is suggested that PSAM-LLR outperforms the A-PSAM-LLR. In the computer simulation, we will compare the BER performance with these two LLR metrics.

4.3   Simulation

Monte Carlo simulation is conducted to obtain the BER for the pilot-aided LDPC-coded single-carrier system. The computer simulation system in Figure 4-1 is implemented in the C/C++ program which can call MATLAB built-in functions through the MATLAB engine. Hence, the efficiency of C/C++ code and the strong capability of MATLAB in handling matrix are combined to accelerate the code development cycle without compromise in the simulation speed. The MALTAB built-in functions called from C/C++ program mainly include:

1)   Besselj() - generate Bessel function.

2)   Inv() - calculate the inverse of a square matrix.

With the program, we can study the impact of system parameters such as pilot spacing, estimator size, LLR metrics, etc, on the BER performance. Results obtained from the program developed here agree with the results presented in [1]. As the focus of the thesis is not repeating the existing research in the pilot-aided single-carrier communication, but exploring the pilot-aided OFDM system by applying similar methodology, we will only give the result for a specific scenario, with the purpose to show the performance difference between A-PSAM-LLR and PSAM-LLR.

The system parameters are summarized in Table 4-1.

Table 4-1   System parameters in LDPC-coded pilot-assisted single-carrier communication system

Parameters	Value
Modulation scheme	BPSK
LDPC code	LDPC (504, 1008) PEGirReg504x1008
LDPC decoding algorithm	Log-domain decoder with maximum iteration 50
Channel model	The Rayleigh flat fading channel is generated using the simulator in [4][5]. Normalized fade rate: $f_d T_s = 0.02$
Interleaver	A block interleaver with size 10080 is implemented. It is a 80×126 array.
Pilot spacing	B=11. Cavers [12] suggests that the pilot spacing shall meet the requirement $B < \dfrac{1}{2f_d T_s}$. When fade rate is 0.02, $B < 25$. Hence, it is reasonable to choose $B = 11$.
LMMSE estimator size	Estimator size: $2W = 20$. Cavers [12] studies the effect of estimator size and suggests that input size can be as small as 5 without causing significant performance degradation. Further increase of input vector size brings only slight improvement.
LLR metrics	A-PSAM-LLR and PSAM-LLR
Eb/No (dB)	2-9

The BER performance is evaluated at different Eb/No. Denote the energy per BPSK symbol as E_s, and LDPC code rate as R, the relationship between E_s and E_b is

$$E_s = \frac{(B-1)R}{B} E_b \qquad (4.17)$$

Hence, the relationship between SNR and $E_b N_0$ is:

$$SNR = E_b / N_0 + \ln \frac{(B-1)R}{B} \qquad (4.18)$$

The BER versus Eb/No with A-PSAM-LLR and PSAM-LLR is shown in Table 4-2.

Table 4-2   **BER for LDPC-coded pilot-assisted single-carrier system over Rayleigh flat fading channel with different LLR metrics**

Eb/No (dB)	BER	
	A-PSAM-LLR metric	PSAM-LLR metric
2	2.45E-01	2.45E-01
3	2.12E-01	2.12E-01
4	1.83E-01	1.80E-01
5	1.27E-01	1.21E-01
6	4.55E-02	3.24E-02
7	6.66E-03	3.31E-03
8	3.21E-04	5.93E-05
9	3.37E-06	5.14E-07

The BER result is plotted in Figure 4-5. It can be seen that PSAM-LLR outperforms A-PSAM-LLR by 0.4dB gain at BER = 10-4.
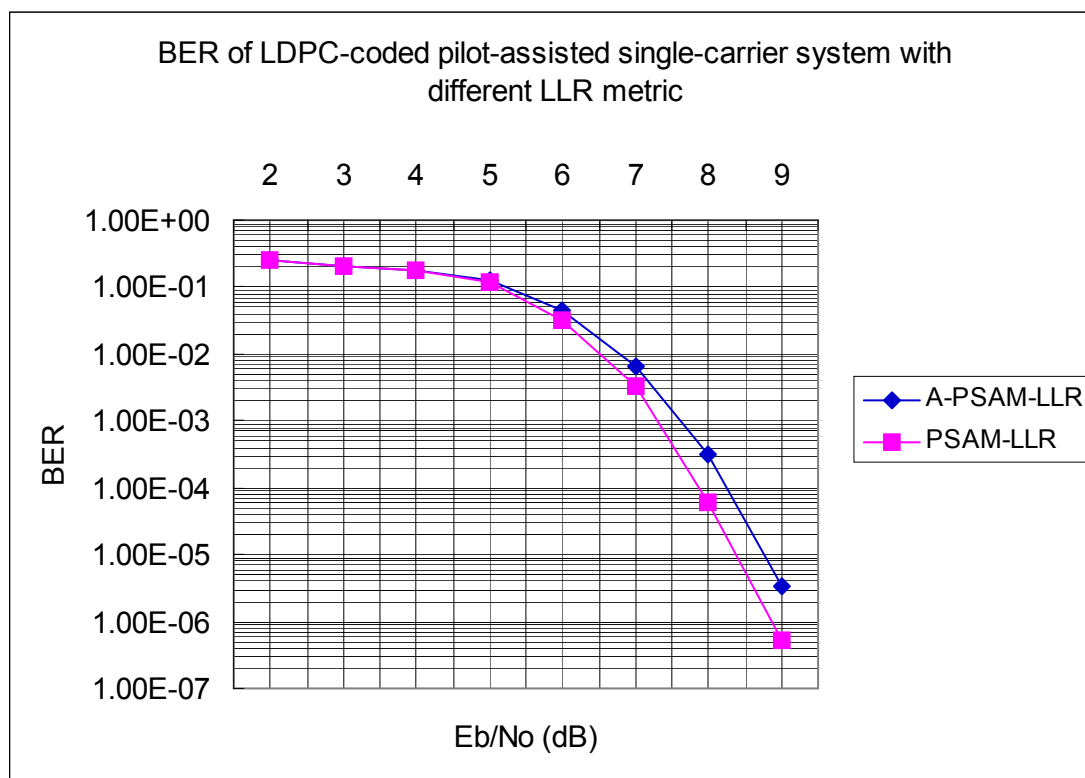
Figure 4-5   **Effect of LLR metric in LDPC-coded pilot-assisted single-carrier system**

4.4   Conclusions

In this Chapter, we study the pilot-aided transmission over Rayleigh flat fading channel. The modulation is BPSK and the coding scheme is LDPC. In the transmitter, pilots are periodically inserted in the data stream. In the receiver, the fading channel is unknown and need to be estimated by the received pilots using the LMMSE estimator. The estimator yields two results: the estimated channel gain and the minimum mean square error. Based on the LMMSE estimator output, two different LLR metrics are derived. The first metric A-PSAM-LLR only uses the estimated channel, while the second metric PSAM-LLR uses both the estimated channel and the minimum mean square error.

Monte Carlo simulation is employed to obtain the BER performance for LDPC decoder using different LLR metrics. Simulation shows that PSAM-LLR has better BER than A-PSAM-LLR by about 0.4dB at high SNR. The simulation result is in agreement with the literature [1]. Hence, PSAM-LLR is a more accurate LLR for the considered single-carrier system. The potential of the PSAM-LLR in OFDM system will be explored in the next chapter.

CHAPTER 5   LDPC-CODED PILOT-ASSISTED OFDM SYSTEM

This chapter will discuss the performance of LDPC code in pilot-assisted OFDM communication system. The aim is to investigate how to derive the LLR metric of each LDPC bit with the channel estimation based on MMSE criteria. The performance with two different LLR metrics is compared and the optimal pilot spacing is studied.

5.1   A Simplified OFDM System Model

A simplified OFDM system model is shown in Figure 5-1. The system consists of several functional blocks: the IFFT and CP insertion in the transmitter, the channel, the FFT and CP removal in the receiver. The Channel Impulse Response (CIR) is represented by the $\{h_k\}$, and Gaussian noise is represented by $\{w(m)\}$.
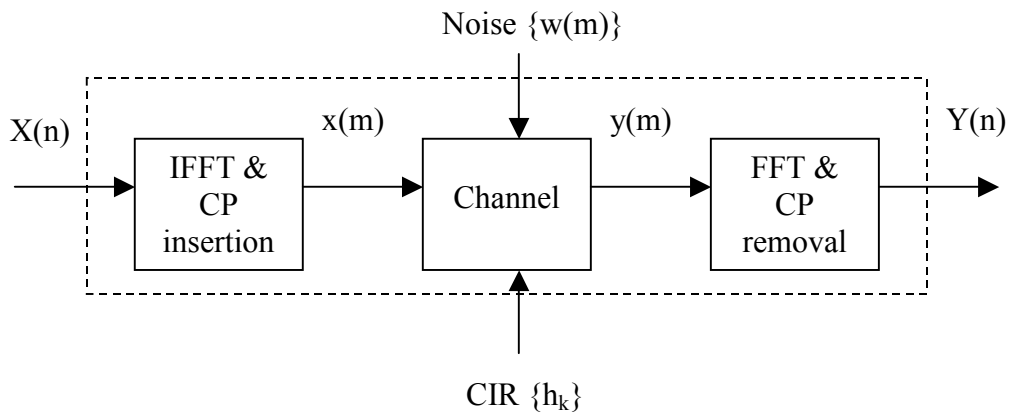
Figure 5-1   Simplified OFDM system model

5.1.1 Multipath Fading Channel

In a mobile communication, due to the scattering, reflection and diffusion caused by the mountain and building, etc, the radio wave may propagate along different paths and arrive with different signal strengths and angles. Such phenomenon is known as multipath fading. The multipath fading channel can be modeled as a linear finite impulse response (FIR) filter with L taps [7].

$$g(t) = \sum_{k=0}^{L-1} h_k \delta(t - \tau_k) \tag{5.1}$$

Here τ_k is the delay spread of the kth path. $\{h_k\}$ represents the path strength.

There are two typical power delay profiles. One is rectangular power delay profile, in which the $\{h_k\}$ are modeled as independent and identically distributed zero-mean complex Gaussian random variables.

$$\sigma_k^2 = E\left[|h_k|^2\right] = 1, k = 0,1,...,L-1 \tag{5.2}$$

Another is exponentially decaying power delay profile, in which the $\{h_k\}$ are zero-mean independent complex Gaussian random variables with its amplitude having Rayleigh distribution with an exponential power delay.

$$\sigma_k^2 = E\left[|h_k|^2\right] = Ce^{\frac{-\tau_k}{\tau_{rms}}} \tag{5.3}$$

Here τ_{rms} is the root mean squared (rms) delay spread.

The path delay $\{\tau_k\}$ is uniformly and independently distributed over the length of the CP. In general, τ_k can be assumed to be multiple integers of the sampling interval. Under such assumption, the channel is modeled as a sample-spaced L-tap FIR filter ([7], [9]).

$$g(t) = \sum_{k=0}^{L-1} h_k \delta(t - kT_s) \tag{5.4}$$

Here T_s is the sampling interval in receiver. We will use this channel model throughout the study.

5.1.2 System Function

The system function, also known as transfer function, describes the relationship between the input and output of a system. System function is essential to the understanding of the system behavior. In the following, the system function of the OFDM system in Figure 5-1 will be derived.

Based on the FFT/IFFT definition and sample-spaced multipath channel model, we have

$$x(m) = \frac{1}{N} \sum_{n=0}^{N-1} X(n)e^{j2\pi mn/N} \qquad m = 0,1,...,N-1 \tag{5.5}$$

$$y(m) = \sum_{k=0}^{L-1} h_k x(m-k) + w(m) \quad m = 0,1,...,N+N_g-1 \tag{5.6}$$

$$Y(n) = \sum_{m=0}^{N-1} y(m)e^{-j2\pi mn/N} \qquad n = 0,1,...,N-1 \tag{5.7}$$

Here N_g is the number of samples in the cyclic prefix, or guard interval. $w(m)$ is a set of statistically independent zero-mean complex Gaussian noise with variance $2\sigma^2$.

Based on the above equations, the transfer function of the OFDM system is given by ([54])

$$Y(n) = X(n)H(n) + W(n) \qquad n = 0,1,...,N-1 \qquad (5.8)$$

Here

$$H(n) = \sum_{k=0}^{L-1} h_k e^{-j2\pi nk/N}$$

$$W(n) = \sum_{m=0}^{N-1} w(m) e^{-j2\pi nm/N} \qquad (5.9)$$

As $w(m)$ is statistically independent zero-mean complex Gaussian noise with variance $2\sigma^2$, it is shown [53] that $W(n)$ is independent and identically distributed zero-mean complex Gaussian random variable with variance $N(2\sigma^2)$.

As $\{h_k\}$ is a set of statistically independent complex Gaussian noise with zero mean and variance σ_k^2, $\{H(n)\}$ is a set of correlated zero-mean complex Gaussian random variable based on the Equation (5.9). The variance of $H(n)$ is

$$Var[H(n)] = E[H(n)H(n)^*] = \sum_{k=0}^{L-1} E[h_k h_k^*] = \sum_{k=0}^{L-1} \sigma_k^2 \qquad (5.10)$$

$W(n)$ and $H(n)$ are independent due to the fact that $W(n)$ is linear function of $w(m)$, $H(n)$ is linear function of h_k, $w(m)$ and h_k are independent Gaussian random variables.

5.1.3 Comparison to the System Function of Single-Carrier System

According to Equation (2.22), the system function for single-carrier system over Rayleigh flat fading channel is

$$r(i) = s(i)c(i) + n(i) \qquad i = 0,1,... \qquad (5.11)$$

According to Equation (5.8), the system function for OFDM system over multipath fading channel is

$$Y(n) = X(n)H(n) + W(n) \qquad n = 0,1,...,N-1 \qquad (5.12)$$

The fundamental difference for these two systems is that the input/output signals are in time domain for single-carrier system and in frequency domain for OFDM system. However, despite the difference, the system functions for the two systems have similar mathematical formula. Here is a comparison between the two system functions.

Table 5-1   **Comparison between the system function of single-carrier system over Rayleigh flat fading channel and OFDM system over multipath fading channel**

Parameter	Single-carrier system over Rayleigh flat fading channel	OFDM system over multipath fading channel
Transmitted signal	$s(i)$, in time domain, i=0,1,…	$X(n)$, in frequency domain, n=0,1,…,N-1
Received signal	$r(i)$, in time domain, i=0,1,…	$Y(n)$, in frequency domain, n=0,1,…,N-1
Channel gain	$c(i)$, modeled as a correlated, zero-mean, complex Gaussian process with its real and imaginary part being independent and identically distributed Gaussian noise.	$H(n)$, modeled as a set of correlated, zero-mean complex Gaussian random variables
Noise	$n(i)$, is a set of statistically independent complex Gaussian noise with zero mean and variance $2\sigma^2$. $n(i)$ is independent from channel gain $c(i)$.	$W(n)$, is a set of statistically independent complex Gaussian noise with zero mean and variance $N(2\sigma^2)$. $W(n)$ is independent from channel gain $H(n)$.

5.2   LDPC-coded Pilot-assisted OFDM System

We consider a LDPC-coded pilot-assisted OFDM baseband system, as shown in Figure 5-2.
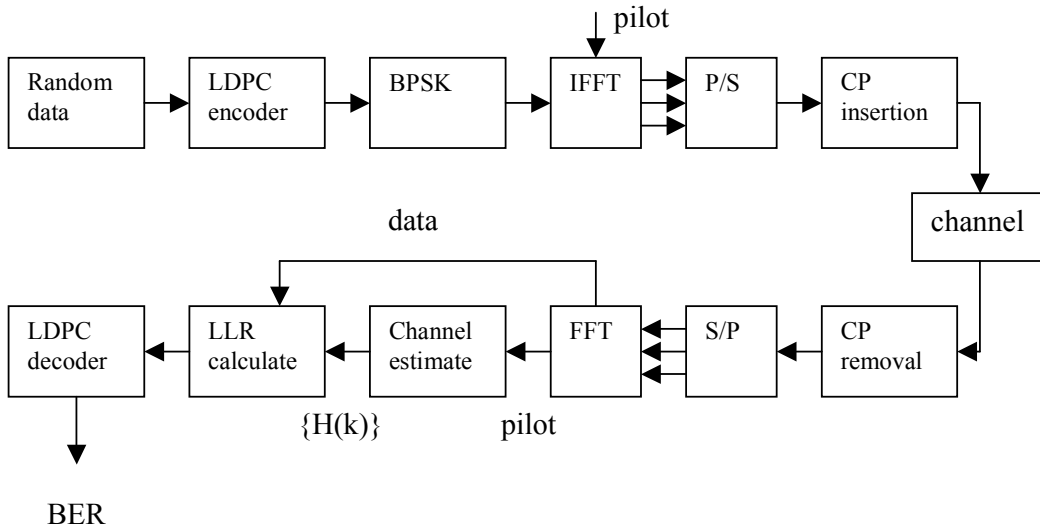
Figure 5-2   **LDPC-coded pilot-assisted OFDM baseband system over multipath channel**

In the transmitter, random bits are encoded by LDPC encoder and the coded bits are BPSK modulated. The resultant data symbols and known pilot symbols are used to modulate different subcarriers in the IFFT block. Here the pilot insertion scheme is comb-type. After the parallel-to-serial (P/S) conversion and insertion of CP, the OFDM signal is transmitted over the multipath fading channel with additive noise.

In the receiver, with perfect symbol synchronization, the signal is sampled and CP is removed. After the serial-to-parallel (S/P), FFT is performed for OFDM demodulation. The received pilot symbols are used in the channel estimation. The received data symbols and the channel estimates {H(k)} are used in generating a proper LLR metric. Finally, LDPC decoder decodes the bits and BER is calculated.

5.3   LMMSE Estimator for Channel Estimation

The purpose of LMMSE estimator is to estimate the channel gain $H(n)$ with the received pilots. Without loss of generality, assume there are N_p pilots per OFDM symbol, with their locations at $\{i_n; 0 \leq n \leq N_p - 1\}$. Hence, the received pilot vector is defined as

$$P = \begin{bmatrix} Y(i_0) & Y(i_1) & ... & Y(i_{N_p-1}) \end{bmatrix}^T \tag{5.13}$$

Let $H = \{H(n); 0 \leq n \leq N - 1\}$ be the column vector containing the channel frequency response at each subcarrier, and let $h = \{h_k; 0 \leq k \leq L - 1\}$ be the column vector that contains the channel impulse response. It is shown [9] that H can be expressed as $H = Gh$, here G is a $N \times L$ matrix with entries

$$[G]_{n,k} = e^{-j2\pi nk/N}, 0 \leq n \leq N - 1, 0 \leq k \leq L - 1 \tag{5.14}$$

To estimate the channel gain $\{H(n)\}$, there are two methods:

1)   Estimate the channel tap $\{h_k\}$, and then obtain the estimated $\{H(n)\}$ through $\hat{H} = G\hat{h}$.

2)   Estimate the channel frequency response $\{H(n)\}$ directly

The two methods will achieve the same result when using LMMSE estimator. Here we use the method (1).

5.3.1   LMMSE Estimation of h and H

The LMMSE estimator for h is expressed as

$$\hat{h} = FP \tag{5.15}$$

Here $\hat{h}$ is a $L \times 1$ vector, P is a $N_p \times 1$ vector and F is a $L \times N_p$ matrix. Applying the orthogonality principle, we have

$$E\left[(h - \hat{h})P^H\right] = 0 \qquad (5.16)$$

Substituting Equation (5.15) into Equation (5.16) gives

$$E\left[hP^H\right] = F \cdot E\left[PP^H\right] \qquad (5.17)$$

Hence

$$F = E\left[hP^H\right] \cdot \left(E\left[PP^H\right]\right)^{-1} \qquad (5.18)$$

$$\hat{H} = GFP \qquad (5.19)$$

In order to calculate the two expectations $E\left[hP^H\right]$ and $E\left[PP^H\right]$, we express the P as follows [9]

$$P = ABh + w \qquad (5.20)$$

Here A is a $N_p \times N_p$ diagonal matrix: $A = diag\{a_0, \ldots, a_{N_p-1}\}$, the elements in the main diagonal are the transmitted pilot symbols. B is a $N_p \times L$ matrix with entries $[B]_{n,k} = e^{-j2\pi k i_n / N}$, $0 \le n \le N_p - 1, 0 \le k \le L - 1$. w is the Gaussian noise. w and h are uncorrelated.

Hence,

$$E\left[hP^H\right] = E\left[h(ABh + w)^H\right] = R_{hh} B^H A^H \qquad (5.21)$$

$$E\left[PP^H\right] = E\left[(ABh + w)(ABh + w)^H\right] = ABR_{hh} B^H A^H + R_{ww}, \qquad (5.22)$$

Here $R_{hh} = E\left[hh^H\right], R_{ww} = E\left[ww^H\right]$.

Substituting Equation (5.21) and (5.22) into Equation (5.18), and subsequently Equation (5.15) and (5.19) gives the estimation as

$$\hat{h} = \left(R_{hh} B^H A^H\right)\left(ABR_{hh} B^H A^H + R_{ww}\right)^{-1} P \qquad (5.23)$$

$$\hat{H} = G\left(R_{hh} B^H A^H\right)\left(ABR_{hh} B^H A^H + R_{ww}\right)^{-1} P \qquad (5.24)$$

If pilot symbols are taken from a Phase Shift Keying (PSK) constellation, i.e., $|a_n| = 1$, the Equation (5.23) and (5.24) are equivalent to the following equations given in [9]

$$\hat{h} = \left(R_{ww} R_{hh}^{-1} + B^H B\right)^{-1} B^H A^H P \qquad (5.25)$$

$$\hat{H} = G\left(R_{ww}R_{hh}^{-1} + B^{H}B\right)^{-1}B^{H}A^{H}P \qquad (5.26)$$

In Equation (5.26), matrix A, B and G are all constant matrices. With the knowledge of the statistic property of noise and channel, the term $G\left(R_{ww}R_{hh}^{-1} + B^{H}B\right)^{-1}B^{H}A^{H}$ is constant matrix. It can be pre-computed and stored in memory for later use. For estimation at all subcarriers, a two-dimensional array N x Np is needed to store the matrix. For estimation at data subcarriers only, a two-dimensional array Nd x Np is needed to store the matrix. The channel estimation is achieved by simply multiplying the pre-computed matrix with the received pilot vector. The computation is straightforward.

5.3.2 The Mean Square Estimation Error of H

As the LMMSE estimation of the frequency channel response at the kth subcarrier is $\hat{H}(k)$, the mean square error for the channel estimation at the kth subcarrier is

$$\xi_{\min}(k) = E\left[\left|H(k) - \hat{H}(k)\right|^{2}\right] \qquad (5.27)$$

Here

$$\hat{H}(k) = G(k,:)\hat{h} \qquad (5.28)$$

$$H(k) = G(k,:)h \qquad (5.29)$$

$G(k,:)$ is a $1 \times L$ vector representing the kth row of the matrix G.

Substituting Equation (5.28) into Equation (5.27) gives

$$\xi_{\min}(k) = E\left[\left(H(k) - \hat{H}(k)\right)\left(H(k) - G(k,:)FP\right)^{H}\right] \qquad (5.30)$$

By applying the orthogonality principle, we have

$$E\left[\left(H - \hat{H}\right)P^{H}\right] = 0 \qquad (5.31)$$

Substituting Equation (5.31) into (5.30) yields

$$\xi_{\min}(k) = E\left[\left(H(k) - \hat{H}(k)\right)\left(H(k)\right)^{H}\right] = \left[\sum_{k=0}^{L-1}\sigma_{k}^{2}\right] - E\left[\hat{H}(k)\left(H(k)\right)^{H}\right] \quad (5.32)$$

Substituting Equation (5.28) and (5.29) into the second term in Equation (5.32), we have

$$
\begin{aligned}
E\left[\hat{H}(k)(H(k))^H\right] &= E\left[G(k,:)\hat{h}(G(k,:)h)^H\right] \\
&= G(k,:)E\left[\hat{h}h^H\right]G(k,:)^H \\
&= G(k,:)E\left[\left(R_{hh}B^H A^H\right)\left(ABR_{hh}B^H A^H + R_{ww}\right)^{-1}Ph^H\right]G(k,:)^H \\
&= G(k,:)E\left[\left(R_{hh}B^H A^H\right)\left(ABR_{hh}B^H A^H + R_{ww}\right)^{-1}(ABh + w)h^H\right]G(k,:)^H \\
&= G(k,:)\left(R_{hh}B^H A^H\right)\left(ABR_{hh}B^H A^H + R_{ww}\right)^{-1}\left(ABR_{hh}\right)G(k,:)^H
\end{aligned}
$$

(5.33)

Substituting Equation (5.33) into Equation (5.32) gives the mean square error for the channel estimation at the kth subcarrier as

$$
\xi_{\min}(k) = \left[\sum_{k=0}^{L-1}\sigma_k^2\right] - G(k,:)\left(R_{hh}B^H A^H\right)\left(ABR_{hh}B^H A^H + R_{ww}\right)^{-1}\left(ABR_{hh}\right)G(k,:)^H
$$

(5.34)

If pilot symbols are taken from a PSK constellation, i.e., $|a_n| = 1$, the Equation (5.34) is equivalent to the following equation given in [9]

$$
\xi_{\min}(k) = R_{ww}\sum_{n=0}^{L-1}\sum_{m=0}^{L-1}\left[V^{-1}\right]_{n,m}e^{j2\pi k(m-n)/N} = R_{ww}G(k,:)V^{-1}G(k,:)^H
$$

(5.35)

Here $V = R_{ww}R_{hh}^{-1} + B^H B$

The MSE given by Equation (5.35) is a constant vector provided that receiver has the knowledge of the statistic property of the noise and the channel. Hence, MSE at each subcarrier can be pre-computed and saved in a N x 1 array for later use. It will be shown in section 5.5 that with proper choice of pilot locations, MSE will be identical for all subcarriers. In that case, only one MSE value need to be computed and stored. With such optimal pilot location arrangement, the computational and storage requirement can be dramatically reduced.

5.4   LLR Metric

In this subchapter, we are interested in deriving the LLR metric for the nth bit given the received symbol Y(n) and the LMMSE channel estimation $\hat{H}(n)$. The LLR metric derivation shall be dependent on the system function of the OFDM system which is

$$
Y(n) = X(n)H(n) + W(n) \qquad n = 0,1,...,N-1
$$

(5.36)

Here $W(n)$ is the noise at the nth subcarrier. Assume the complex Gaussian noise added to the time domain OFDM signal has noise variance $2\sigma^2$, then for a N-point OFDM system, the noise at each subcarrier shall have noise variance $N(2\sigma^2)$ [53]. Specifically, if we denote $W(n) = W_r(n) + jW_i(n)$, then the real and complex part of $W(n)$ is independent

and identically distributed zero mean Gaussian noise, with $W_r(n) \sim N(0, N\sigma^2)$, $W_i(n) \sim N(0, N\sigma^2)$.

When the channel is perfectly known at the receiver, the ideal LLR metric is defined as:

$$\lambda(n)_{ideal} = \frac{4\sqrt{E_s}}{N_0} \text{Re}\left[Y(n)H(n)^*\right] \tag{5.37}$$

It has been shown in CHAPTER 4 that for LDPC-coded pilot-assisted BPSK-modulated single-carrier system over Rayleigh flat fading channel, two LLR metrics can be defined, as indicated in Equation (4.15) and (4.16). Considering the fact that the single-carrier system and OFDM system has a similar system function, indicated in Table 5-1, we can define two LLR metrics for OFDM system. Adopting the same notation used in [1], we name the first metric as A-PSAM-LLR and the second metric as PSAM-LLR.

The A-PSAM-LLR metric is defined as

$$\lambda(n)_{A-PSAM-LLR} = \frac{4\sqrt{E_s}}{N_0} \text{Re}\left[Y(n)\hat{H}(n)^*\right] \tag{5.38}$$

The PSAM-LLR metric is defined as

$$\lambda(n)_{PSAM-LLR} = \frac{1}{\frac{E_s}{N_0}\xi_{min}(n)+1} \left\{ \frac{4\sqrt{E_s}}{N_0} \text{Re}\left[Y(n)\hat{H}(n)^*\right] \right\} \tag{5.39}$$

Here $N_0 = N(2\sigma^2)$ in both Equations.

While the A-PSAM-LLR metric considers only the channel estimation $\hat{H}(n)$, the PSAM-LLR metric takes into account both the estimated channel gain $\hat{H}(n)$ and the minimum mean square error $\xi_{min}(n)$. In the computer simulation section, we will compare the performance of these two LLR metrics in different scenarios.

The MSE given by Equation (5.35) is a constant provided that the statistic property of the noise and the channel is known to the receiver. Hence, the scaling factor $\dfrac{1}{\frac{E_s}{N_0}\xi_{min}(n)+1}$ can be pre-computed and stored in an N x 1 array. Compared with the derivation of A-PSAM-LLR, the derivation of PSAM-LLR requires one extra multiplication with the scaling factor. It will be shown in section 5.7 that such slightly increased computational complexity is much

worthwhile as PSAM-LLR has a better performance than A-PSAM-LLR and requires less iteration to converge.

5.5   Optimal Pilot Arrangement

In the literature, there have been much research done on the optimal pilot placement and similar conclusions are reached by a number of researchers.   Negi and Cioffi [29] show that for accurate channel estimation, the number of pilots shall be no less than the maximum channel length. In addition, the equally spaced pilot tones are the best among other sets when the noise is AWGN. And more mathematically satisfying results are obtained when N/N_p is an integer. Specifically, assume that N_p pilots are inserted in one OFDM symbol which comprises totally N subcarriers and N is a multiple of N_p, it is found that the pilot sets

$$\left\{i, i + \frac{N}{N_p}, ..., i + \frac{N(N_p - 1)}{N_p}\right\}, i = 0, 1, ..., \frac{N}{N_p} - 1$$ are the optimal in the sense of MMSE.

Shuichi et al [33] study the OFDM system over frequency selective fading channel and show that the equispaced and equipowered pilot symbols are optimal in terms of minimizing the mean square channel estimation error.

We consider an OFDM system with parameters listed in Table 5-2. We will experiment with different pilot placement schemes and plot the minimum mean square error of the LMMSE channel estimation as Equation (5.35). By showing the MMSE results under different pilot insertion schemes, we hope to discover more about the pilot insertion strategy.

Table 5-2   Parameters of an OFDM system over multipath fading channel for pilot insertion study

Parameters	Value
DFT size N	64
Cyclic prefix	16 samples
Channel length L	Equivalent to 8 sample duration
Channel power delay profile	Rectangular
Pilot symbols	BPSK constellation
SNR	10dB

5.5.1 Uniformly Spaced Pilots

When pilots are uniformly spaced, different pilot spacing, or equivalently different Np, will affect the channel estimation. We divide the pilot spacing or Np into some categories, and compare the performance. The categories that we use are listed here:

1) Np can divide N versus Np cannot divide N. In other words, N/Np is integer or not.

2) Np is less than, equal to, and larger than the maximum channel length.

5.5.1.1 N/Np

In a N-point OFDM system with subcarrier index from 0 to N-1, if the pilot spacing is B and the first pilot subcarrier index is always 0, then the pilots will be at subcarriers with index 0, B, 2B, … $\left(\left\lfloor \dfrac{N-1}{B} \right\rfloor\right)B$. Hence, total number of pilots in one OFDM symbol is $\mathrm{Np} = \left\lfloor \dfrac{N-1}{B} \right\rfloor + 1$. Whether Np can divide N or not depends on the value of B.

We now consider four different pilot spacing values: 2, 3, 4 and 5. For pilot spacing 2 and 4, Np is 32 and 16, respectively. Np can divide N for these two pilot spacing. For pilot spacing 3 and 5, Np is 22 and 13, respectively. Np cannot divide N for these two pilot spacing.

The mean square error for these four pilot spacing settings is plotted versus subcarriers in Figure 5-3.
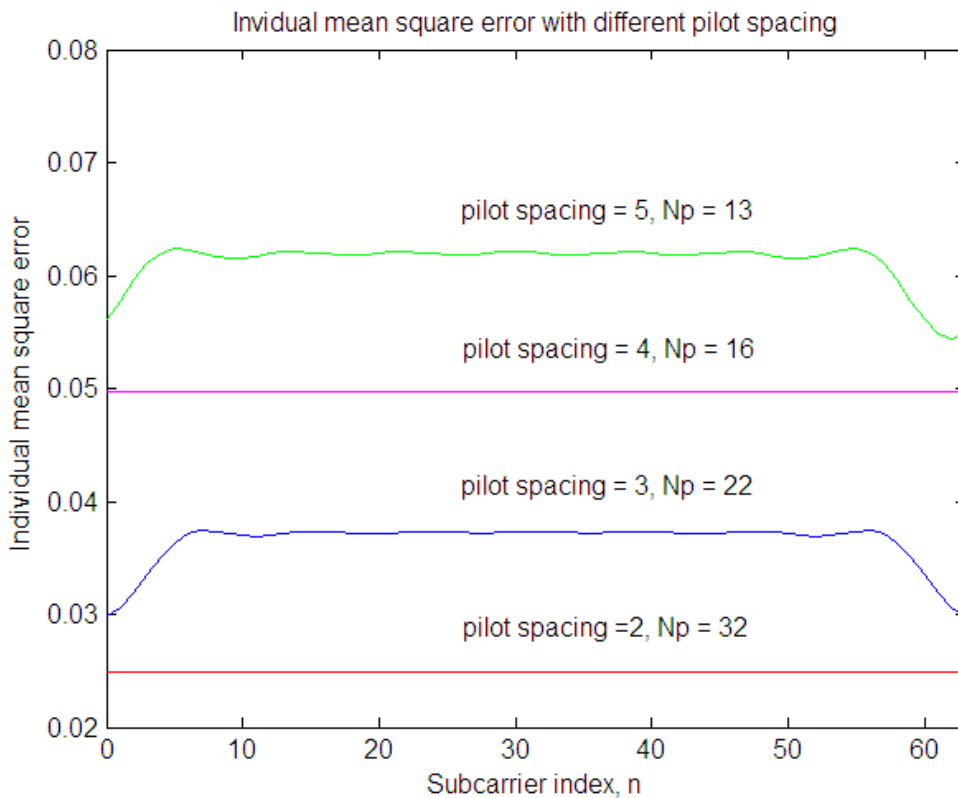
Figure 5-3   MSE versus subcarriers with uniformly spaced pilots

It can be seen from Figure 5-3 that when Np divides N, e.g, Np = 16 and 32, the mean square error is identical over the signal bandwidth. On the other hand, when Np cannot divide the N, the mean square error at different subcarriers is not identical. For subcarriers in the middle, the mean square error is nearly identical, but the mean square error for subcarriers at the edge has much difference. For instance, when pilot spacing is 3, the mean square error at subcarrier index 5 is about 0.036, while the mean square error decreases to about 0.03 at the subcarrier index 0.

It is preferred that Np can divide N because of two considerations:

1) The MSE is the same for all subcarriers if Np divides N. Hence, only one value need to be saved in the memory. In contrast, MSE is different for all subcarriers if Np cannot divide N. Hence, a total of N MSE values shall be saved, which requires large memory and increases hardware/software complexity.

2) In general, N shall be chosen to be power of 2 in order to allow the FFT/IFFT operation. Hence, Np that divides N must also be power of 2. In hardware implementation, it is always desirable to choose values that are power of 2 as resources like timer, counter, etc, can be more conveniently designed with less power consumption.

Another observation from Figure 5-3 is that smaller pilot spacing will lead to better channel estimation and less estimation error. It is reasonable since smaller pilot spacing means more pilots are used in the channel estimation. However, it shall be noteworthy that improved channel estimation with more pilots comes at the cost of decreased spectrum utilization.

5.5.1.2 Np

In order to show the relationship between the number of pilots and the maximum channel length, we choose Np to be 6,7,8 and 10. The first two Np values are less than the maximum channel length which is 8. The last two Np values are equal to and larger than the maximum channel length, respectively. We also assume that the pilots are uniformly spaced. The mean square errors for different pilot spacing are plotted in Figure 5-4.
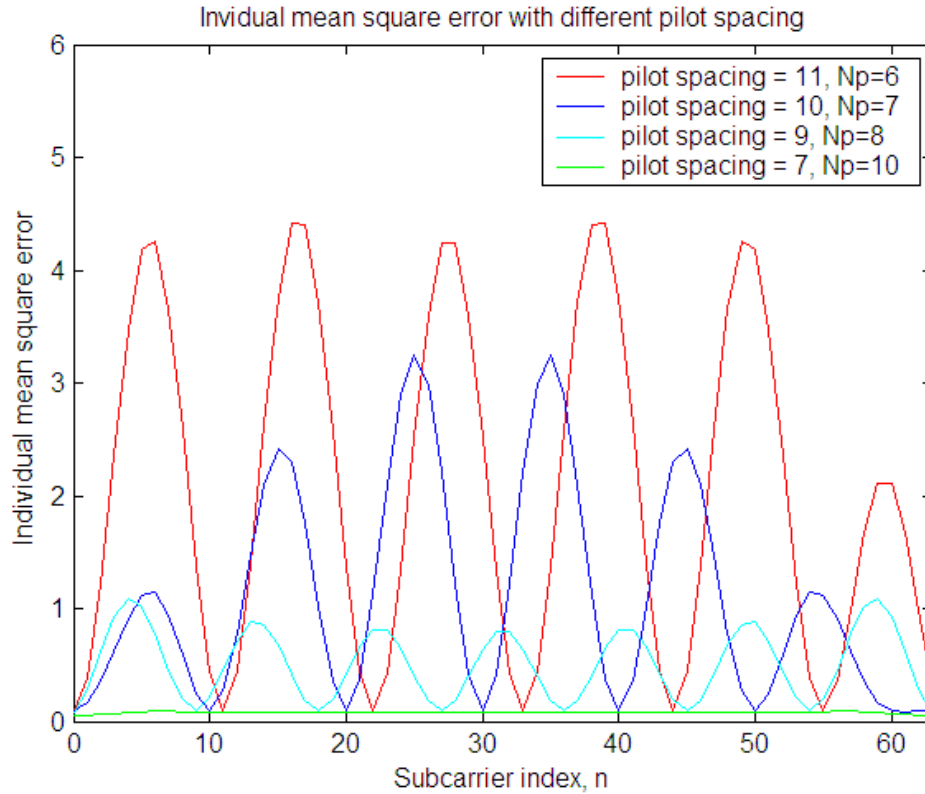
Figure 5-4   MSE versus subcarriers with uniformly spaced pilots

Figure 5-4 shows that when N_p is 10 which is greater than the maximum channel length, MSE is small and almost identical over the signal bandwidth.

However, when N_p is 6 and 7, which are less than the maximum channel length, MSE fluctuates over the signal bandwidth with a repetitive cycle. Specifically, MSE is the lowest at the pilot subcarriers. MSE gradually increases and reaches a local maximum at data subcarrier which lies exactly in the middle of two adjacent pilot subcarriers. Moreover, the local maximum can be significantly higher than the local minimum at pilot subcarriers. For example, when N_p is 6, MSE at pilot subcarriers is about 0.1, while MSE at data subcarriers can be as high as 4. In summary, channel estimation at pilot subcarriers is the most accurate. Channel estimation at any data subcarrier depends on its location relative to the adjacent pilot subcarriers. The further away the data subcarrier from the nearest pilot subcarrier, the worse the MSE becomes.

When N_p is 8 which is equal to the maximum channel length, MSE exhibits similar repetitive pattern, although the worst MSE at data subcarrier is much lower than that in N_p = 6 or 7. For example, the worse MSE with N_p = 8 is about 1, compared with the worse MSE of 3 and 4, for N_p = 6 and 7, respectively.

42

Hence, the conclusion is reached that for accurate channel estimation, Np must be equal to or greater than the maximum channel length, which is L=8 in the considered scenario.

5.5.2 Nonuniformly Spaced Pilots

In order to illustrate the general performance of nonuniformly spaced pilots and compare the performance between nonuniformly spaced pilots and uniformly spaced pilots, we generate three different sets of nonuniformly spaced pilots and plot them together with the uniformly spaced pilots in Figure 5-5. The first subplot shows the uniformly spaced pilots, whereas the other three subplots show the nonuniformly spaced pilots. For all these pilot schemes, Np is set to 16.
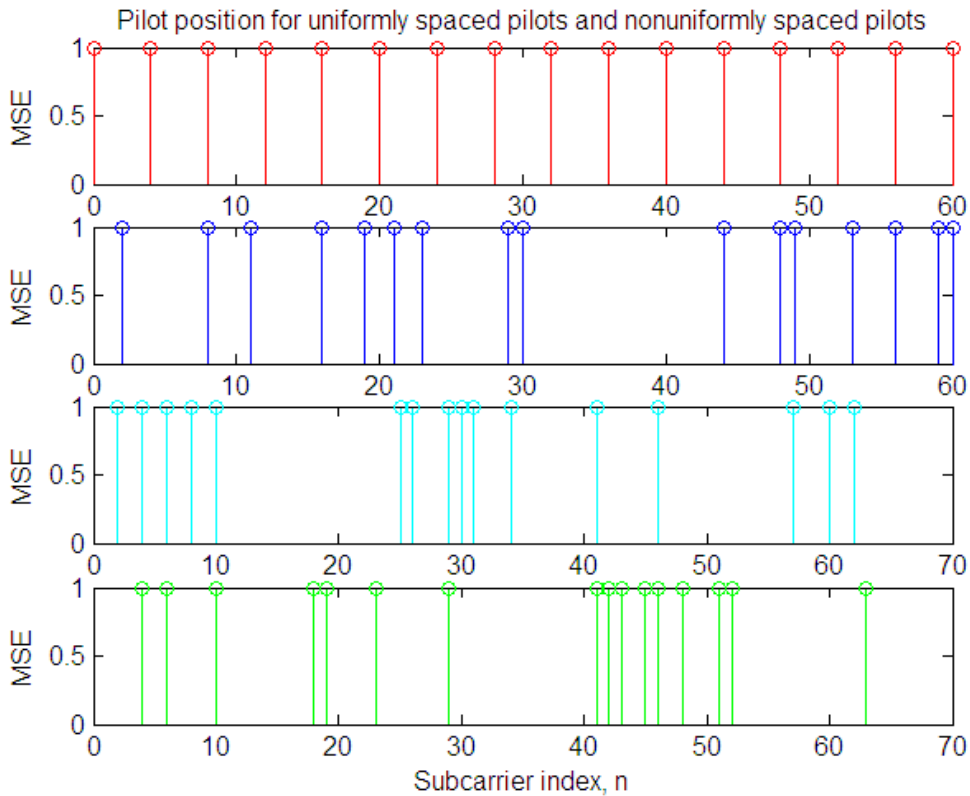
Figure 5-5   Pilot position for uniformly spaced pilots and nonuniformly spaced pilots

The minimum mean square error for the uniformly pilot set and the three nonuniformly pilot sets are plotted in Figure 5-6.
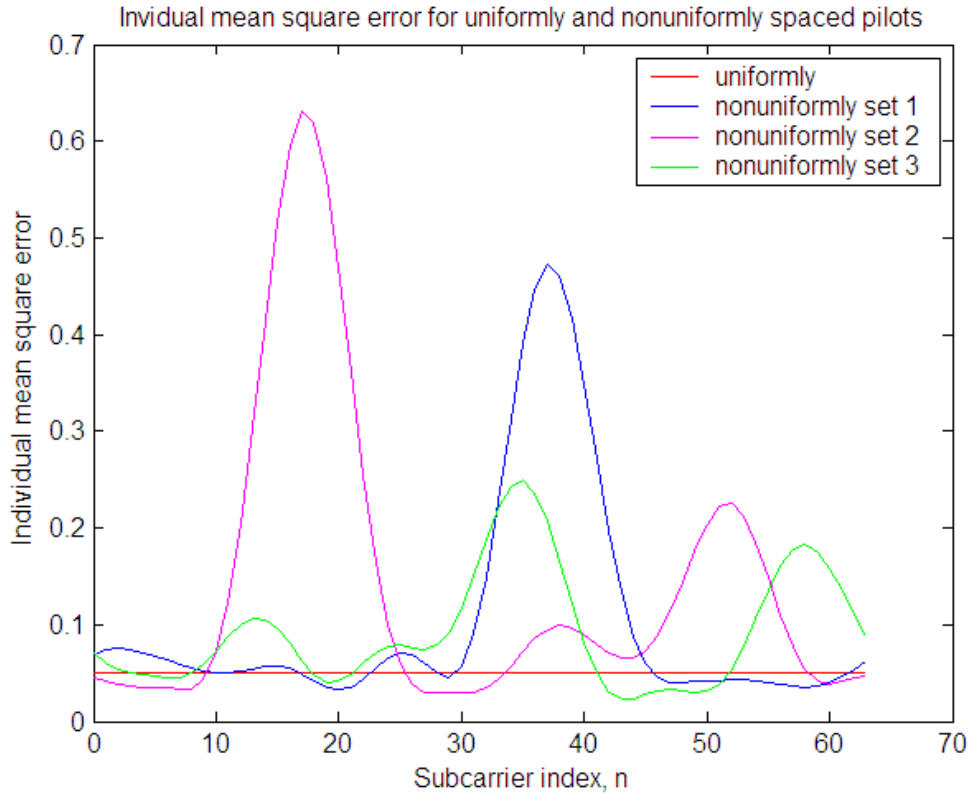
Figure 5-6   **MSE versus subcarriers with uniformly and nonuniformly spaced pilots**

It can be seen from Figure 5-6 that when pilot tones are not uniformly spaced, the estimation mean square error will fluctuate dramatically throughout the signal bandwidth. Although at certain subcarriers the MSE with nonuniformly spaced pilots may be lower than that with uniformly spaced pilots, at most subcarriers the MSE with nonuniformly spaced pilots are much higher than that with uniformly spaced pilots. For best decoding, a flat MSE curve is desired as it ensures the same level of accuracy of channel estimation for all subcarriers. Hence, the uniformly spaced pilots are the optimal.

5.5.3 Summary

From what we have observed in the experiment, we can reach the following conclusion regarding how to select the optimal pilot set.

1. N_p shall be equal to or greater than the maximum channel length. Otherwise the channel estimation error is unacceptably large.

2. Uniformly spaced pilots is preferred over nonuniformly spaced pilots, as it results in a flat or nearly flat MSE over all subcarriers, while nonuniformly spaced pilots leads to much fluctuation across the spectrum, which is undesirable.

3. When pilots are uniformly spaced

   1) It is preferred that N_p divides N to ensure that the MSE is flat over the whole bandwidth.

2)   Increasing Np will decrease the minimum mean square error.

3)   The choice of Np is a tradeoff between channel estimation reliability and spectral efficiency. Higher Np, or denser pilots can boost channel estimation accuracy but reduce the spectral efficiency. On the other hand, lower Np, or sparser pilots can degrade channel estimation accuracy but improve the spectral efficiency.

Hence, in the LDPC-coded pilot-assisted OFDM system that we study, we would like to choose uniformly spaced pilots with Np that satisfies two conditions: (1) Np can divide N. (2) Np is equal to or larger than the maximum channel length. There may be a number of Np that satisfy the above two conditions. Hence, the optimal Np can only be determined after computer simulation to obtain the BER. Np that gives the best BER versus Eb/No will be seen as the optimal Np.

5.6   Simulation Introduction

In this chapter, Monte Carlo simulation is employed to obtain the BER for the LDPC-coded pilot-assisted OFDM system. The simulation system will be introduced. Simulation will be run for different configurations.

5.6.1 Simulation System

The computer simulation system is shown in Figure 5-7.
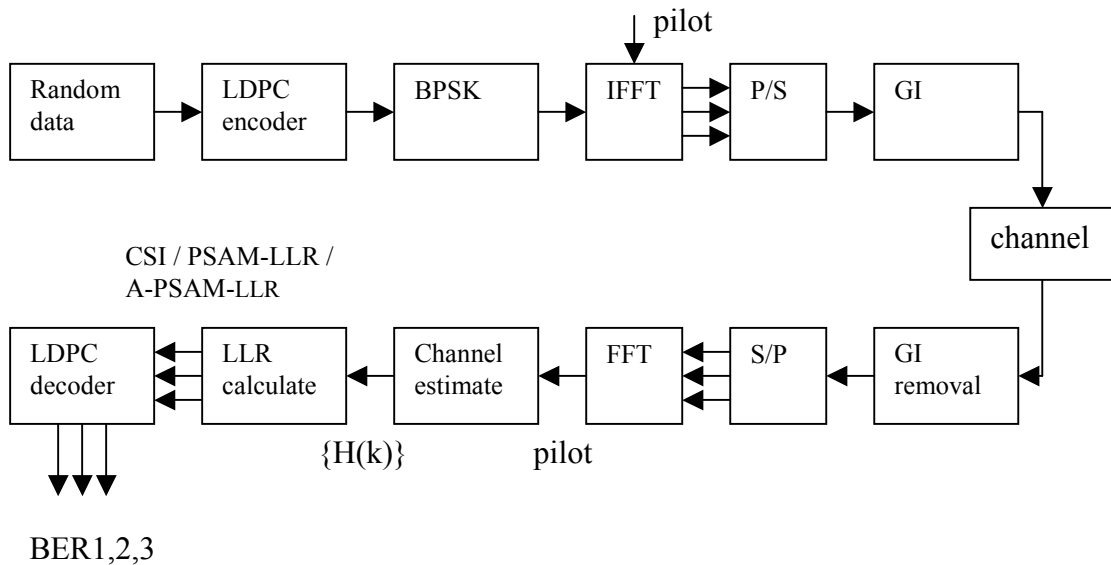
Figure 5-7   Simulation of LDPC-coded pilot-assisted OFDM system

In the receiver, three LLR metrics are calculated. Ideal LLR is calculated based on ideal channel state information (CSI), while PSAM-LLR and A-PSAM-LLR is based on the

estimated channel. Therefore, three different BER will be obtained. The BER for the ideal LLR is used as a performance benchmark.

The system parameters are listed in Table 5-3.

Table 5-3   Parameters for the OFDM simulation system

Parameter	Value
FFT points	64, 128
Cyclic prefix	16 sampling intervals
Modulation scheme	BPSK
Pilots arrangement	Comb type pilot arrangement. Uniformly spaced with energy equal to data symbols
Pilot spacing	2,4,8,16,32
LDPC code	LDPC (504, 1008) PEGirReg504x1008
Channel model	Sample-spaced multipath channel, modeled by a L-tap FIR filter
Maximum channel length	L=8 and 12
Power delay profile	Rectangular and exponential delay profile
Eb/No (dB)	2-12

For channel with rectangular delay profile, the amplitude of each path satisfies

$$E[|h_k|^2]=1, k=0,1,\ldots,L-1 \tag{5.40}$$

For channel with the exponential delay profile, the amplitude of each path satisfies

$$E[|h_k|^2]=\exp(-k/10), k=0,1,\ldots,L-1 \tag{5.41}$$

The rectangular and exponential delay profile with 12 paths is shown in Figure 5-8 and Figure 5-9, respectively.
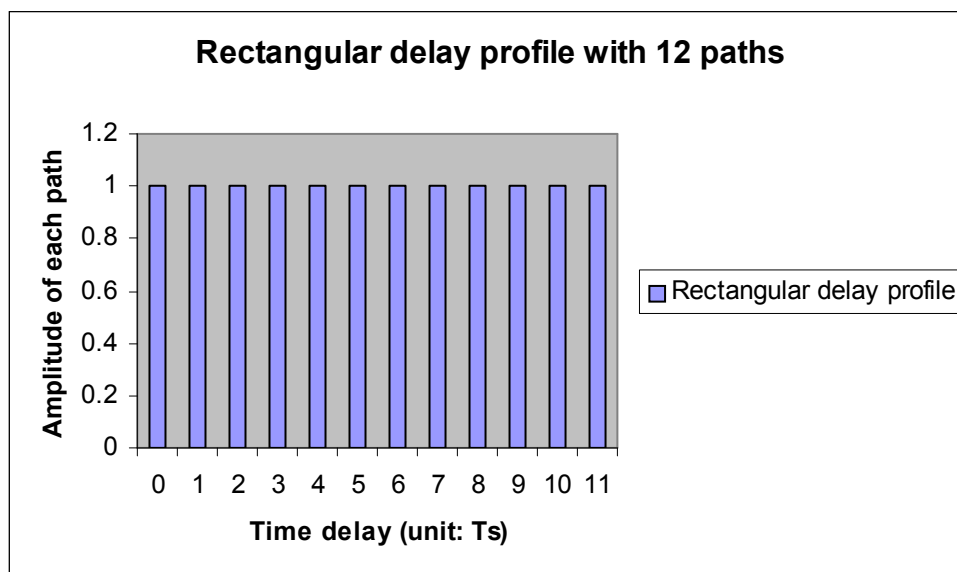
Figure 5-8   Rectangular power delay profile with maximum path delay 12
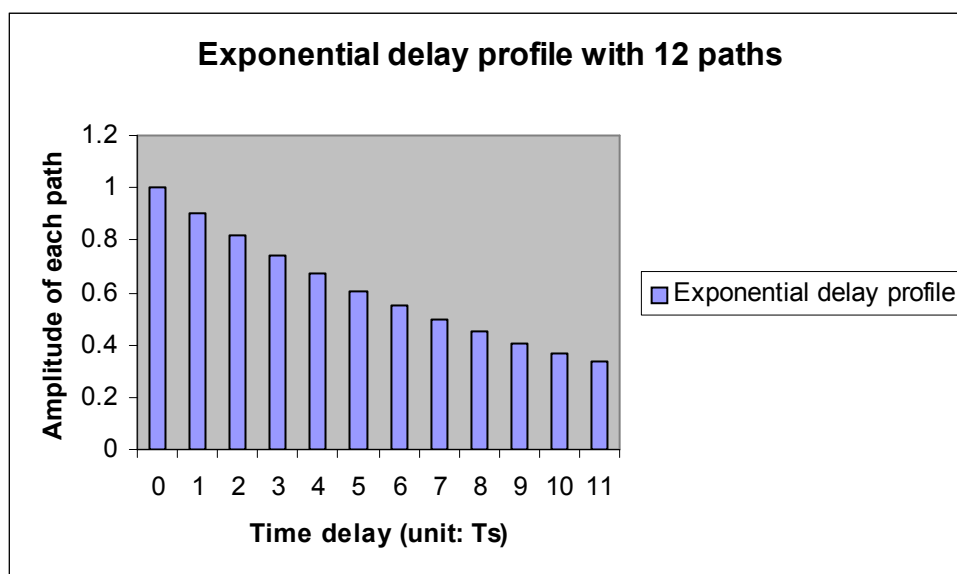
Figure 5-9   Exponential power delay profile with maximum path delay 12

5.6.2 Simulation Platform

The simulation system is built on the Microsoft Visual Studio 2010, an integrated development environment (IDE) from Microsoft, and MATLAB R2011a, a popular technical computing language and interactive environment for algorithm development. The program comprises C/C++ code that will call some MATLAB built-in functions through the MATLAB engine. The procedure of using MATLAB engine is detained in section 5.6.2. By using the MATLAB engine, the simulation platform can be quickly built by avoiding some complicated programming work in C/C++.

An example of MATLAB function called through the MATLAB engine is the inv(), whih calculates the inverse of a square matrix. It is used in the LMMSE channel estimator. The call of inv() via the MATLAB engine is demonstrated in Figure 5-10.

```
start
```

```
Input c_in, matrix size N
```

```
Start the engine        ep = engOpen("")
```

```
Create a mxArray variable        mxArray *mat_in =
                                 mxCreateDoubleMatrix(N, N,
                                 mxCOMPLEX);
```

```
Copy the input matrix to        memcpy((char *) mxGetPr(mat_in), (char *)
mxArray variable                c_in_r, N*N*sizeof(double));
                                memcpy((char *) mxGetPi(mat_in), (char *)
                                c_in_i, N*N*sizeof(double));
```

```
Place the mxArray variable
into MATLAB workspace           engPutArray(ep, mat_in);
```

```
Matrix inversion                engEvalString(ep, "mat_out =
                                inv(mat_in)");
```

```
Get the result in mxArray       mxArray *mat_out =
variable                        engGetArray(ep, "mat_out");
```

```
Copy to the output matrix       memcpy((char *) c_out_r, (char *)
                                mxGetPr(mat_out), N*N*sizeof(double));
                                memcpy((char *) c_out_i, (char *)
                                mxGetPi(mat_out), N*N*sizeof(double));
```

```
Free memory                     mxDestroyArray(mat_in);
                                mxDestroyArray(mat_out);
```

```
Close engine                    engClose(ep);
```

```
Output c_out
```

```
end
```

Figure 5-10   Procedure of calling MATLAB function inv() through MATLAB engine

5.6.3 Program Flowchart

The program flowchart is shown in Figure 5-11. The input parameters are Nfft, pilot spacing, power delay profile, maximum path delay, Eb/N0 and error threshold. The output is the BER for ideal CSI, PSAM-LLR and A-PSAM-LLR. The signal processing functional blocks in the OFDM transmitter and receivers are clearly indicated in the figure. The LDPC decoder is log-domain decoder with maximum iteration 50.
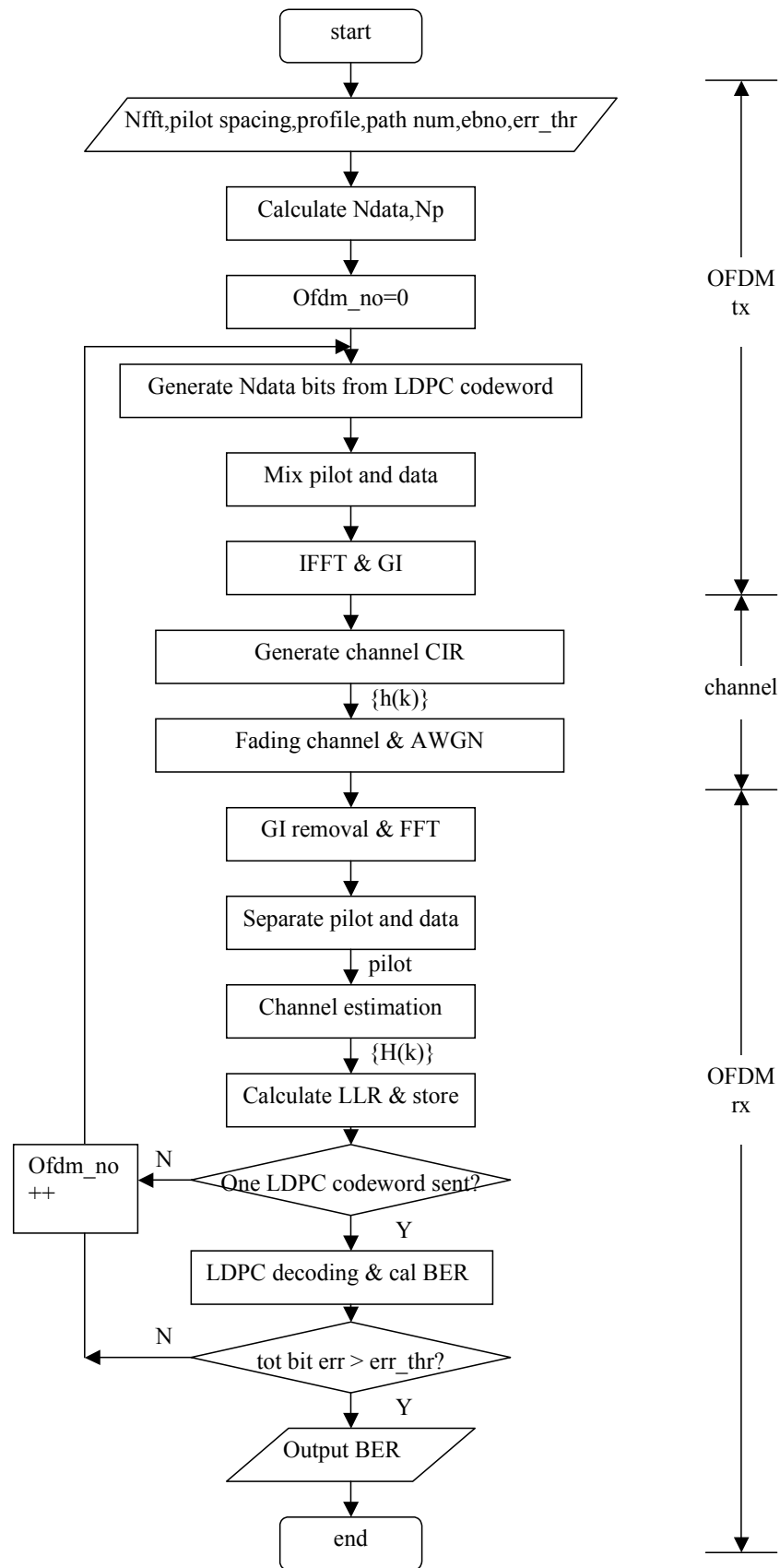
Figure 5-11   Program flowchart for LDPC-coded pilot-assisted OFDM simulation system

The mapping of LDPC codewords to the data subcarriers is handled by the functional block "generate Ndata bits from LDPC codeword" in Figure 5-11. The mapping is illustrated in Figure 5-12. The Ndata bits in one OFDM symbol may come from one LDPC codeword, or two LDPC codewords.
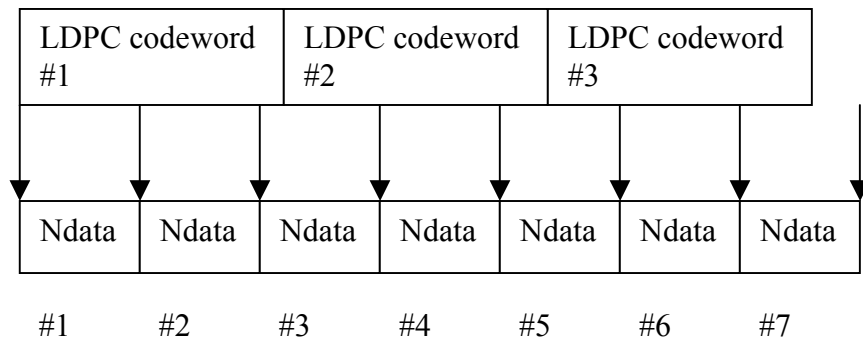
Figure 5-12   Illustration of mapping the LDPC codeword to the Ndata subcarriers

In the example given in Figure 5-12, the first LDPC codeword is mapped to the OFDM symbols #1 - #3, the second LDPC codeword is mapped to the OFDM symbols #3 - #5 and the third LDPC codeword is mapped to the OFDM symbols #5 - #7. Hence, the OFDM symbol #3 contains bits from OFDM symbol #1 and #2. Likewise, the OFDM symbol #5 contains bits from OFDM symbol #2 and #3.

The procedure in the functional block "generate Ndata bits from LDPC codeword" is described in Figure 5-13.
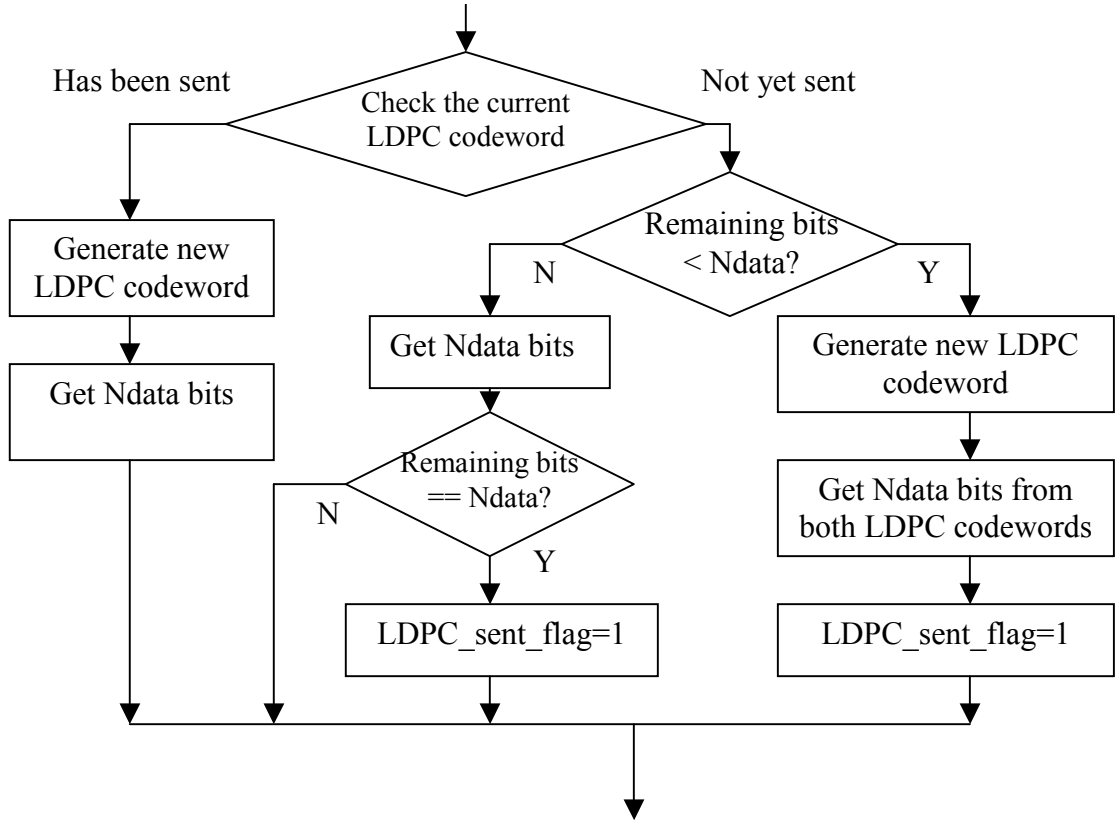
Figure 5-13   Program flowchart of the generation of Ndata bits for one OFDM symbol

5.6.4 Performance Measurement Criteria

The performance is measured in BER versus Eb/No, which is an important parameter in digital communication and data transmission. It is a normalized SNR measure, also known as the "SNR per bit". As the pilots occupy the bandwidth, for a fair comparison, BER shall be plotted versus Eb/No instead of the SNR. In the following, we will define the SNR for OFDM system, then convert the SNR to Eb/No.

Let x(n) and X(n) denote the time domain and frequency domain OFDM signal. As X(n) and x(n) are a discrete Fourier transform pair, they have the following relationship based on the Parseval's theorem

$$\sum_{n=0}^{N-1}\left|x(n)\right|^2 = \frac{1}{N}\sum_{k=0}^{N-1}\left|X(k)\right|^2 \tag{5.42}$$

We assume BPSK symbol average energy is Es. In ideal channel, the average power of OFDM signal is

$$S = \frac{1}{N}\sum_{n=0}^{N-1}\left|x(n)\right|^2 = \frac{1}{N^2}\sum_{k=0}^{N-1}\left|X(k)\right|^2 = \frac{E_s}{N} \tag{5.43}$$

53

In the multipath fading channel with L paths, the total average power of the received OFDM signal will be

$$S = \frac{E_s}{N}\left(\sum_{k=0}^{L-1}|h_k|^2\right)$$

(5.44)

Hence, the signal-to-noise ratio is

$$SNR = \frac{E_s}{N}\left(\sum_{k=0}^{L-1}|h_k|^2\right)\bigg/N_0$$

(5.45)

Assume the pilot is uniformly inserted, and the pilot spacing is denoted as B, which means one out of B subcarriers is used for transmitting pilots. Due to the insertion of pilot symbols, the signal power needed to transmit a data bit is Es*B/(B − 1). Considering the LDPC code rate R, the signal power needed to transmit an information bit would be Es*R*B/(B − 1). Hence, the relationship between Eb/No and SNR is

$$E_b / N_o = SNR\frac{B}{(B-1)R}$$

(5.46)

When Eb/No and SNR is expressed using the logarithmic decibel scale, their relationship is

$$(E_b / N_o)_{dB} = (SNR)_{dB} + 10\log_{10}\frac{B}{(B-1)R}$$

(5.47)

5.7 Simulation Result and Discussion

In this chapter, simulation results for different scenarios will be presented, followed by discussion on the optimal pilot spacing and LLR metric.

Simulation is performed on 64-point and 128-point OFDM system. The channel can have 8 and 12 paths. The power delay profile can be rectangular and exponential. The Eb/No range is from 2dB to 10dB, but can be extended to 11dB or 12dB in a few scenarios to obtain a BER lower than 1e-4.

The pilot spacing is chosen to be power of 2, such as 2, 4, 8, 16, etc. According to section 5.5, channel estimation is very poor when the number of pilots per OFDM symbol is less than the maximum path delay. Hence, we will run simulation with pilot spacing which results in sufficient number of pilots. For example, in 64-point OFDM system, when the maximum path delay is 8, we can choose the pilot spacing 2, 4 and 8, corresponding to 32, 16 and 8 pilots per OFDM symbol, respectively. We will not run simulation for pilot spacing like 16, 32, etc, as these settings will result in less than 8 pilots per OFDM symbol.

The simulation scenarios are listed in Table 5-4.

Table 5-4   Summary of simulation scenarios

Scenario No	Scenario Description				
	Number of FFT points	Maximum path delay	Power delay profile	Possible pilot spacing	Number of pilots
1	64	8	Rectangular	2,4,8	32,16,8
2	64	8	Exponential	2,4,8	32,16,8
3	64	12	Rectangular	2,4	32,16
4	64	12	Exponential	2,4	32,16
5	128	8	Rectangular	2,4,8,16	64,32,16,8
6	128	8	Exponential	2,4,8,16	64,32,16,8
7	128	12	Rectangular	2,4,8	64,32,16
8	128	12	Exponential	2,4,8	64,32,16

5.7.1 BER result for Different Scenarios

The simulation results for the 8 scenarios are given in Table 5-5 to

Table 5-12. The notation "NA" in the tables refers to "not available".

Table 5-5   **BER for scenarios 1: 64-point OFDM, rectangular delay profile and 8 paths**

Eb/No (dB)	BER					
	Pilot spacing 2		Pilot spacing 4		Pilot spacing 8	
	A-PSAM-LLR	PSAM-LLR	A-PSAM-LLR	PSAM-LLR	A-PSAM-LLR	PSAM-LLR
2	2.91E-01	2.91E-01	2.77E-01	2.78E-01	2.96E-01	2.95E-01
3	2.64E-01	2.63E-01	2.48E-01	2.47E-01	2.69E-01	2.67E-01
4	2.34E-01	2.33E-01	2.18E-01	2.16E-01	2.41E-01	2.38E-01
5	2.09E-01	2.08E-01	1.85E-01	1.80E-01	2.13E-01	2.07E-01
6	1.77E-01	1.75E-01	1.47E-01	1.34E-01	1.83E-01	1.71E-01
7	1.13E-01	1.07E-01	5.24E-02	3.70E-02	1.32E-01	1.03E-01
8	2.07E-02	1.59E-02	4.40E-03	2.19E-03	4.69E-02	2.62E-02
9	4.88E-04	2.77E-04	8.22E-05	3.41E-05	5.28E-03	2.02E-03
10	4.33E-06	1.90E-06	9.56E-07	2.06E-07	1.86E-04	5.88E-05
11	NA	NA	NA	NA	2.74E-06	6.06E-07

Table 5-6   BER for scenarios 2: 64-point OFDM, exponential delay profile and 8 paths

Eb/No (dB)	BER					
	Pilot spacing 2		Pilot spacing 4		Pilot spacing 8	
	A-PSAM-LLR	PSAM-LLR	A-PSAM-LLR	PSAM-LLR	A-PSAM-LLR	PSAM-LLR
2	2.90E-01	2.90E-01	2.76E-01	2.75E-01	2.94E-01	2.93E-01
3	2.63E-01	2.63E-01	2.44E-01	2.43E-01	2.66E-01	2.64E-01
4	2.36E-01	2.35E-01	2.17E-01	2.16E-01	2.40E-01	2.38E-01
5	2.07E-01	2.06E-01	1.89E-01	1.86E-01	2.10E-01	2.05E-01
6	1.75E-01	1.73E-01	1.44E-01	1.31E-01	1.85E-01	1.71E-01
7	1.12E-01	1.05E-01	5.29E-02	3.71E-02	1.28E-01	1.01E-01
8	1.98E-02	1.54E-02	4.79E-03	2.57E-03	4.63E-02	2.58E-02
9	5.64E-04	3.47E-04	1.07E-04	2.80E-05	5.19E-03	1.88E-03
10	2.62E-06	1.36E-06	1.36E-06	2.82E-07	2.02E-04	6.29E-05
11	NA	NA	NA	NA	2.99E-06	1.39E-06

Table 5-7   BER for scenarios 3: 64-point OFDM, rectangular delay profile and 12 paths

Eb/No	BER			
(dB)	Pilot spacing 2		Pilot spacing 4	
	A-PSAM-LLR	PSAM-LLR	A-PSAM-LLR	PSAM-LLR
2	3.07E-01	3.07E-01	2.97E-01	2.96E-01
3	2.79E-01	2.79E-01	2.69E-01	2.68E-01
4	2.57E-01	2.56E-01	2.42E-01	2.41E-01
5	2.27E-01	2.25E-01	2.14E-01	2.11E-01
6	1.93E-01	1.91E-01	1.90E-01	1.82E-01
7	1.59E-01	1.53E-01	1.35E-01	1.10E-01
8	7.16E-02	5.68E-02	3.87E-02	2.06E-02
9	4.66E-03	2.41E-03	1.52E-03	4.27E-04
10	1.90E-05	6.99E-06	8.26E-06	9.90E-07

Table 5-8   BER for scenarios 4: 64-point OFDM, exponential delay profile and 12 paths

Eb/No	BER			
(dB)	Pilot spacing 2		Pilot spacing 4	
	A-PSAM-LLR	PSAM-LLR	A-PSAM-LLR	PSAM-LLR
2	3.06E-01	3.06E-01	2.93E-01	2.92E-01
3	2.79E-01	2.79E-01	2.68E-01	2.68E-01
4	2.55E-01	2.54E-01	2.40E-01	2.37E-01
5	2.25E-01	2.23E-01	2.13E-01	2.08E-01
6	1.93E-01	1.91E-01	1.82E-01	1.71E-01
7	1.57E-01	1.50E-01	1.29E-01	1.04E-01
8	6.86E-02	5.56E-02	3.39E-02	1.85E-02
9	5.08E-03	2.54E-03	1.65E-03	7.05E-04
10	2.54E-05	7.97E-06	1.48E-05	4.32E-06

Table 5-9   **BER for scenarios 5: 128-point OFDM, rectangular delay profile and 8 paths**

Eb/No (dB)	BER							
	Pilot spacing 2		Pilot spacing 4		Pilot spacing 8		Pilot spacing 16	
	A-PSAM-LLR	PSAM-LLR	A-PSAM-LLR	PSAM-LLR	A-PSAM-LLR	PSAM-LLR	A-PSAM-LLR	PSAM-LLR
2	2.69E-01	2.69E-01	2.42E-01	2.42E-01	2.59E-01	2.57E-01	2.89E-01	2.87E-01
3	2.42E-01	2.42E-01	2.14E-01	2.14E-01	2.30E-01	2.28E-01	2.58E-01	2.56E-01
4	2.09E-01	2.09E-01	1.83E-01	1.82E-01	1.91E-01	1.88E-01	2.37E-01	2.33E-01
5	1.82E-01	1.81E-01	1.26E-01	1.22E-01	1.46E-01	1.39E-01	2.01E-01	1.93E-01
6	1.33E-01	1.32E-01	5.39E-02	4.76E-02	9.84E-02	8.29E-02	1.73E-01	1.56E-01
7	4.38E-02	4.15E-02	6.27E-03	4.92E-03	2.30E-02	1.57E-02	1.05E-01	8.01E-02
8	3.27E-03	2.95E-03	4.04E-04	2.59E-04	3.06E-03	1.63E-03	3.96E-02	2.47E-02
9	8.16E-05	6.59E-05	1.18E-05	9.47E-06	2.04E-04	1.15E-04	8.01E-03	4.11E-03
10	5.26E-07	3.72E-07	2.80E-07	0.00E+00	1.77E-05	1.09E-05	9.11E-04	4.04E-04
11	NA	NA	NA	NA	NA	NA	1.02E-04	5.63E-05
12	NA	NA	NA	NA	NA	NA	1.77E-05	1.10E-05

Table 5-10   BER for scenarios 6: 128-point OFDM, exponential delay profile and 8 paths

Eb/No (dB)	BER							
	Pilot spacing 2		Pilot spacing 4		Pilot spacing 8		Pilot spacing 16	
	A-PSAM-LLR	PSAM-LLR	A-PSAM-LLR	PSAM-LLR	A-PSAM-LLR	PSAM-LLR	A-PSAM-LLR	PSAM-LLR
2	2.67E-01	2.67E-01	2.42E-01	2.42E-01	2.55E-01	2.53E-01	2.89E-01	2.88E-01
3	2.37E-01	2.37E-01	2.14E-01	2.13E-01	2.26E-01	2.24E-01	2.59E-01	2.57E-01
4	2.12E-01	2.12E-01	1.86E-01	1.85E-01	1.98E-01	1.95E-01	2.27E-01	2.24E-01
5	1.84E-01	1.84E-01	1.32E-01	1.28E-01	1.62E-01	1.54E-01	2.04E-01	1.95E-01
6	1.33E-01	1.32E-01	5.28E-02	4.65E-02	9.21E-02	7.49E-02	1.71E-01	1.53E-01
7	4.19E-02	3.95E-02	6.85E-03	4.78E-03	2.14E-02	1.52E-02	1.01E-01	7.70E-02
8	3.56E-03	3.21E-03	3.02E-04	2.00E-04	2.75E-03	1.46E-03	3.88E-02	2.42E-02
9	7.24E-05	5.27E-05	1.35E-05	1.06E-05	2.80E-04	1.28E-04	7.53E-03	3.53E-03
10	4.88E-07	2.06E-07	3.00E-07	5.85E-07	2.27E-05	1.31E-05	1.15E-03	6.27E-04
11	NA	NA	NA	NA	NA	NA	1.27E-04	7.26E-05
12	NA	NA	NA	NA	NA	NA	1.60E-05	1.02E-05

Table 5-11 **BER for scenarios 7: 128-point OFDM, rectangular delay profile and 12 paths**

Eb/No (dB)	BER					
	Pilot spacing 2		Pilot spacing 4		Pilot spacing 8	
	A-PSAM-LLR	PSAM-LLR	A-PSAM-LLR	PSAM-LLR	A-PSAM-LLR	PSAM-LLR
2	2.79E-01	2.78E-01	2.64E-01	2.64E-01	2.80E-01	2.80E-01
3	2.55E-01	2.54E-01	2.33E-01	2.32E-01	2.52E-01	2.51E-01
4	2.28E-01	2.27E-01	2.02E-01	2.00E-01	2.27E-01	2.24E-01
5	1.93E-01	1.92E-01	1.70E-01	1.65E-01	1.94E-01	1.88E-01
6	1.59E-01	1.57E-01	1.03E-01	9.12E-02	1.54E-01	1.37E-01
7	7.74E-02	7.21E-02	2.13E-02	1.48E-02	7.19E-02	5.01E-02
8	8.49E-03	6.64E-03	1.47E-03	7.39E-04	1.36E-02	7.13E-03
9	1.58E-04	1.17E-04	3.28E-05	1.35E-05	1.22E-03	4.79E-04
10	5.87E-07	4.00E-07	4.41E-07	0.00E+00	3.59E-05	1.30E-05

Table 5-12   **BER for scenarios 8: 128-point OFDM, exponential delay profile and 12 paths**

Eb/No (dB)	BER					
	Pilot spacing 2		Pilot spacing 4		Pilot spacing 8	
	A-PSAM-LLR	PSAM-LLR	A-PSAM-LLR	PSAM-LLR	A-PSAM-LLR	PSAM-LLR
2	2.80E-01	2.80E-01	2.59E-01	2.58E-01	2.76E-01	2.76E-01
3	2.53E-01	2.53E-01	2.32E-01	2.32E-01	2.45E-01	2.44E-01
4	2.26E-01	2.25E-01	2.01E-01	2.00E-01	2.22E-01	2.17E-01
5	1.94E-01	1.94E-01	1.58E-01	1.54E-01	1.88E-01	1.81E-01
6	1.61E-01	1.59E-01	8.78E-02	7.64E-02	1.43E-01	1.22E-01
7	7.36E-02	6.86E-02	2.05E-02	1.50E-02	6.91E-02	4.79E-02
8	9.41E-03	7.38E-03	1.30E-03	9.05E-04	1.32E-02	7.36E-03
9	1.06E-04	8.43E-05	2.40E-05	1.15E-05	8.14E-04	2.86E-04
10	8.63E-07	2.70E-07	0.00E+00	0.00E+00	4.15E-05	1.50E-05

5.7.2 Discussions on Optimal Pilot Spacing

The BER with PSAM-LLR for the 8 scenarios are plotted in Figure 5-14 to Figure 5-21. The "S2" in the legend refers to pilot spacing of 2, the legend "S4" refers to pilot spacing of 4, etc.

Figure 5-14 **BER for scenarios 1: 64-point OFDM, rectangular, 8 paths, PSAM-LLR with different pilot spacing**

Figure 5-15 **BER for scenarios 2: 64-point OFDM, exponential, 8 paths, PSAM-LLR with different pilot spacing**

Figure 5-16 **BER for scenarios 3: 64-point OFDM, rectangular, 12 paths, PSAM-LLR with different pilot spacing**

Figure 5-17   **BER for scenarios 4: 64-point OFDM, exponential, 12 paths, PSAM-LLR with different pilot spacing**

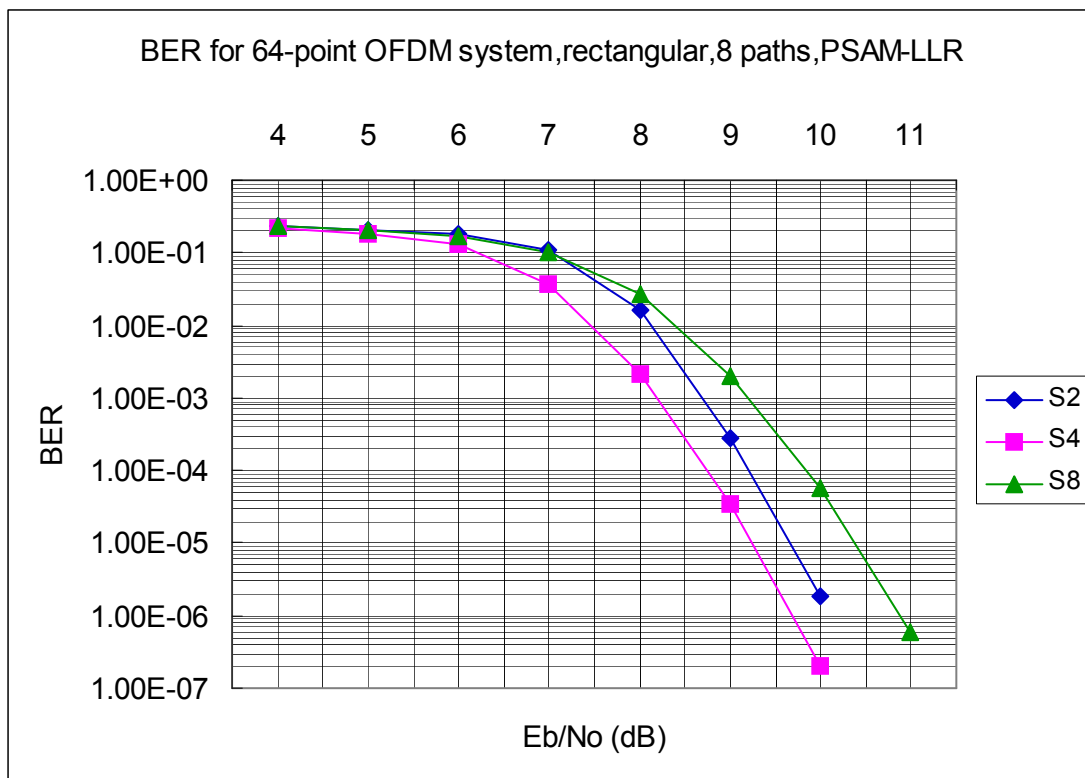BER for 128-point OFDM system,rectangular,8 paths,PSAM-LLR

Figure 5-18   **BER for scenario 5: 128-point OFDM, rectangular, 8 paths, PSAM-LLR with different pilot spacing**
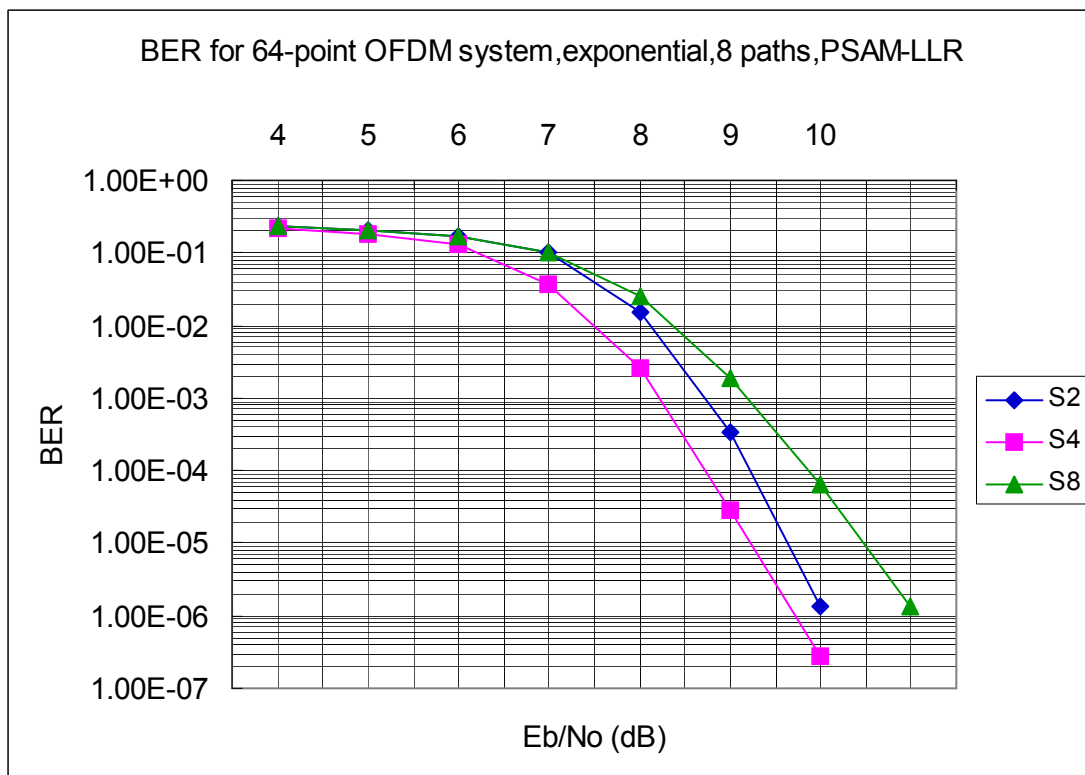
Figure 5-19   BER for scenario 6: 128-point OFDM, exponential, 8 paths, PSAM-LLR with different pilot spacing

Figure 5-20   BER for scenario 7: 128-point OFDM, rectangular, 12 paths, PSAM-LLR with different pilot spacing

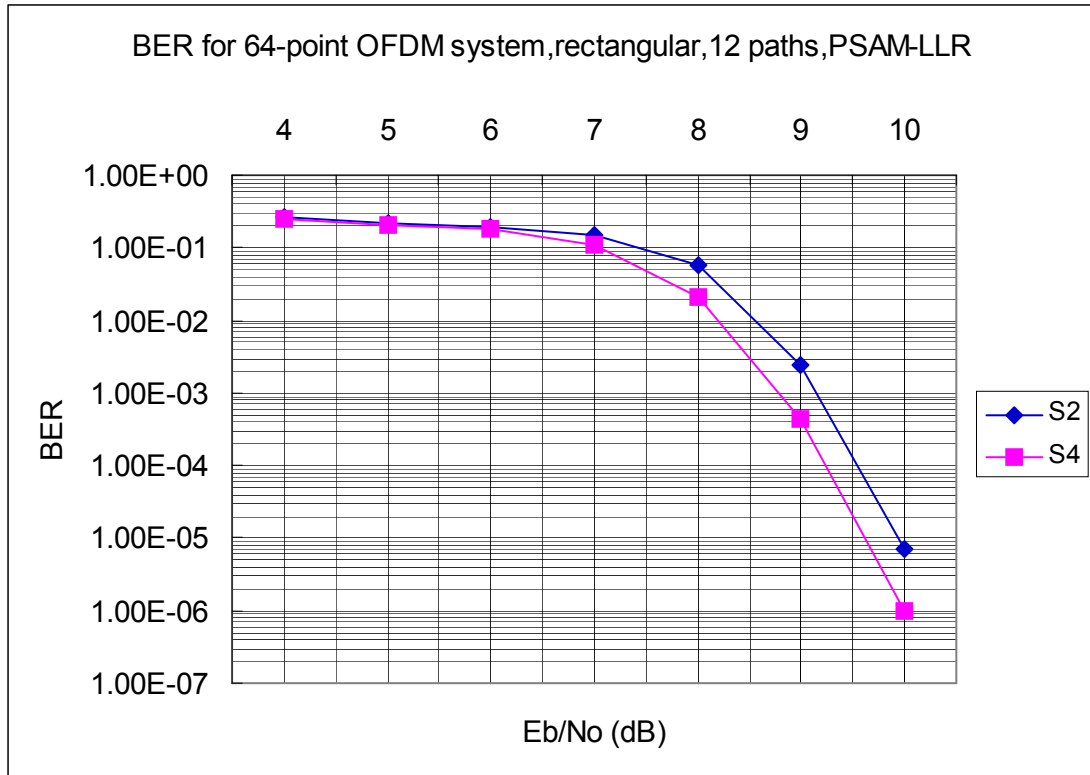**Figure 5-21   BER for scenario 8: 128-point OFDM, exponential, 12 paths, PSAM-LLR with different pilot spacing**
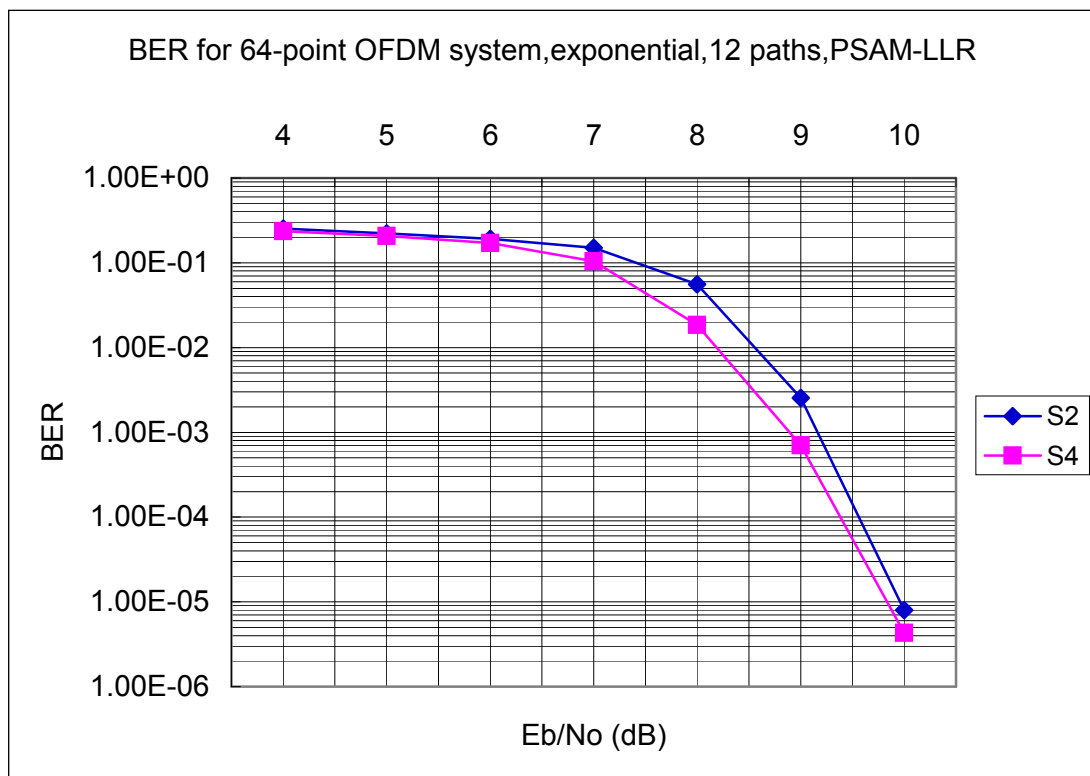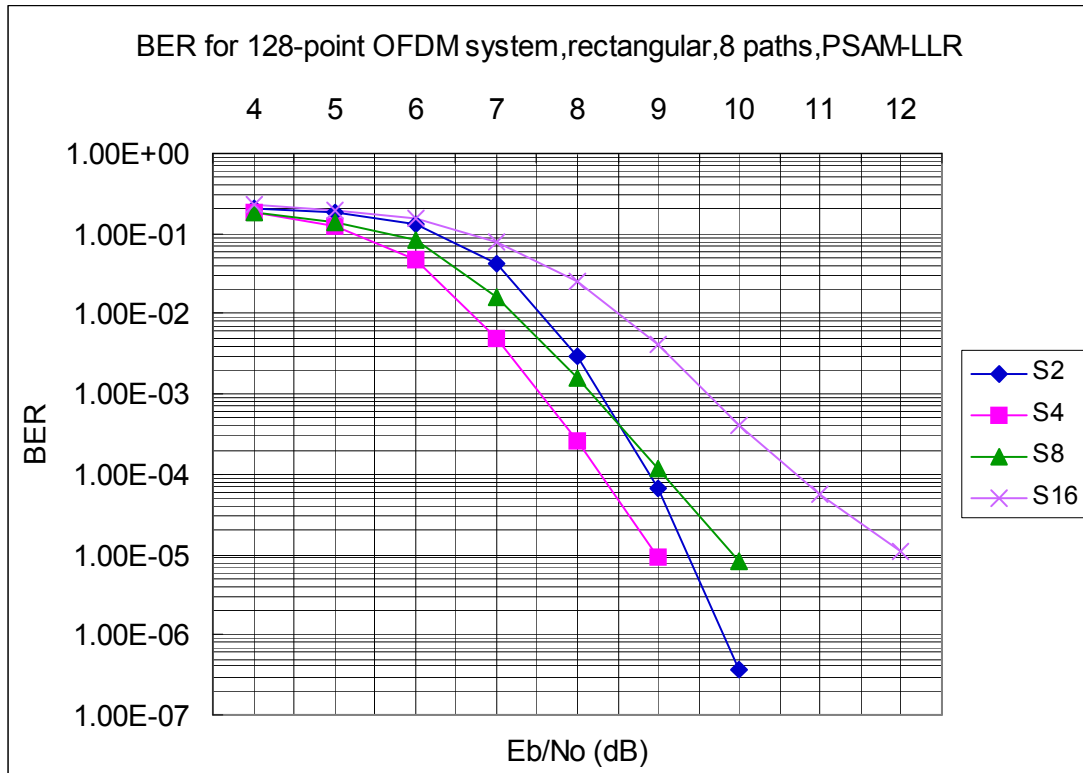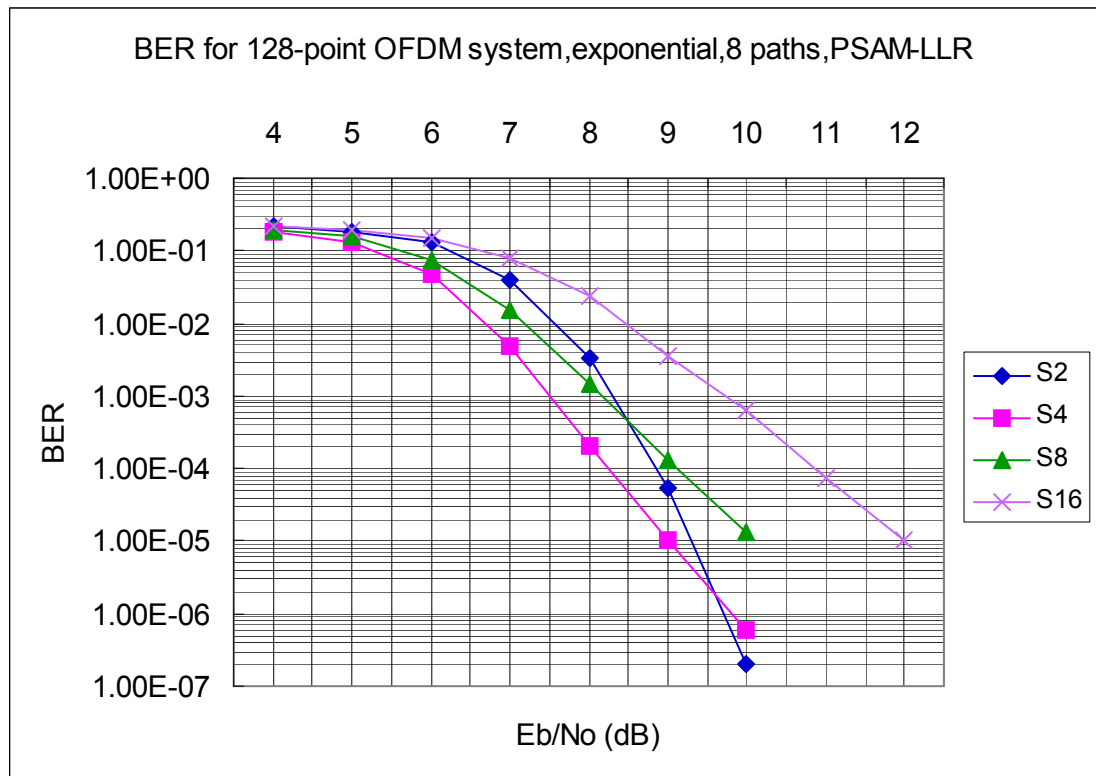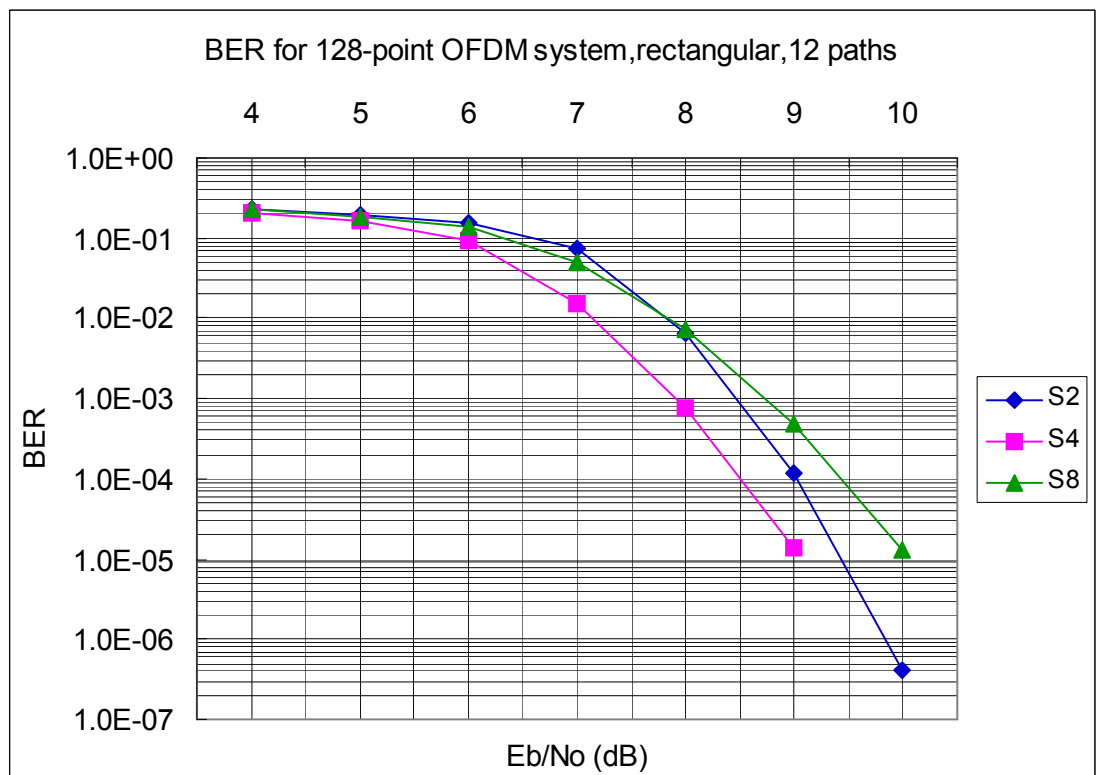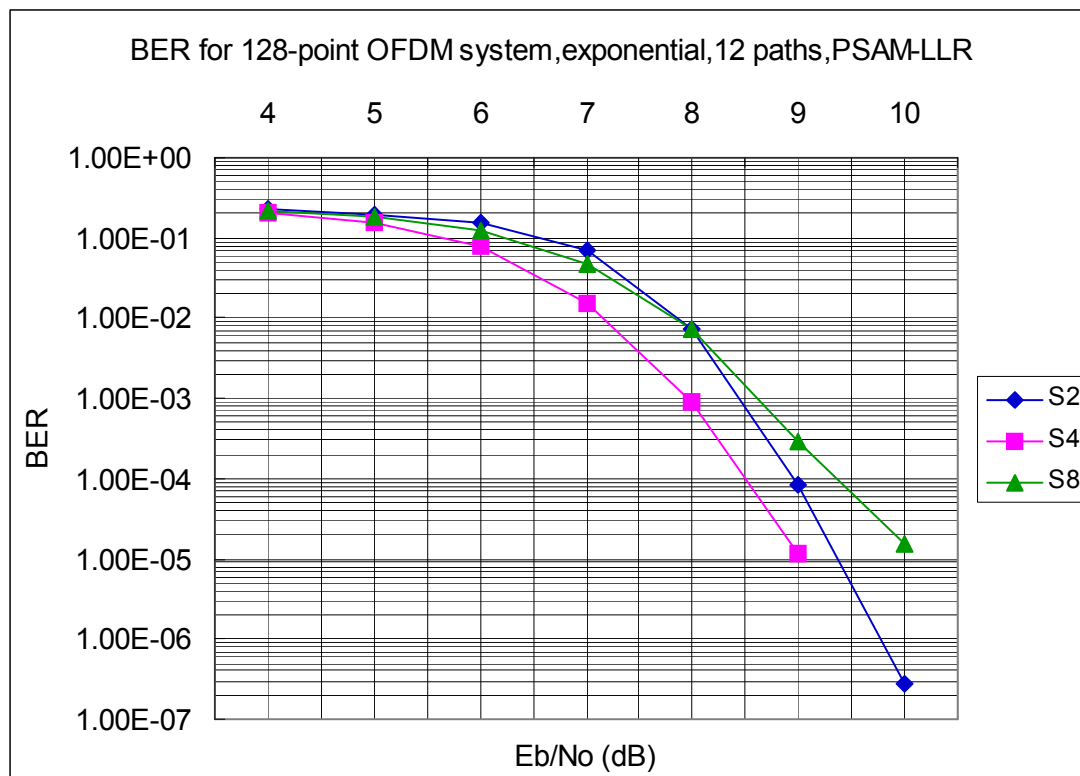
Based on the above BER plots, we can find that the Eb/No required to achieve the BER of 1e-4 are as listed in Table 5-13. The notation "NA" in the table is the abbreviation for "not applicable".

Table 5-13   Eb/No (dB) for achieving BER of 1e-4 in different scenarios when PSAM-LLR is used

Scenario	Eb/No (dB) for achieving BER of 1e-4			
	Pilot spacing 2	Pilot spacing 4	Pilot spacing 8	Pilot spacing 16
1	9.20	8.74	9.85	NA
2	9.22	8.72	9.86	NA
3	9.54	9.24	NA	NA
4	9.56	9.38	NA	NA
5	8.89	8.29	9.05	10.71
6	8.84	8.24	9.11	10.85
7	9.03	8.50	9.43	NA
8	8.96	8.49	9.37	NA

It can be seen that when pilot spacing decreases, the BER performance generally improves. For example, Table 5-13 shows that in scenario 1, when pilot spacing decreases from 8 to 4, the BER performance improves by about 1.1dB. The reason for the BER improvement is that decreased pilot spacing results in more pilots being involved in the channel estimation. Hence, the channel estimation is more accurate and the BER performance will improve.

However, when pilot spacing decreases to a very small value of 2, the performance at low and medium Eb/No range degrades rather than improves. For example, Table 5-13 shows that in scenario 1, when pilot spacing decreases from 4 to 2, the BER performance degrades by about 0.5dB. Similar trend can be observed for other scenarios. The reason is that when pilot spacing is extremely small, the bandwidth is wasted too much on the pilot transmission, and hence has an adverse impact on the BER versus Eb/No performance.

There are some interesting observations regarding the BER performance with pilot spacing 2. Although the performance with pilot spacing 2 is worse than that with pilot spacing 8 at low and medium Eb/No range, its performance can exceed that with pilot spacing 8 at high Eb/No. For example, in scenario 8, the BER performance with pilot spacing 2 becomes better than pilot spacing 8 when Eb/No is greater than 8dB. Another example is that in scenario 6, the BER performance with pilot spacing 2 becomes comparable to that with pilot spacing 4 when Eb/No is greater than 10dB.

Although in some scenarios, the BER performance with pilot spacing 2 is the best at high Eb/No, it is observed that in most scenarios, pilot spacing 4 leads to the best performance at

low and medium Eb/No range. Considering that pilot spacing 2 reduces the data rate too excessively and impairs the data throughput, the optimal choice of pilot spacing shall be 4.

It shall be emphasized that our claim that optimal pilot spacing is 4 is valid only for a number of specific system configurations considered in this chapter. The generalization of such conclusion to all channel conditions or OFDM systems requires future study, in both analytical work and simulation.

5.7.3 Discussions on LLR Metrics

5.7.3.1 BER Performance

The BER with PSAM-LLR compared with BER with A-PSAM-LLR in 8 scenarios is shown in Figure 5-22 to Figure 5-29. It shall be noted that to save the display space, we use "S2" in the legend to refer to pilot spacing of 2, "S4" to refer to pilot spacing of 4, etc. The legend "LA" refers to A-PSAM-LLR, while the legend "L" refers to PSAM-LLR.

Figure 5-22   BER for scenarios 1: 64-point OFDM, rectangular, 8 paths, PSAM-LLR vs A-PSAM-LLR with different pilot spacing

Figure 5-23 **BER for scenarios 2: 64-point OFDM, exponential, 8 paths, PSAM-LLR vs A-PSAM-LLR with different pilot spacing**

Figure 5-24 **BER for scenarios 3: 64-point OFDM, rectangular, 12 paths, PSAM-LLR vs A-PSAM-LLR with different pilot spacing**

Figure 5-25 **BER for scenarios 4: 64-point OFDM, exponential, 12 paths, PSAM-LLR vs A-PSAM-LLR with different pilot spacing**

Figure 5-26   BER for scenario 5: 128-point OFDM, rectangular, 8 paths, PSAM-LLR vs A-PSAM-LLR with different pilot spacing
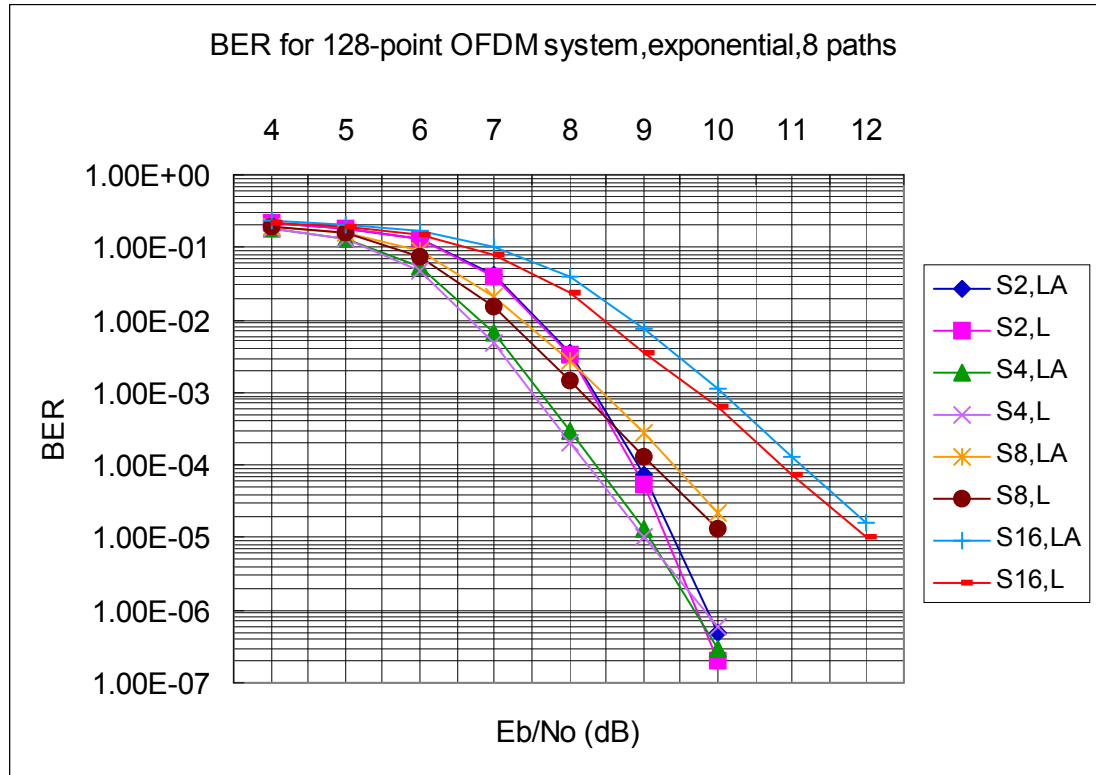
Figure 5-27   BER for scenario 6: 128-point OFDM, exponential, 8 paths, PSAM-LLR vs A-PSAM-LLR with different pilot spacing
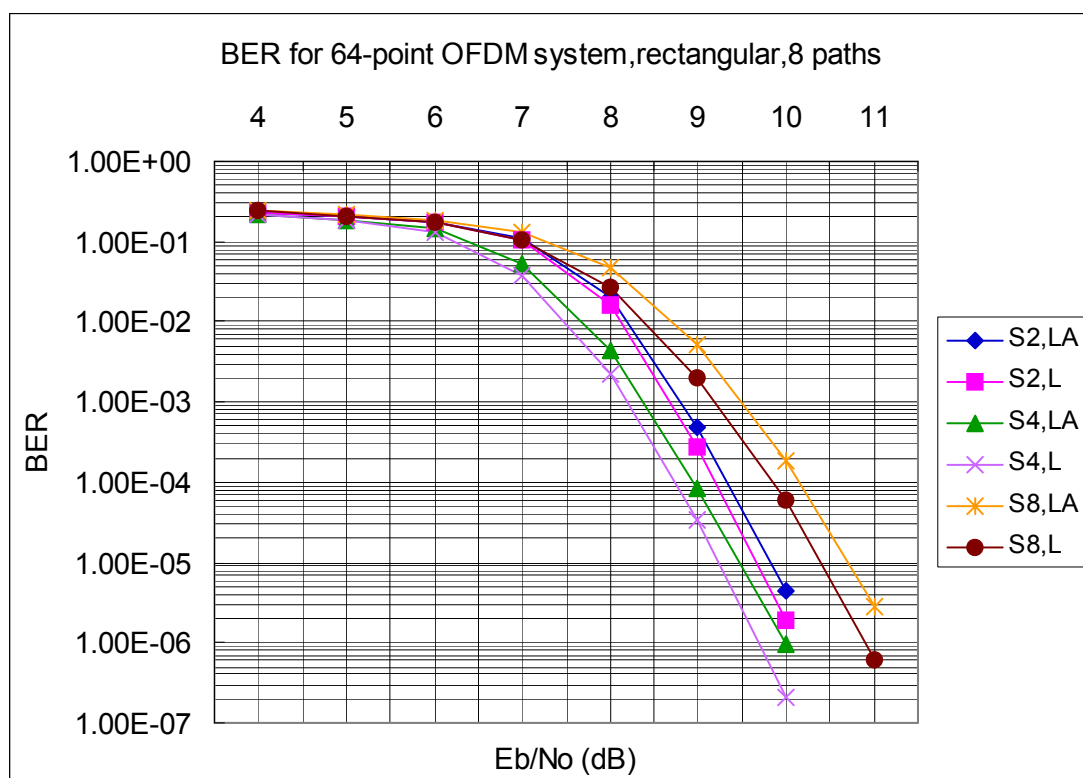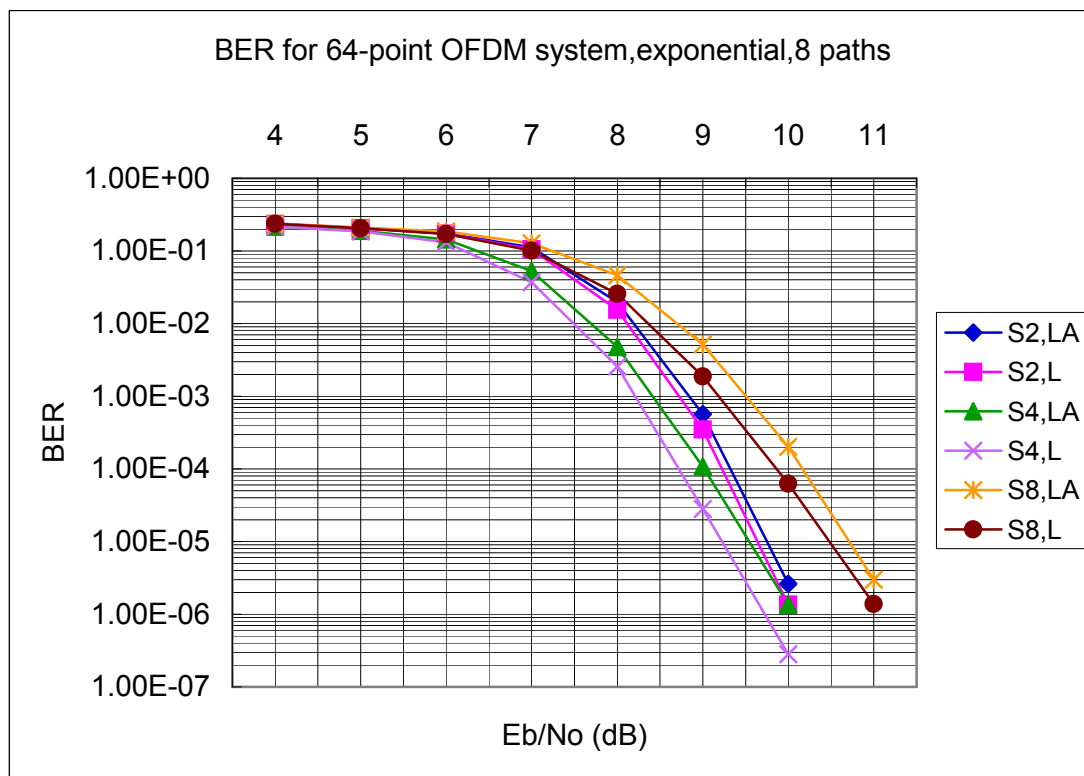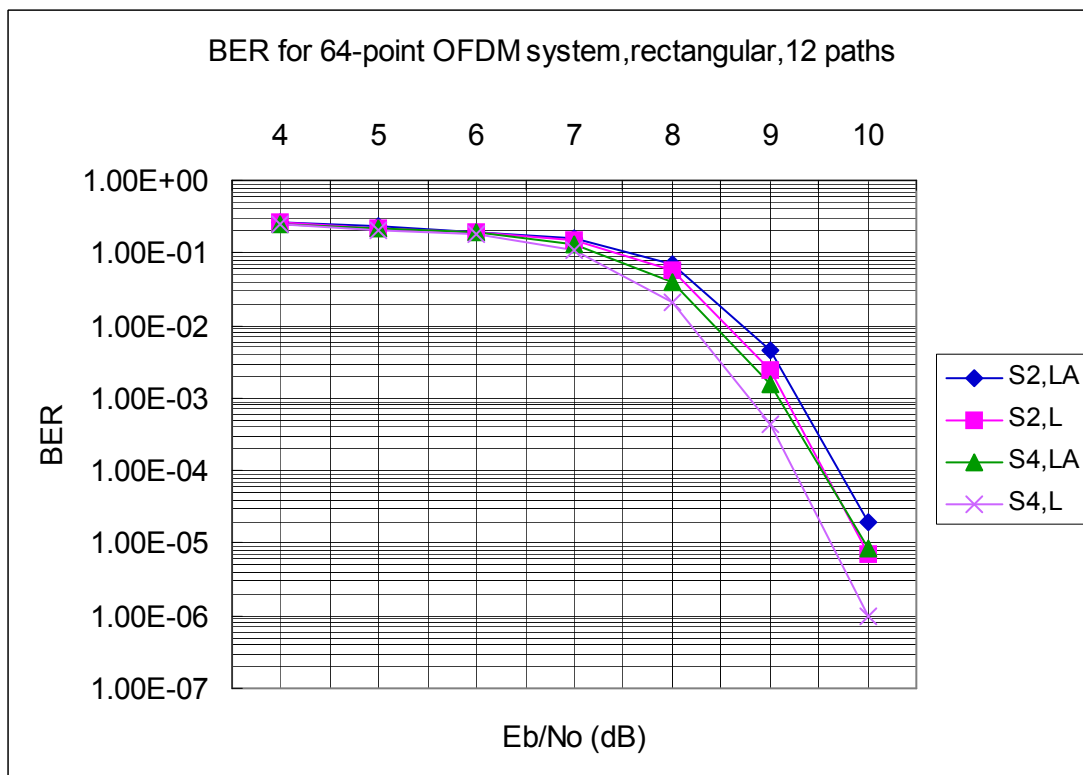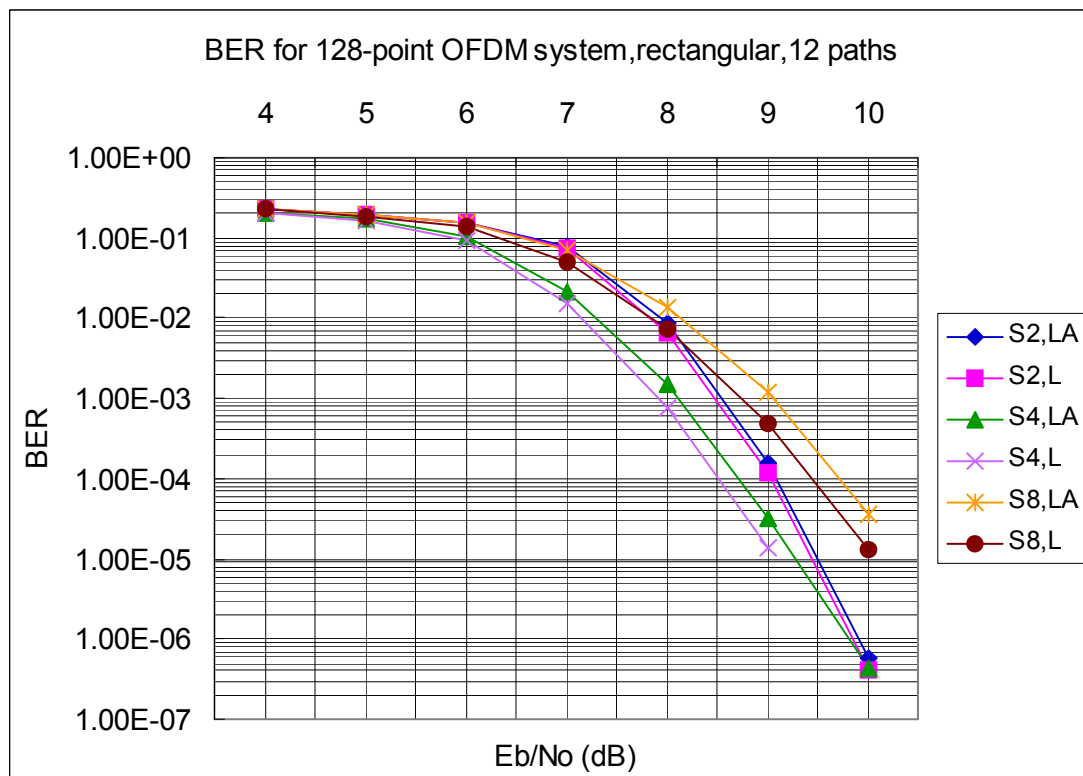
Figure 5-28   BER for scenario 7: 128-point OFDM, rectangular, 12 paths, PSAM-LLR vs A-PSAM-LLR with different pilot spacing
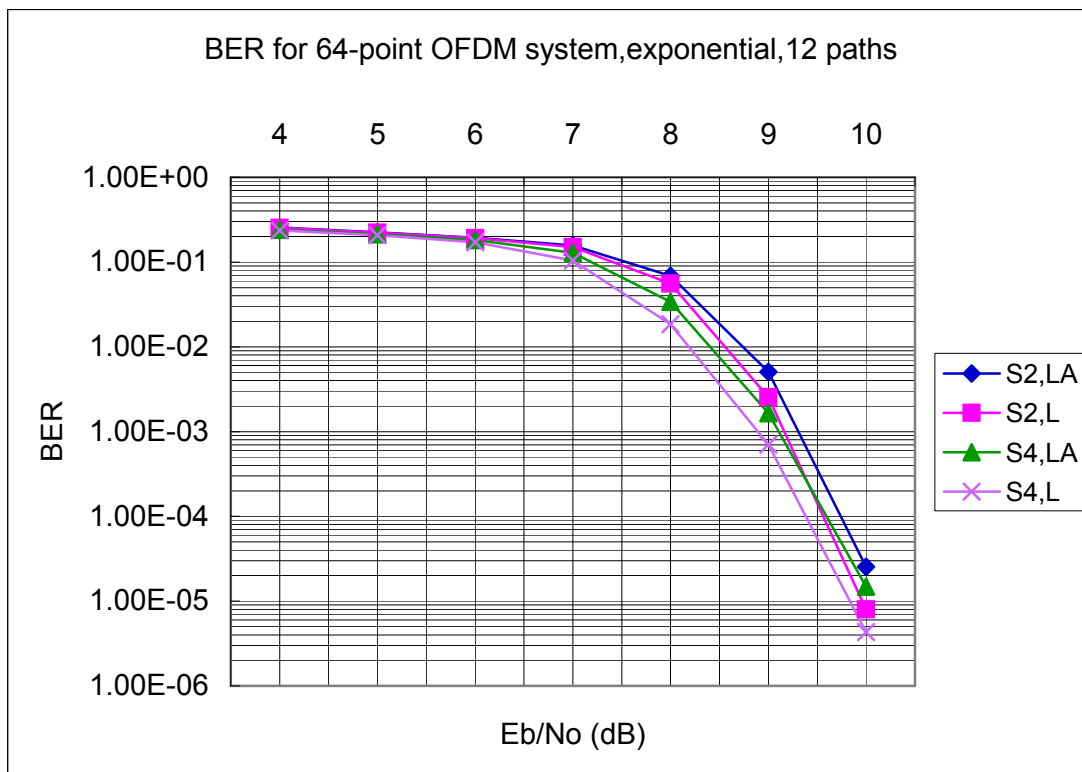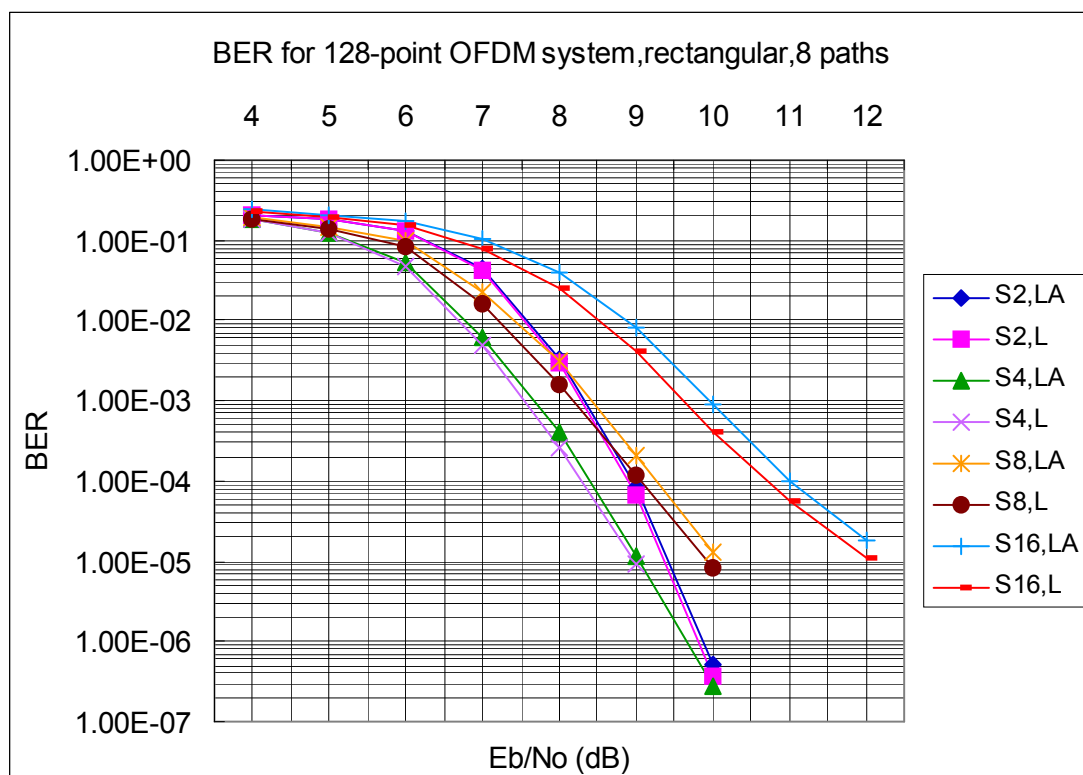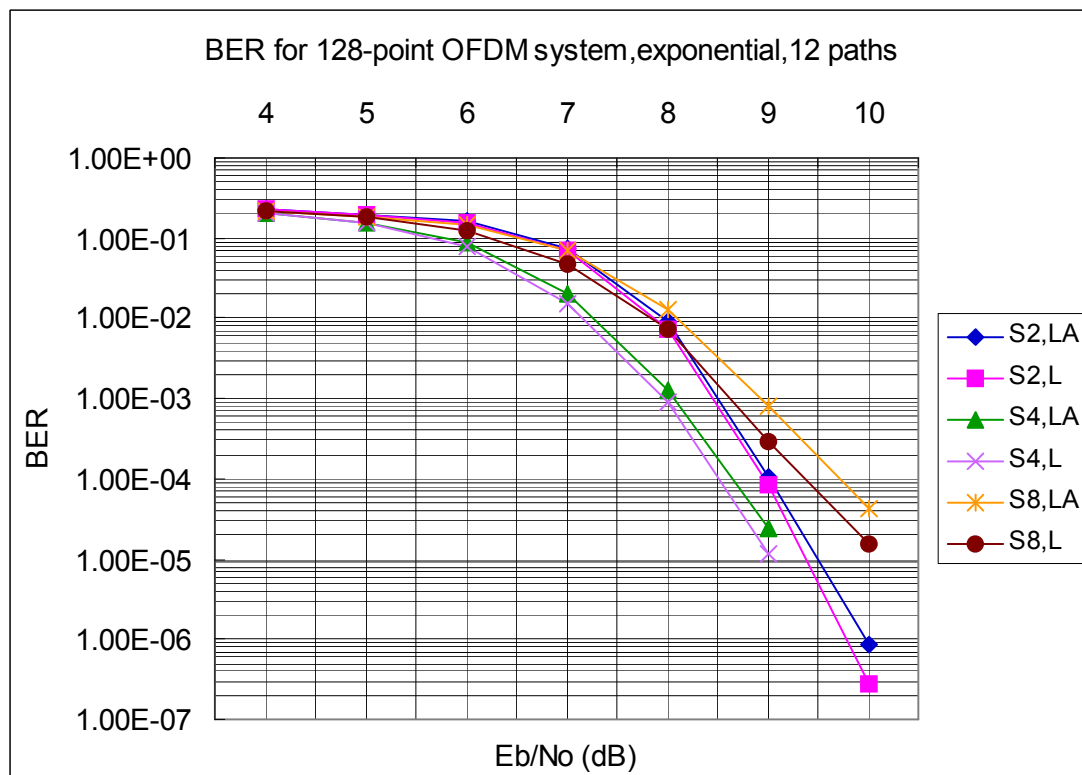

Figure 5-29   BER for scenario 8: 128-point OFDM, exponential, 12 paths, PSAM-LLR vs A-PSAM-LLR with different pilot spacing

Based on the above BER plots, the Eb/No required to achieve the BER of 1e-4 for different scenarios can be summarized in Table 5-14.

Table 5-14   Eb/No (dB) for achieving BER of 1e-4 in different scenarios when A-PSAM-LLR or PSAM-LLR is used

scenario	Eb/No (dB) for achieving BER of 1e-4							
	Pilot spacing 2		Pilot spacing 4		Pilot spacing 8		Pilot spacing 16	
	A-PSAM-LLR	PSAM-LLR	A-PSAM-LLR	PSAM-LLR	A-PSAM-LLR	PSAM-LLR	A-PSAM-LLR	PSAM-LLR
1	9.34	9.20	8.95	8.74	10.15	9.85	NA	NA
2	9.32	9.22	9.02	8.72	10.17	9.86	NA	NA
3	9.70	9.54	9.52	9.24	NA	NA	NA	NA
4	9.74	9.56	9.59	9.38	NA	NA	NA	NA
5	8.95	8.89	8.40	8.29	9.26	9.05	11.01	10.71
6	8.92	8.84	8.36	8.24	9.41	9.11	11.12	10.85
7	9.08	9.03	8.71	8.50	9.71	9.43	NA	NA
8	9.01	8.96	8.67	8.49	9.69	9.37	NA	NA

Denote the Eb/No required to achieve BER of 1e-4 for A-PSAM-LLR and PSAM-LLR as $EbNo_{A-PSAM-LLR}$ and $EbNo_{PSAM-LLR}$, respectively, the performance difference between A-PSAM-LLR and PSAM-LLR can be indicated by the difference between the two Eb/No values.

$$\Delta EbNo = EbNo_{A-PSAM-LLR} - EbNo_{PSAM-LLR} \qquad (5.48)$$

The $\Delta EbNo$ in different scenarios are summarized in Table 5-15. The average of $\Delta EbNo$ for different pilot spacing is calculated.

Table 5-15   Compare A-PSAM-LLR with PSAM-LLR in terms of Eb/No (dB) for achieving BER of 1e-4 in different scenarios

Scenario	ΔEb/No (dB) for achieving BER of 1e-4			
	Pilot spacing 2	Pilot spacing 4	Pilot spacing 8	Pilot spacing 16
1	0.14	0.21	0.30	NA
2	0.10	0.30	0.31	NA
3	0.16	0.28	NA	NA
4	0.18	0.21	NA	NA
5	0.06	0.11	0.21	0.30
6	0.08	0.12	0.30	0.27
7	0.05	0.21	0.28	NA
8	0.05	0.18	0.32	NA
Average	0.1	0.2	0.29	0.29

Table 5-15 shows that for all scenarios and all pilot spacing, the PSAM-LLR always outperforms the A-PSAM-LLR. For example, in scenario 1, when pilot spacing is 4, the BER of PSAM-LLR is better than that of A-PSAM-LLR by 0.21dB. With pilot spacing 4, the performance gain of PSAM-LLR over A-PSAM-LLR varies between 0.1dB to 0.3dB for different scenarios, and the average performance gain over all the scenarios is about 0.2dB.

Furthermore, the performance gain of PSAM-LLR over A-PSAM-LLR is related to the pilot spacing. Specifically, with the increased pilot spacing, the performance gap between PSAM-LLR and A-PSAM-LLR is increased. For example, in scenario 2, the performance gain increases from 0.1dB to 0.3dB when pilot spacing increases from 2 to 4. Similar trend is observed in other scenarios. Hence, when pilot spacing is small, the performance of PSAM-LLR is only slightly better than that of A-PSAM-LLR. When pilot spacing is large, the performance with PSAM-LLR will be more significantly better than that with A-PSAM-LLR.

The average of ΔEb/No over different pilot spacing is shown in Table 5-15. It can be seen that when pilot spacing is 2, the performance gain of PSAM-LLR over A-PSAM-LLR is 0.1dB. When pilot spacing is increased to 4, the performance gain of PSAM-LLR over A-PSAM-LLR increases to 0.2dB. When pilot spacing is 8 and 16, the performance gain can reach 0.3dB. The result clearly shows that PSAM-LLR outperforms A-PSAM-LLR, particularly for larger pilot spacing setting.

The reason for such phenomenon is that A-PSAM-LLR ignores the channel estimation mean square error and uses the inaccurate channel estimate only in its LLR derivation. In contrast, PSAM-LLR takes into account the channel estimation as well as the estimation mean square error in its LLR derivation. When pilot spacing is very small, i.e. 2, the channel estimation is accurate enough. Hence, the consideration of channel estimation error in PSAM-LLR does not bring too much performance improvement. However, when pilot spacing is large, the estimation error becomes large. In such cases, the estimation mean square error provides some useful information about the reliability of the received bits and can make a lot of difference. By considering the estimation mean square error, the PSAM-LLR is a more accurate and reliable LLR. It is reasonable that PSAM-LLR can achieve a better performance than the A-PSAM-LLR.

5.7.3.2 Iteration in LDPC Decoder

The iteration required in LDPC decoder is an important measurement criterion. As each iteration incurs processing delay and considerable power consumption, it is desirable that iteration be kept minimum without compromise of performance. Hence, it is necessary to compare the iteration required by PSAM-LLR and A-PSAM-LLR to reach a certain performance.

We consider the scenario 3. Table 5-16 shows the BER of PSAM-LLR and A-PSAM-LLR when Eb/No is 10dB and LDPC decoder uses different iteration.

Table 5-16   BER for PSAM-LLR and A-PSAM-LLR at Eb/No 10dB in scenario 3: 64-point OFDM system, rectangular and 12 paths

Iteration	BER with ideal CSI	BER with A-PSAM-LLR	BER with PSAM-LLR
1	7.75e-002	1.06e-001	1.06e-001
2	4.23e-002	7.78e-002	7.75e-002
3	1.47e-002	5.06e-002	5.00e-002
4	3.65e-003	2.93e-002	2.86e-002
5	6.90e-004	1.53e-002	1.46e-002
6	1.02e-004	7.35e-003	6.81e-003
7	1.32e-005	3.35e-003	2.98e-003
8	1.68e-006	1.51e-003	1.27e-003
9	2.63e-007	7.17e-004	5.60e-004
10	3.76e-008	3.76e-004	2.70e-004

11	0.00e+000	2.25e-004	1.48e-004
12	0.00e+000	1.52e-004	9.34e-005
13	0.00e+000	1.15e-004	6.61e-005
14	0.00e+000	9.43e-005	5.09e-005
15	0.00e+000	8.22e-005	4.15e-005
16	0.00e+000	7.36e-005	3.52e-005
17	0.00e+000	6.68e-005	3.06e-005
18	0.00e+000	6.12e-005	2.76e-005
19	0.00e+000	5.84e-005	2.56e-005
20	0.00e+000	5.49e-005	2.39e-005
21	0.00e+000	5.18e-005	2.21e-005
22	0.00e+000	4.95e-005	2.10e-005
23	0.00e+000	4.74e-005	1.94e-005
24	0.00e+000	4.64e-005	1.87e-005
25	0.00e+000	4.49e-005	1.78e-005
26	0.00e+000	4.32e-005	1.70e-005
27	0.00e+000	4.19e-005	1.64e-005
28	0.00e+000	4.04e-005	1.62e-005
29	0.00e+000	3.93e-005	1.52e-005
30	0.00e+000	3.75e-005	1.50e-005
31	0.00e+000	3.61e-005	1.41e-005
32	0.00e+000	3.48e-005	1.38e-005
33	0.00e+000	3.40e-005	1.35e-005
34	0.00e+000	3.25e-005	1.32e-005
35	0.00e+000	3.13e-005	1.24e-005
36	0.00e+000	3.07e-005	1.21e-005
37	0.00e+000	2.98e-005	1.18e-005
38	0.00e+000	2.90e-005	1.14e-005

| 39	0.00e+000	2.84e-005	1.12e-005
40	0.00e+000	2.75e-005	1.08e-005
41	0.00e+000	2.66e-005	1.05e-005
42	0.00e+000	2.62e-005	9.84e-006
43	0.00e+000	2.55e-005	9.70e-006
44	0.00e+000	2.51e-005	9.44e-006
45	0.00e+000	2.41e-005	9.27e-006
46	0.00e+000	2.40e-005	8.98e-006
47	0.00e+000	2.36e-005	8.75e-006
48	0.00e+000	2.32e-005	8.34e-006
49	0.00e+000	2.23e-005	8.26e-006
50	0.00e+000	2.21e-005	8.01e-006

The result is plotted in Figure 5-30.
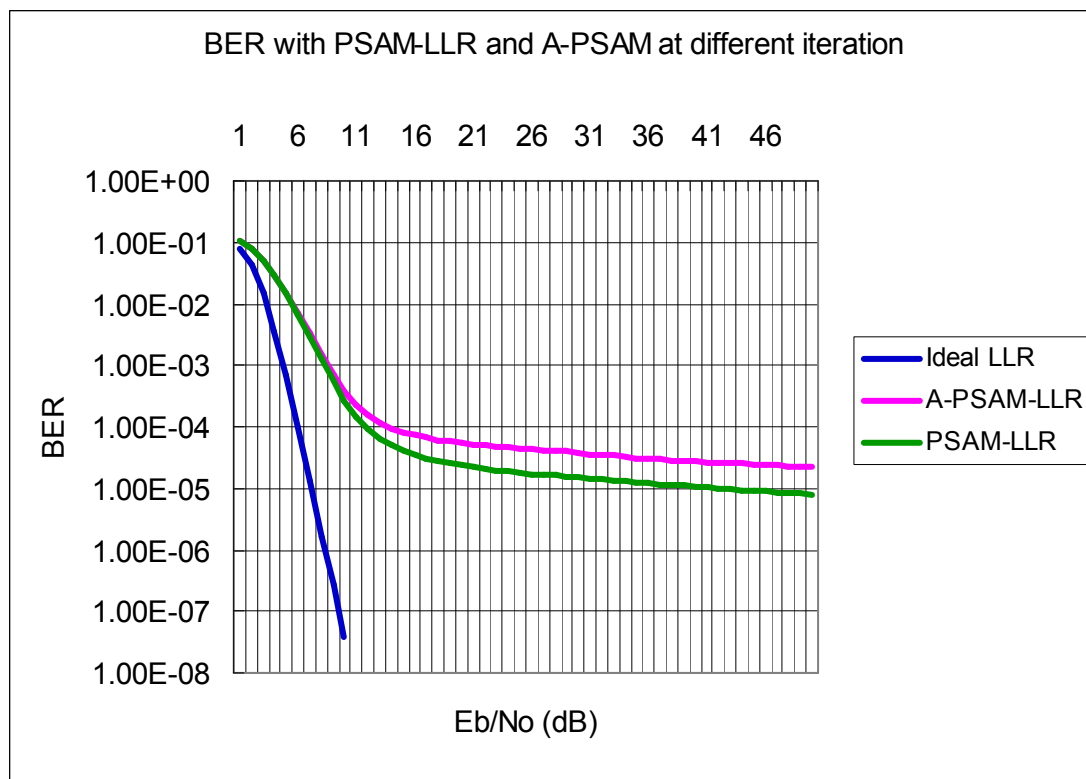
Figure 5-30   **BER with PSAM-LLR and A-PSAM-LLR at different iteration**

Figure 5-30 shows that BER with PSAM-LLR converges faster than A-PSAM-LLR when the iteration is greater than 10. For example, when PSAM-LLR is used, BER of 1e-4 is achieved after about 12 iterations. In contrast, when A-PSAM-LLR is used, BER of 1e-4 is achieved after 14 iterations. Hence, 2 iterations can be saved if PSAM-LLR is adopted.

It is shown in both Table 5-16 and Figure 5-30 that while it takes the decoder with A-PSAM-LLR 50 iterations to achieve a BER of 2.21e-005, the decoder with PSAM-LLR can achieve the same performance with only 22 iterations. Hence, a total of 28 iterations can be saved, leading to considerable reduction in the computational complexity and processing delay.

Similar trend is observed in other scenarios.

5.7.3.3 Implementation Complexity

Equation (5.38) and (5.39) shows that the derivation of PSAM-LLR requires the calculation of a scaling factor which is $\dfrac{1}{\dfrac{E_s}{N_0}\xi_{\min}(n)+1}$. It is shown in section 5.5 that when pilots are uniformly spaced and number of pilots are power of 2, the mean square error $\xi_{\min}(n)$ is a constant and the scaling factor is also a constant. Hence, the requirement for memory is low.

Basically, the choice between the two LLR metrics is a tradeoff between computational complexity and the BER performance. Although the multiplication of the scaling factor requires some computational resource, the extra complexity is worthwhile considering the performance improvement and the reduced iteration brought by the PSAM-LLR.

5.7.4 Summary

Based on the simulation result for different scenarios and the discussion on the pilot spacing and different LLR metrics, we can make the following summary.

1) About optimal pilot spacing

   - Denser pilot leads to better channel estimation, and consequently the better BER versus SNR. However, the poorer utilization of the signal spectrum will cause the BER versus Eb/No to degrade. Hence, pilot spacing of 2 does not lead to the best performance among other possible pilot spacing settings.

   - Simulation shows that when pilots are uniformly spaced, the BER performance is the best with pilot spacing of 4.

   - In summary, the pilot spacing of 4 is recommended as the optimal choice.

2) About the LLR metric

- With the same maximum iteration of 50 in LDPC decoder, PSAM-LLR and A-PSAM-LLR has similar performance in the low Eb/No range. It shows that A-PSAM-LLR is a good approximation of PSAM-LLR.

- PSAM-LLR leads to better performance at high Eb/No. For example, at BER of 1e-4, the performance with PSAM-LLR is better than that with A-PSAM-LLR by about 0.1 - 0.3dB, depending on the scenarios. And the larger the pilot spacing, the more significant performance difference between the A-PSAM-LLR and PSAM-LLR is observed.

- LDPC decoder initialized with PSAM-LLR requires less iteration to converge. Simulation shows that when initialized with PSAM-LLR, the LDPC decoder with 20 iterations can achieve a BER which is achievable by LDPC decoder initialized with A-PSAM-LLR after 50 iterations.

- The PSAM-LLR requires slightly more complex computation due to the calculation of the scaling factor. However, considering that PSAM-LLR has better performance and requires less iteration, the slightly increase in the computation can be justified.

- In summary, PSAM-LLR is the recommended LLR metric to be used in LDPC decoder.

CHAPTER 6   CONCLUSION AND FUTURE WORK

This chapter summarizes the main contributions of the thesis and discusses possible directions for further research.

6.1   Main Contributions

The main work in this thesis is to study the LDPC-coded pilot-assisted OFDM system with the focus on finding the optimal pilot insertion and optimal LLR metric for LDPC decoding.

The research is inspired by the work in [1], in which Haifeng Yuan et al. studied the pilot-assisted LPDC-coded single-carrier system and proposed the PASM-LLR metric which is found to outperform the A-PSAM-LLR metric, also known as the conventional LLR metric. The two metrics are both based on the LMMSE estimator, or Wiener filter, but differ in that PSAM-LLR metric considers both the channel estimation and estimation mean square error in the LLR derivation, while A-PSAM-LLR metric only considers the channel estimation.

Based on such pioneering work, the LDPC-coded pilot-assisted OFDM system over multipath fading channel is studied. The research is divided into theoretical portion and simulation portion. The theoretical work is carried out in several stages. Firstly, by modeling the multipath channel to a sample-spaced FIR filter, the system function in frequency domain is derived and found to have a similar mathematical form to that of the single-carrier system. Secondly, by using the LMMSE estimator, the channel at every subcarrier is estimated. Thirdly, due to the analogy in the system function between single-carrier system and OFDM system, we derive two LLR metrics for the OFDM system. By following the naming convention in the literature, we name the two LLR metrics as PSAM-LLR and A-PSAM-LLR, respectively. Finally, the LDPC decoding is performed with the two LLR metrics.

Based on the above theoretical work, we build a simulation platform with C/C++ and MATLAB language. Simulations are performed for system with configurable parameters such as FFT points, pilot spacing, maximum delay spread, power delay profile, etc. The simulation result is analyzed with the focus on these issues:

(1)   What is the optimal pilot spacing?

(2)   Is PSAM-LLR better than A-PSAM-LLR in terms of BER performance? Which LLR metric is recommended in real application considering the performance and the implementation complexity?

The simulation gives answer to these questions. The simulation shows that the optimal pilot spacing in various scenarios is 4. It is found that PSAM-LLR metric outperforms the A-

PSAM-LLR metric in the OFDM system. Moreover, the performance gain with PSAM-LLR varies with different pilot spacing. The performance improvement with PSAM-LLR is more significant when pilot spacing is large, e.g. pilot spacing of 8 or 16, and less significant when the pilot spacing is small, e.g. pilot spacing of 2 or 4. Although the implementation of PSAM-LLR requires extra computational efforts, the considerable performance improvement and much relaxed iteration requirement still make it a cost-effective choice. Hence, PSAM-LLR is recommended in real application.

In summary, the main contribution of the research is to illustrate the impact of different pilot spacing and LLR metrics on the performance of the LPDC-code pilot-assisted OFDM system. The result obtained in the research may provide reference to system designers, raising their awareness of the importance of pilot spacing and helping them select the optimal pilot insertion scheme. The research also benefits the receiver designers, enabling them to select the LDPC decoder initialized with the most accurate LLR metric.

6.2   Directions for Future Research

There are several limitations of the research. First, only one channel model is considered, by which the multipath fading channel is modeled as a sample-spaced FIR filter. Second, only BPSK modulation is considered. Third, only the pilots in one OFDM symbol are used in the channel estimation. We can overcome these limitations by expanding our research scope. In the future work, we may investigate other channel models, such as WSSUS channel (wide sense stationary with uncorrelated scattering channel) [48]. We may consider more complex modulation schemes such as QPSK (Quadrature Phase Shift Keying) and QAM (Quadrature Amplitude Modulation), and investigate if 2-D channel estimation by using pilots in a frequency-time grid will further improve the performance. The prospect of the extended research shall be promising.

CHAPTER 7   BIBLIOGRAPHY

[1]   Haifeng Yuan; Pooi Yuen Kam; , "Log-Likelihood Ratios for LDPC Codes with Pilot-Symbol-Assisted BPSK Transmission over Flat Rayleigh Fading Channels," *Vehicular Technology Conference Fall (VTC 2009-Fall), 2009 IEEE 70th* , vol., no., pp.1-5, 20-23 Sept. 2009

[2]   W. C. Jakes, *Microwave Mobile Communication*. New York: Wiley, 1974

[3]   Dent, P.; Bottomley, G.E.; Croft, T.; , "Jakes fading model revisited," *Electronics Letters* , vol.29, no.13, pp.1162-1163, 24 June 1993

[4]   Zheng, Y.R.; Chengshan Xiao; , "Improved models for the generation of multiple uncorrelated Rayleigh fading waveforms," *Communications Letters, IEEE* , vol.6, no.6, pp.256-258, Jun 2002

[5]   Yahong Rosa Zheng; Chengshan Xiao; , "Simulation models with correct statistical properties for Rayleigh fading channels," *Communications, IEEE Transactions on* , vol.51, no.6, pp. 920- 928, June 2003

[6]   Jilei Hou; Siegel, P.H.; Milstein, L.B.; , "Performance analysis and code optimization of low density parity-check codes on Rayleigh fading channels," *Selected Areas in Communications, IEEE Journal on* , vol.19, no.5, pp.924-934, May 2001

[7]   Edfors, O.; Sandell, M.; van de Beek, J.-J.; Wilson, S.K.; Borjesson, P.O.; , "OFDM channel estimation by singular value decomposition," *Communications, IEEE Transactions on* , vol.46, no.7, pp.931-939, Jul 1998

[8]   Srivastava, V.; Chin Keong Ho; Patrick Ho Wang Fung; Sumei Sun; , "Robust MMSE channel estimation in OFDM systems with practical timing synchronization," *Wireless Communications and Networking Conference, 2004. WCNC. 2004 IEEE* , vol.2, no., pp. 711- 716 Vol.2, 21-25 March 2004

[9]   Morelli, M.; Mengali, U.; , "A comparison of pilot-aided channel estimation methods for OFDM systems," *Signal Processing, IEEE Transactions on* , vol.49, no.12, pp.3065-3073, Dec 2001

[10]   Benedetto, S.; Montorsi, G.; , "Unveiling turbo codes: some results on parallel concatenated coding schemes," *Information Theory, IEEE Transactions on* , vol.42, no.2, pp.409-428, Mar 1996

[11]   Ramsey, J.; , "Realization of optimum interleavers," *Information Theory, IEEE Transactions on* , vol.16, no.3, pp. 338- 345, May 1970

[12]   Cavers, J.K.; , "An analysis of pilot symbol assisted modulation for Rayleigh fading channels [mobile radio]," *Vehicular Technology, IEEE Transactions on* , vol.40, no.4, pp.686-693, Nov 1991

[13]   R.W. Chang, "Synthesis of band-limited orthogonal signals for multichannel data transmission," *Bell Sys. Tech*. J., vol. 45, December 1966.

[14]   Weinstein, S.; Ebert, P.; , "Data Transmission by Frequency-Division Multiplexing Using the Discrete Fourier Transform," *Communication Technology, IEEE Transactions on* , vol.19, no.5, pp.628-634, October 1971

[15]   Cimini, L., Jr.; , "Analysis and Simulation of a Digital Mobile Channel Using Orthogonal Frequency Division Multiplexing," *Communications, IEEE Transactions on* , vol.33, no.7, pp. 665- 675, Jul 1985

[16]   Cavers, J.K.; Liao, M.; , "A comparison of pilot tone and pilot symbol techniques for digital mobile communication," *Global Telecommunications Conference, 1992. Conference Record., GLOBECOM '92. Communication for Global Users., IEEE* , vol., no., pp.915-921 vol.2, 6-9 Dec 1992

[17]   W. C. Y. Lee, *Mobile Communications Engineering*. New York: McGraw-Hill, 1982.

[18]   R. H. Clarke, "A Statistical Theory of Mobile Radio Reception," *Bell Sys. Tech*. I., vol. 47, no. 6, July-Aug. 1968, pp. 957-1000.

[19]   R. G. Gallager, *Low-Density Parity-Check Codes*. Cambridge, MA: MIT Press, 1963.

[20]   Tanner, R.; , "A recursive approach to low complexity codes," *Information Theory, IEEE Transactions on* , vol.27, no.5, pp. 533- 547, Sep 1981

[21]   MacKay, D.J.C.; , "Good error-correcting codes based on very sparse matrices," *Information Theory, IEEE Transactions on* , vol.45, no.2, pp.399-431, Mar 1999

[22]   M. Luby, M. Mitzenmacher, M. A. Shokrollahi, D. A. Spielman, and V. Stemann, "Practical Loss-Resilient Codes", *Proc. 29th Symp. on Theory of Computing*, 1997, pp. 150–159.

[23]   M. Luby, M. Mitzenmacher, A. Shokrollahi, and D. Spielmann. "Analysis of low-density codes and improved designs using irregular graph". *Proc. 30th -Annual ACM Symposium on Theory of Computing*, pages 249-258, 1998.

[24]   Richardson, T.J.; Urbanke, R.L.; , "The capacity of low-density parity-check codes under message-passing decoding," *Information Theory, IEEE Transactions on* , vol.47, no.2, pp.599-618, Feb 2001

[25]   Richardson, T.J.; Shokrollahi, M.A.; Urbanke, R.L.; , "Design of capacity-approaching irregular low-density parity-check codes," *Information Theory, IEEE Transactions on* , vol.47, no.2, pp.619-637, Feb 2001

[26]   Sae-Young Chung; Richardson, T.J.; Urbanke, R.L.; , "Analysis of sum-product decoding of low-density parity-check codes using a Gaussian approximation," *Information Theory, IEEE Transactions on* , vol.47, no.2, pp.657-670, Feb 2001

[27]   D.   Makay's   Database,   [online]. http://www.inference.phy.cam.ac.uk/mackay/codes/data.html#l26

[28]   Meng-Han Hsieh; Che-Ho Wei; , "Channel estimation for OFDM systems based on comb-type pilot arrangement in frequency selective fading channels," *Consumer Electronics, IEEE Transactions on* , vol.44, no.1, pp.217-225, Feb 1998

[29]   Negi, R.; Cioffi, J.; , "Pilot tone selection for channel estimation in a mobile OFDM system ," *Consumer Electronics, IEEE Transactions on* , vol.44, no.3, pp.1122-1128, Aug 1998

[30]   Rinne, J.; Renfors, M.; , "Pilot spacing in orthogonal frequency division multiplexing systems on practical channels," *Consumer Electronics, IEEE Transactions on* , vol.42, no.4, pp.959-962, Nov 1996

[31]   Coleri, S.; Ergen, M.; Puri, A.; Bahai, A.; , "Channel estimation techniques based on pilot arrangement in OFDM systems," *Broadcasting, IEEE Transactions on* , vol.48, no.3, pp. 223- 229, Sep 2002

[32]   Li, Y.; Cimini, L.J., Jr.; Sollenberger, N.R.; , "Robust channel estimation for OFDM systems with rapid dispersive fading channels," *Communications, IEEE Transactions on* , vol.46, no.7, pp.902-915, Jul 1998

[33]   Shuichi Ohno; Giannakis, G.B.; , "Capacity maximizing MMSE-optimal pilots for wireless OFDM over frequency-selective block Rayleigh-fading channels," *Information Theory, IEEE Transactions on* , vol.50, no.9, pp. 2138- 2145, Sept. 2004

[34]   3GPP TS 05.05 74 V8.20.0 (2005-11)

[35]   Bello, P.; , "Selective Fading Limitations of the Kathryn Modem and Some System Design Considerations," *Communication Technology, IEEE Transactions on* , vol.13, no.3, pp.320-333, September 1965

[36]   Zimmerman, M.; Kirsch, A.; , "The AN/GSC-10 (KATHRYN) Variable Rate Data Modem for HF Radio," *Communication Technology, IEEE Transactions on* , vol.15, no.2, pp.197-204, April 1967

[37]   E. Powers and M. Zimmermann, "A digital implementation of a multichannel data modem," in *Proceedings of the IEEE International Conference on Communications*. (Philadelphia, USA), 1968

[38]   Chang, R.; Gibby, R.; , "A Theoretical Study of Performance of an Orthogonal Multiplexing Data Transmission Scheme," *Communication Technology, IEEE Transactions on* , vol.16, no.4, pp.529-540, August 1968

[39]   Saltzberg, B.; , "Performance of an Efficient Parallel Data Transmission System," *Communication Technology, IEEE Transactions on* , vol.15, no.6, pp.805-811, December 1967

[40]   MacKay, D.J.C.; Neal, R.M.; , "Near Shannon limit performance of low density parity check codes ," *Electronics Letters* , vol.32, no.18, pp.1645, 29 Aug 1996

[41]   Moher, M.L.; Lodge, J.H.; , "TCMP-a modulation and coding strategy for Rician fading channels ," *Selected Areas in Communications, IEEE Journal on* , vol.7, no.9, pp.1347-1355, Dec 1989

[42]   van de Beek, J.-J.; Edfors, O.; Sandell, M.; Wilson, S.K.; Borjesson, P.O.; , "On channel estimation in OFDM systems," *Vehicular Technology Conference, 1995 IEEE 45th* , vol.2, no., pp.815-819 vol.2, 25-28 Jul 1995

[43]   P. Hoher, S. Kaiser, and P. Robertson, "Pilot-symbol-aided channel estimation in time and frequency," in *Proc. IEEE Global Telecommun. Conf. (GLOBECOM'97), Commun. Theory Mini Conf.*, Nov. 1997, pp. 90–96.

[44]   Hoeher, P.; Kaiser, S.; Robertson, P.; , "Two-dimensional pilot-symbol-aided channel estimation by Wiener filtering," *Acoustics, Speech, and Signal Processing, 1997. ICASSP-97., 1997 IEEE International Conference on* , vol.3, no., pp.1845-1848 vol.3, 21-24 Apr 1997

[45]   Magnus Sandell and Ove Edfors, "A comparative study of pilot-based estimators for wireless OFDM, " Research Report TULEA 1996:19, Div. of Signal Processing, LuleL University of Technology, 1996.

[46]   Tufvesson, F.; Maseng, T.; , "Pilot assisted channel estimation for OFDM in mobile cellular systems," *Vehicular Technology Conference, 1997 IEEE 47th* , vol.3, no., pp.1639-1643 vol.3, 4-7 May 1997

[47]   Yuping Zhao; Aiping Huang; , "A novel channel estimation method for OFDM mobile communication systems based on pilot signals and transform-domain processing," *Vehicular Technology Conference, 1997 IEEE 47th* , vol.3, no., pp.2089-2093 vol.3, 4-7 May 1997

[48]   Hoeher, P.; , "A statistical discrete-time model for the WSSUS multipath channel ," *Vehicular Technology, IEEE Transactions on* , vol.41, no.4, pp.461-468, Nov 1992

[49]   Coates, R.F.W.; Janacek, G.J.; Lever, K.V.; , "Monte Carlo simulation and random number generation," *Selected Areas in Communications, IEEE Journal on* , vol.6, no.1, pp.58-66, Jan 1988

[50]   Ozdemir, M.K.; Arslan, H.; , "CHANNEL ESTIMATION FOR WIRELESS OFDM SYSTEMS," *Communications Surveys & Tutorials, IEEE* , vol.9, no.2, pp.18-48, Second Quarter 2007

[51]   Young Gil Kim; Sang Wu Kim; , "Optimum selection diversity for BPSK signals in Rayleigh fading channels," *Communications, IEEE Transactions on* , vol.49, no.10, pp.1715-1718, Oct 2001

[52]   Jilei Hou; Siegel, P.H.; Milstein, L.B.; , "Performance analysis and code optimization of low density parity-check codes on Rayleigh fading channels," *Selected Areas in Communications, IEEE Journal on* , vol.19, no.5, pp.924-934, May 2001

[53]   J. Schoukens and J. Renneboog, "Modeling the noise influence on the Fourier coefficients after a discrete Fourier transform," *IEEE Trans. Instrum. Meas.*, vol. IM-35, No.3, pp.278-286, Sept. 1986

[54]   Baoguo Yang; Letaief, K.B.; Cheng, R.S.; Zhigang Cao; , "Channel estimation for OFDM transmission in multipath fading channels based on parametric channel modeling," *Communications, IEEE Transactions on Communications*, vol.49, no.3, pp.467-479, Mar 2001